FLORIDA INTERNATIONAL UNIVERSITY

Miami, Florida

NON-DESTRUCTIVE EVALUATION OF POLYMERIC MATERIALS USING ULTRASONICS AND MAGNETO-ELECTRIC NANOPARTICLES

A dissertation submitted in partial fulfillment of

the requirements for the degree of

DOCTOR OF PHILOSOPHY

in

MATERIAL SCIENCE AND ENGINEERING

by

Gonzalo Seisdedos Rodriguez

2023

To: Dean John L. Volakis
College of Engineering and Computing

This dissertation, written by Gonzalo Seisdedos Rodriguez, and entitled Non-Destructive Evaluation of Polymeric Materials using Ultrasonics and Magneto-Electric Nanoparticles, having been approved in respect to style and intellectual content, is referred to you for judgment.

We have read this dissertation and recommend that it be approved.

Daniela Radu

Seung Jae Lee

Benjamin Boesl, Co-Major Professor

Dwayne McDaniel, Co-Major Professor

Date of Defense: March 22, 2023

The dissertation of Gonzalo Seisdedos Rodriguez is approved.

Dean John L. Volakis
College of Engineering and Computing

Andrés G. Gil
Vice President for Research and Economic Development
and Dean of the University Graduate School

Florida International University, 2023

DEDICATION

This dissertation is dedicated to my parents for the sacrifices they have made since I was born for me to have a good education. I thank them for their support and encouragement during the challenges of these past few graduate school years. It is also dedicated to my sister for being always there any time I needed it. This goes to my friends here in Miami as well as family and friends back in Spain.

ACKNOWLEDGMENTS

I first want to give a special thanks to Dr. Benjamin Boesl for the last five years of continuous support and mentoring. His guidance and advice have helped me tremendously to make very important personal and professional decisions that have shaped my future career. Special mention also to Dr. Dwayne McDaniel for helping me get introduced to materials-related research when I was an undergrad. Both Dr. McDaniel and Dr. Boesl have been my major advisors throughout graduate school and have dedicated time and effort to help me complete the course work and research to achieve graduation. I would like to mention Tommy, Cristian, and Eric from LANL for their amazing personal and scientific support.

My gratitude also extends to Dr. Daniela Radu and Dr. Seung Jae Lee for being part of my committee. Both have given valuable input to improve my work throughout graduate school. It is important as well to mention the financial support from the NASA CRE2DO and NSF PREM IMPACT FIU. Their contribution also extends to my professional development. Thank you as well to the ONR and PRE-CCAP for supporting the projects that are part of this dissertation. I would also like to mention the Applied Research Center (ARC), the Mechanical and Materials Engineering Department (MME), and Advanced Materials Engineering Research Institute (AMERI) for laboratory support.

A separate paragraph is needed to highlight my friends here in Miami: la bicho palo (Elena), la bebe (Betty), las bebas (Laia and Yoli), la rosiro (Rocio), el del cadi (Riki), el garciius airlines (David), la de los tapers con lentejas (Paula), and el calvo (Jose). For all the long-lasting friendships and invaluable memories that we have built together. You will always be the best of colacado.

My family here in Florida, including my parents and sister, already knows that I would have not been able to reach where I am today without them. Special mention to el chuchi as well, who is also known as the frisbee catcher (Draco). From my family back in Spain I would like to highlight my abuelos, tios, and primos. Special mention to la tati, la dinamita, el obeso, as well as all the bbs in Polinya (not the cats).

ABSTRACT OF THE DISSERTATION

NON-DESTRUCTIVE EVALUATION OF POLYMERIC MATERIALS USING ULTRASONICS AND MAGNETO-ELECTRIC NANOPARTICLES

by

Gonzalo Seisdedos Rodriguez

Florida International University, 2023

Miami, Florida

Professor Benjamin Boesl, Co-Major Professor

Professor Dwayne McDaniel, Co-Major Professor

Polymeric materials, such as Thermosets, are becoming more widely used in demanding applications due to their ability to tailor the properties of structures while reducing weight and cost. The manufacturing conditions of polymeric materials are critical since they determine the resulting polymer structure, which influences the final properties and performance characteristics. It is essential to monitor these polymers during the manufacturing process to understand the relationship between the fabrication conditions and the final quality of the parts. Although destructive testing is commonly used to characterize polymer properties, this type of testing requires specific sample preparation and geometry. Furthermore, lab-type instrumentation used for destructive testing cannot be taken to the field for in-situ testing.

This work presents three non-destructive evaluation methods to characterize the curing process and the viscoelastic properties of various epoxies. The magneto-electric effect was capitalized by monitoring changes in the surface charge density of dispersed magneto-electric nanoparticles by evaluating the output magnetic signal under an applied

magnetic field. This method was used to monitor the curing process of an adhesive as well as the water ingression after exposing the polymer to 95 % relative humidity and 70 ºC. Ultrasonics were utilized to evaluate changes in the cure kinetics and final properties of the epoxies due to variations in their polymer chemistry, i.e., different stoichiometries and the presence of a residual solvent. Changes in longitudinal and shear sound speeds proved how the fabrication process influenced the curing and the viscoelastic properties of various epoxies.

The chemical structure during cure was monitored using Fourier transform infrared spectroscopy. The evolution of the polymer's molecular structure while curing corroborated the trends obtained using ultrasonics. The evaluated curing kinetics were modeled using the Hill equation to better understand numerically the curing processes and allow for future predictions. Combining ultrasonics and FTIR has the potential to effectively characterize the properties of polymers in both an in-field and manufacturing setting, aiding in the tailoring process, and ensuring their reliability in demanding applications.

TABLE OF CONTENTS

LIST OF TABLES

TABLE PAGE

LIST OF FIGURES

FIGURE PAGE

ABBREVIATIONS AND ACRONYMS

AC	Alternating Current
ABCJ	Adhesively Bonded Composite Joint
ASTM	American Society for Testing Materials
CFRP	Carbon Fiber Reinforced Polymer
DCB	Double Cantilever Beam
DDS	Diaminodiphenylsulfone
DGEBA	Diglycidyl Ethers of Bisphenol-A
DI	Deionized
DMA	Dynamic Mechanical Analysis
DSC	Differential Scanning Calorimetry
ENF	End Notch Flexure
FIB	Focused Ion Beam
FTIR	Fourier Transform Infrared Spectroscopy
GRG	Generalized Reduced Gradient
IPA	Isopropyl Alcohol
IR	Infrared Radiation
ME	Magneto-electric
MEN	Magneto-electric Nanoparticles
NDE	Non-Destructive Evaluation
NDT	Non-Destructive testing
PLA	Polylactic Acid
PMC	Polymer Matrix Composites

PPE	Personal Protective Equipment
SEM	Scanning Electron Microscope
SHM	Structural Health Monitoring
TEM	Transmission Electron Microscope
TETA	Triethylenetetramine
T_g	Glass Transition Temperature
TGA	Thermal Gravimetric Analysis
Vol %	Volume Percent
VSM	Vibrating Sample Magnetometry
Wt %	Weight Percent

Chapter 1 Introduction

The primary objective of this research was to create two distinct non-destructive testing (NDT) methods for assessing the characteristics of polymeric materials. The two different methods consist of the following:

1. synthesizing and dispersing Magneto-Electric Nanoparticles (MENs) into an aerospace epoxy adhesive, and then monitoring changes in their surface charge density by evaluating the output magnetic signal under an applied magnetic field, and
2. using ultrasonics to detect changes in the longitudinal and shear sound speeds of thermoset epoxies during the curing process, and after it has been manufactured, due to the varying polymeric structure.

The implementation of MENs and ultrasonics offers a cost-effective alternative to traditional destructive testing techniques. These two techniques allow for non-destructive, in-situ monitoring of polymeric materials, thereby providing a range of possibilities. Through the successful implementation of MENs and ultrasonics, it is now possible to accurately and efficiently assess the condition of polymeric materials.

This report provides a comprehensive overview of polymeric materials, their importance, and the associated challenges. It also reviews the current state-of-the-art techniques used to characterize the properties of polymers. To further understand the materials and the methodology used to non-destructively evaluate the cure kinetics and final properties of two epoxies, three chapters are devoted to the study. The first chapter investigates the use of MENs to characterize an aerospace epoxy adhesive. The second examines the effects of residual solvent on the cure kinetics and final properties of an epoxy

adhesive when evaluated via ultrasonics. Finally, the third chapter explores the combination of ultrasonics and Fourier transform infrared spectroscopy (FTIR) to tailor an epoxy resin when varying its chemical structure. Significant contributions of this work to the field of materials science and engineering include:

1. the novel implementation of magneto-electric nanoparticles to non-destructively evaluate polymers using the magneto-electric effect,
2. the development of an ultrasonics setup for the in-situ, non-destructive evaluation of the cure kinetics and viscoelastic properties of polymeric materials, and
3. the unique combination of ultrasonics and FTIR to understand the effects of the chemical structure on the curing process and the final properties of polymers.

The novel methodologies presented can be implemented in the research and development of new polymeric materials, thereby facilitating their widespread implementation in high-demand applications.

1.1 Polymeric Materials

Polymeric materials are a type of material composed of long, repeating chains of molecules [1]–[3]. They are typically synthetic materials, though some are derived from natural sources [4], [5]. Polymers are lightweight compared to metals and ceramics and have a wide range of properties. They can be hard and rigid, or soft and flexible [6], [7]. They can also be heat resistant and be used in high-temperature applications [8], [9].

One of the main advantages of polymeric materials is their cost-effectiveness. Polymers are typically less expensive than other ceramics and metals, making them a

popular choice for many applications. Polymers often have easier manufacturability than metals and ceramics, which can lower production costs. Another advantage of polymers is that they are environmentally friendly. Many polymers are made from renewable sources, such as plant-based materials. Additionally, some polymers are biodegradable, meaning they can be broken down into harmless components which reduces the risk of environmental pollution [10], [11].

Another great benefit of polymeric materials is their versatility. Polymers can be tailored to create materials with specific properties [12], [13]. For example, polyurethane can be used to create a durable, waterproof material suitable for outdoor use[14]. Polystyrene is used to create lightweight, insulating materials [15], [16], while polyethylene can be used to make durable, waterproof packaging [17], [18]. Modifying polymers has become a priority for companies and researchers to further expand their application range especially in high demanding applications in terms of temperature, load, or environmental conditions.

1.2 Thermosets

Thermosets are a type of polymer that can be used as a structural material in many industrial applications. They are known for their resistance to high temperatures [8], good electrical insulation properties [19], and excellent chemical resistance [20]. Thermosets are formed from a reaction between two or more components, typically a resin and a curing agent, that create a strong, rigid material. Since one of the major advantages of thermosets is their high heat resistance, they are ideal for applications where the material will be exposed to high temperatures, such as aircraft and automotive parts, as well as in electrical components. Additionally, thermosets are resistant to many chemicals, such as acids and bases, making them suitable for use in corrosive environments [21].

The rigidity of thermosets also makes them a good choice for structures that require durability and strength. This is because the material develops a strong bond that cannot be reversed, even when exposed to high temperatures or chemicals. In addition, thermosets are lightweight materials that can be easily molded into shapes, making them ideal for complex designs. Thermoset parts can be mass-produced, allowing for large-scale production of components with consistent quality. This makes them a great option for industries that require large quantities of parts that need to meet high standards.

1.2.1 Cure process

The curing process of thermosets, such as epoxies, involves a chemical reaction that transforms a liquid mixture into a solid form [22]. This mixture is typically composed of resin, curing agents, catalysts, and other components that are activated by heat. One of the main families of epoxies is the glycidyl epoxies, which are known for their low molecular weight [23]. Diglycidyl ether of bisphenol A (also known as DGEBA) is the most common epoxy of the glycidyl family [23], which has an oxirane functional group consisting of a ring containing three members between an oxygen and two carbon atoms [24]. This is illustrated in Figure 1.1 which shows a 3D model of the oxirane ring.

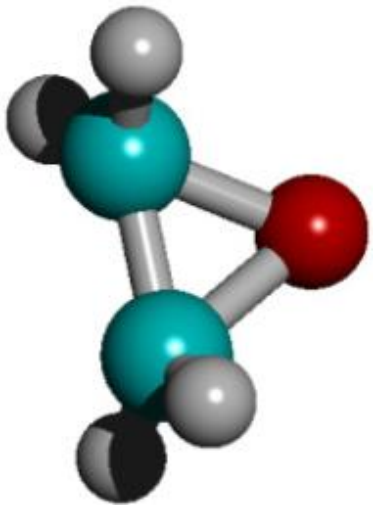

Figure 1.1. 3D model of the oxirane ring [23].

A three-dimensional network is formed due to the opening of the epoxy rings, which is caused by the difference in electronegativity between the oxygen and carbon atoms that results in the oxirane group reacting with nucleophilic compounds such as amines [23]. Triethylenetetramine (TETA), a hexafunctional compound containing two primary and two secondary amine groups, is a common curing agent used to crosslink epoxy [25]. This type of hardener is usually used for room to moderate temperature cures. As seen in Figure 1.2 the reaction between the epoxy resin and the amine serves as the basis of the crosslinking.

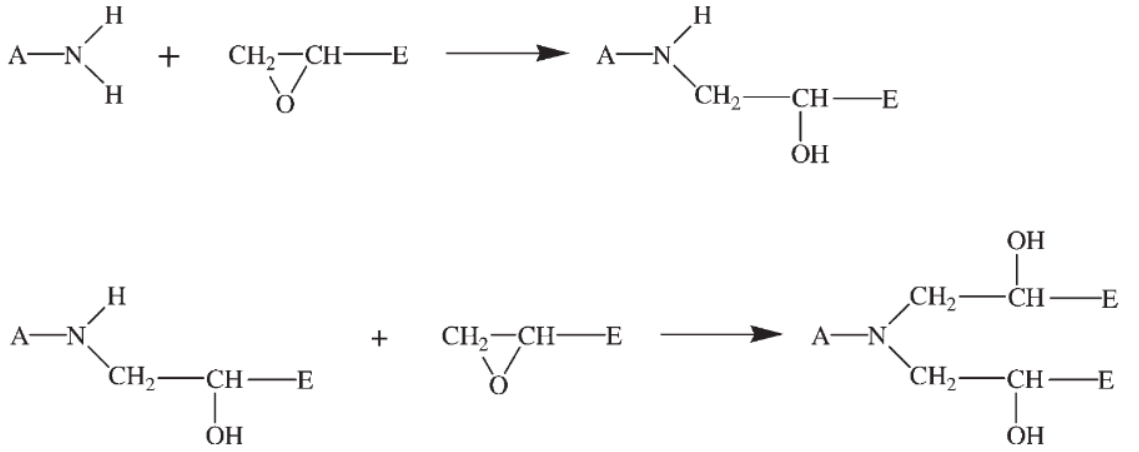

Figure 1.2. Cure reaction between an epoxy resin and an amine. Ring opening by a primary amine (top) and secondary amine reacting with a second epoxy group [19].

As the reaction progresses, the molecular weight and polydispersity of the resin increase, causing two distinct phase transformations to occur: gelation and vitrification [22], [26]. Gelation involves a transformation from a viscous liquid to an elastic gel, rendering the reaction irreversible and leading to a shear response in the material since it can no longer flow [26]. At gelation, the extent of the reaction can be determined using equation 1.1 as follows [27]:

$$\alpha_{gel}\beta_{gel} = \frac{1}{(f_e-1)(f_a-1)} \tag{1.1}$$

where α_{gel} is the epoxy conversion, β_{gel} is the amine conversion, f_e is the functionality of the epoxy, and f_a is the functionality of the amine. The functionality of the epoxy and the amine typically have a value of 2 and 4, respectively.

As the reaction progresses, the cross-linking and molecular weight increase, leading to an increase in the glass transition temperature and viscosity [23]. This marks the vitrification stage of the polymer, where it becomes a rigid, glassy solid. Subsequently, the reaction rate drops and further cross-linking is diffusion/mobility dependent [28], [29]. However, vitrification is a reversible process, and heating the polymer above the glass

transition temperature allows for more cross-linking to occur [23]. To enhance the mechanical and thermal properties of the polymer, it is common for cured parts to receive a post-cure heat treatment [22], [23]. Figure 1.3 presents a schematic of the cross-linking process of a polymer.

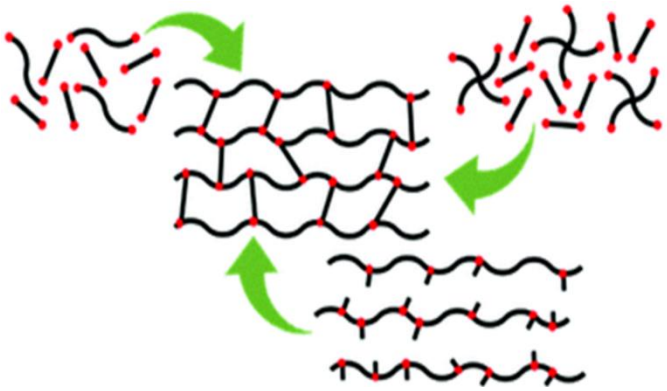

Figure 1.3. Cross-linking process in polymers during cure [30].

1.2.2 Adhesives and Resins

Epoxy-amine resins are widely used in the manufacture of composites, coatings, and adhesives due to their excellent mechanical, thermal, and electrical properties [25], [28]. The versatility of these thermosets enables the tailoring of their characteristics for a wide range of applications. In the aerospace industry, their use as a matrix in fiber-reinforced composites is of particular significance [31], [32]. Nowadays, a paramount objective of aircraft design is the reduction of overall weight, for which composite materials are ideal, as they exploit the properties of various materials for lightweight applications [33].

Most composite parts are currently joined using mechanical fasteners, such as rivets and bolts. While these traditional joining methods enable rapid assembly/disassembly for inspection and repair, they require holes to be drilled in the composite panel. Unfortunately,

this drilling can cause delamination and damage to the composite (as seen in Figure 1.4), and can also produce concentrated stress around the holes [34]. Figure 1.4 shows how a traditional end mill generates delamination in the composite panel. In addition, Moreover, rivets and bolts add numerous components to the aircraft which are typically made of high-density metals, thus increasing the aircraft's total weight and making it more susceptible to corrosion.

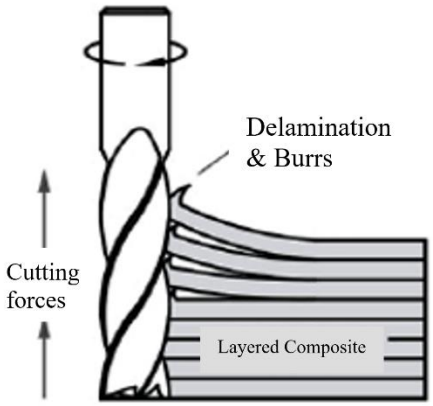

Figure 1.4. Delamination in layered composites caused by drilling [35].

For these reasons, substituting mechanical fasteners with adhesive bonds has become of great interest in many industries. As evidenced in Figure 1.5 this substitution results in a more uniform load distribution and consequently reduces stress concentration. In addition, S. Pitta et al. found that adhesive bonds can be up to three times stronger than riveted joints [36]. Despite this, adhesive bonds have yet to be fully incorporated into primary load structures due to their unpredictable performance, leading to the over-design of composite panels and a reduced efficiency overall [37].

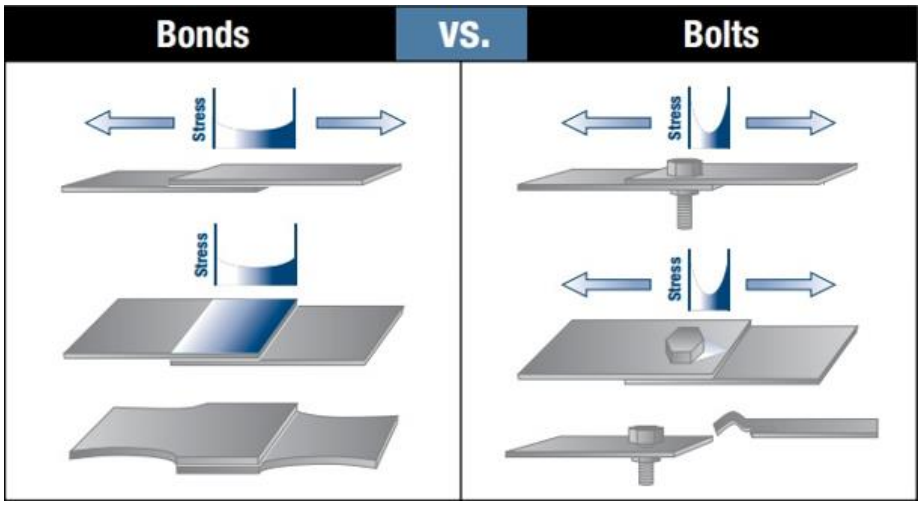

Figure 1.5 Stress distribution in bonded and bolted joints [38].

Unlike mechanical fasteners, it is difficult to inspect adhesive bonds for damage after assembly due to the inability to accurately evaluate the health of the bond after prolonged exposure to external factors, such as elevated temperature, humidity, radiation, and cyclic fatigue. Consequently, it is essential to consider additional measures during the design and manufacturing process of a composite, particularly if it is to be used for primary load structures.

1.2.3 Challenges

Standardizing adhesive bonding has proven to be a great challenge due to the difficulties in obtaining a consistent and acceptable bond quality. This technology is still considered unreliable for primary aircraft structures due to the unpredictable in-service durability, leading to major concerns that limit the widespread implementation of polymeric adhesives. Adding mechanical fasteners into adhesive bonds for reinforcement can defeat the main purpose of this technology, which is the mitigation of stress concentrations and fiber delamination due to drilling holes into the composite. As such, it is important to identify the factors that negatively influence the performance of adhesive

bonds to design and implement alternative adhesive composites to prevent catastrophic crack propagation. Consistent testing of these composites is essential to gain confidence in adhesive bonding before it can be implemented into primary load structures.

1.2.3.1 Manufacturing Concerns

Despite the advantages of using adhesive bonding, the implementation of adhesively bonded composite joints (ABCJs) has been limited due to the variability in bond performance, which is especially prominent when related to process control [39]. While manufacturers provide guidelines for bonding procedures, the performance of such joints remains significantly variable. Weak bonds, bondline voids, and contamination can lead to the failure of such joints, making them a critical issue in the adhesion community today [40].

The lack of standardization in process control to capture and quantify the variability in adhesive bonds during manufacturing can pose a significant challenge. This is because many factors, such as surface preparation methods [41], bondline thickness [42], and curing cycle [43], can influence the mechanical response of a bond. Studies have demonstrated that the bond quality is highly sensitive to contamination, which can arise from human error, incorrect storage and handling, and improper curing. For instance, Van Voast et al. found that even a contamination level of only 2% siloxane, a silicon-based material, can substantially affect adhesion [44]. Similarly, C. Jeenjitkaew et al. observed a 70% reduction in fracture toughness when the composite panels were contaminated with Frekote release agent containing 4% silicon [45]. Thus, quality control is of paramount importance in the production of adhesive bonds to mitigate the effects of factors that increase crack propagation.

The use of solvents during the manufacturing of polymers is essential for reducing the viscosity of the polymer during the coating process or to aid in the dispersion of fillers into the polymer matrix [21], [46], [47]. However, the improper removal of the solvent is known to have detrimental effects on the physical and chemical properties of the polymer [48]–[52]. For example, J. Trinidad et al. demonstrated that the presence of solvents in sodium dodecyl sulfate decorated graphene hybrid electrically conductive adhesives significantly decreased the lap-shear strength of the material due to bubble formation and the creation of voids [53]. N. Othman et al. also found that the addition of 16 wt.% of acetone to an epoxy resin caused a decrease in tensile strength and hardness of 17 and 9 % respectively, as well as a significant reduction in adhesion strength from 13 MPa to 4.9 MPa (-62 %) [21]. Additionally, K. Qiu et al. showed that the addition of 5 wt. % of cellular nanocrystals as a filler to an epoxy resin led to a decrease in crosslinking density and caused a decrease in the glass transition temperature (Tg) of the resin by ~8.5 °C due to reduced homogeneity of the material [54]. These findings emphasize the importance of having an accurate evaluation method to detect residual solvent content in the final structure of a polymeric material to avoid its deleterious effects on the properties of the material.

The incorrect ratio of resin to hardener in an epoxy formulation can affect its curing process, leading to a variation in microstructure due to changes in crosslinking density and molecular weight [25], [26]. K. Frank et al. demonstrated that an excess of 25 % epoxy in a system containing DGEBA cured with 3,3’-diaminodiphenylsulfone (DDS) resulted in a decrease in crosslinking density of over 50 % [55]. Temperature and pressure also play an important role in the curing process of polymers and should be carefully monitored and controlled if specific mechanical properties are desired. However, in some manufacturing

and repair applications, these variables may not be controllable, necessitating an evaluation of the final product to ensure quality control.

1.2.3.2 Durability

Unlike mechanical fasteners, adhesive bonding cannot be disassembled, making part transportation challenging during manufacturing. Additionally, repairs to bonded parts are not easily conducted during service, making it essential to have an accurate understanding of the behavior of adhesive bonds under the conditions they will be subjected to over their lifetime. This is particularly relevant in the aerospace industry, as aircraft operate in highly humid and temperature-fluctuating environments which can expedite the degradation of the adhesive polymer. Therefore, the adhesive bonds must be able to withstand a minimum of thirty years of operation, the approximate operable lifespan of an aircraft.

I. Katsivalis et al. performed dogbone tensile testing on bulk adhesive and determined that environmental exposure produced a reduction in strength and stiffness and an increase in the adhesive's ductility [56]. They also showed through double cantilever beam (DCB) testing how there was a large reduction in the interface strength between the adhesive and composite due to moisture diffusion. B. Wan et al. also concluded that the presence of water deteriorates the bond performance with time [57]. They also mentioned that dry conditions are important during the application of the adhesive and curing process because the presence of water negatively affects the bond quality considerably.

1.2.4 Tailoring mechanical properties

Epoxy resins and adhesives present a unique advantage in their versatility as the final properties can be tailored through adjustment of the chemistry, i.e. the ratio of resin

to curing agent. For example, an epoxy-amine system featuring an excess of amine can increase fracture toughness while reducing fatigue crack propagation [6], [58] However, this can also reduce the glass transition temperature and increase moisture ingression which can have a negative effect on the properties of the material [20], [59]. Finding an optimal stoichiometry to achieve the desired properties for a given application is essential.

The chemistry of the polymer is integral to its curing process. When epoxy and curing agent are mixed, microgel particles form containing low molar mass, which then link together to form a continuous phase. At this stage of the cure, vitrification occurs, wherein the reaction rate decreases and further crosslinking is diffusion/mobility dependent. [28], [29]. However, some un-crosslinked molecules are unable to properly react, thus resulting in an incomplete cure unless the epoxy is subjected to its glass transition temperature (Tg) [60]. Excess epoxy may be used to prevent the presence of unreacted amine. [61]. Nonetheless, altering the system's stoichiometry can result in changes in the chemical structure, as demonstrated by F. Meyer et al. who decreased the amine content of a DGEBA/DDS epoxy-amine resin system by 25%, resulting in an increase of molecular weight from 265 to 596 amu due to an increase in crosslinking density [62]. Therefore, understanding how the epoxy chemistry network interacts with stoichiometry is essential to tailor the material's properties and optimize the use of fillers and other additives in the resin [63].

The mechanical and thermal properties of epoxies are also influenced by the epoxy/amine stoichiometry as a consequence of varying chemical structure [19], [64]. J. Szabelski et al. tested the adhesive joint strength of an Epidian 57/PAC epoxy resin cured at 25 ºC for seven days [65]. They showed how the joint strength decreased from 27.10

MPa to 23.49 and 13.65 MPa with – 30 % and + 30% of PAC hardener content, respectively. They also demonstrated that both curing and testing at increased temperatures enhances joint strength when having a reduced amount of hardener. Higher temperature increased mobility which allowed for all the epoxy molecules to diffuse and bond with the hardener. M. A. Andres et al. demonstrated how amine-rich mixtures experienced increased flexural strength and ductility, while the epoxy-rich counterpart showed a more brittle behavior with a decreased strength [31]. This is corroborated by S. Pandini et al. and J. R. M. D'Almeida et al., who obtained a brittle to ductile transition with increasing hardener amount and observed plastic deformation in hardener-rich formulations [66], [67].

The glass transition temperature (Tg) of a bisphenol A epoxy resin with a diamine curing agent was observed to vary significantly based on the epoxy/amine stoichiometry. H. Wang et al. demonstrated a decrease in Tg from 87.2 to 73.7 °C when the epoxy was reduced by 20%, due to a reduced cross-linking density [68]. Similarly, F. Bignotti et al. observed a decrease in Tg when excess amounts of both epoxy and hardener were used, and the highest Tg was achieved when using the recommended epoxy/hardener ratio specified by the manufacturer [19]. These findings indicate that Tg can be used to determine the optimum stoichiometry of a system, in order to gain improved thermal properties.

1.3 Evaluating the properties of polymers

Evaluating the properties of materials and structures is essential to properly understand their capabilities. Characterizing the mechanical properties of a polymer aids in determining the load and strain that it can undergo before reaching a critical point, while

thermally analyzing this material can give information about its glass transition temperature and its thermal decomposition. Performing fatigue and environmental testing allows to evaluate the longevity of the polymer, which is key for its durability in long-term applications.

Before implementing an epoxy adhesive to bond carbon fiber-reinforced composites for aerospace applications, it is essential to analyze how the adhesive will perform under working conditions. Aircraft are designed to operate in a wide range of temperatures, such as -55 to 50 ºC (-65 to 122 ºF) at ground level, and temperatures as low as -80 ºC (-112 ºF) can be reached during flight at an altitude of 12,200 meters (39,400 feet) [69]. Therefore, testing that the properties of the adhesive will be maintained under these temperatures is crucial for the integrity of the structure. Additionally, verifying that the adhesive joint can withstand all types of loads, including tensile, shear, bending, or torsional, that it will undergo during service is also essential to prevent catastrophic failure. Every polymeric material used in the aircraft, such as the resin utilized to manufacture carbon fiber composites, must be designed and tested to withstand the loads it will undergo during its lifetime. Both destructive and non-destructive methods can be used to evaluate the properties of materials, however, non-destructive testing can provide a more cost-effective way to perform intensive quality control during manufacturing.

1.3.1 Destructive Testing

Destructive testing, which involves the utilization of laboratory-type instrumentation that necessitates specific sample preparation and geometry, is primarily employed to characterize the mechanical properties of materials [70]–[76]. This approach involves subjecting samples to extreme loading conditions until they are either fully or

partially destroyed. This type of testing has additionally been used to ascertain the curing kinetics of polymeric materials. Examples of tests include dynamic mechanical analysis (DMA), differential scanning calorimetry (DSC), thermogravimetric analysis (TGA), tensile testing, lap-shear testing, and end-notched flexure. In the manufacturing process, this type of destructive testing is implemented for quality control. However, such equipment cannot be taken to the field for in-situ testing. As a result, developing a non-destructive in-situ method to evaluate the degree of reaction and the viscoelastic properties of polymers during cure and after they have been manufactured has become essential [77].

1.3.2 Non-destructive testing

Non-destructive evaluation (NDE) involves characterizing materials without damaging them, allowing for the inspection of surface and subsurface features and flaws. Common NDE techniques such as ultrasonics, infrared, electromagnetic, acoustic emission, and radiographic testing can be used to evaluate the properties of materials, identify internal damage, and investigate flaws [79] [78]. To ensure an accurate evaluation of a material, a combination of different NDE techniques is often utilized [78].

NDE offers numerous advantages when compared to destructive testing, such as cost-effectiveness, since the evaluated structure or part can be reused [80]. NDE is not as expensive as destructive testing and does not require large laboratory equipment [79], [80]. Moreover, some of the NDE techniques, like ultrasonics, allow for in-field testing to be performed, thereby eliminating the need to disassemble and transport the specific part requiring inspection to a different location, which can be time-consuming, and some structures, like adhesive joints, cannot be disassembled [81], [82]. Additionally, NDE can be used for quality control of a product and in-situ monitoring during its manufacturing

process without damaging it. This offers more reliability than destructively testing a small percentage of the manufactured products in each batch and assuming that these properties will be maintained along the rest of the batch. The advantages of NDE have led researchers and industries to adopt these techniques for the evaluation of materials and structures in industries such as the military and defense, aerospace, automotive, and construction [69], [78], [83]. In many of those cases, more than one NDT method is required to increase the effectiveness of the evaluation. To ensure a successful evaluation, it is important to understand the capabilities and limitations of each NDE method [83].

NDT methods are primarily divided into two distinct categories: contact and non-contact. Contact methods, such as traditional ultrasonic testing, eddy current testing, and penetrant testing, typically require good contact with the sample in order to obtain reliable evaluations [79]. In contrast, non-contact methods offer a more expedited testing process since physical contact with the sample is not required. Examples of non-contact methods include transmission ultrasonics, radiography testing, thermography, and electromagnetic testing [79]. This research focuses on the utilization of electromagnetic testing as a non-contact method and ultrasonics as a contact method.

1.3.2.1 Magneto-electric nanoparticles

Magneto-electric nanoparticles (MENs) are a special type of nanoparticles that exhibit the magneto-electric (ME) effect since they are composed of a piezoelectric and piezomagnetic phase [84], [85]. The coupling between these two phases allows for the magnetization to change when an electric field is applied, while the electric polarization can be modified by inducing a magnetic field [86], [87]. MENs are synthesized with a core-shell structure, where the shell constitutes the magnetostrictive phase and the core is the

piezoelectric phase [88]. Figure 1.6a shows how the flux density is proportional to the surface charge of the nanoparticles, which can be altered using a magnetic field. Figure 1.6b displays an example of a hysteresis loop where it is shown how the application of a magnetic force causes an increase in the flux density and part of which is retained after the magnetic force is brought back to zero (point b).

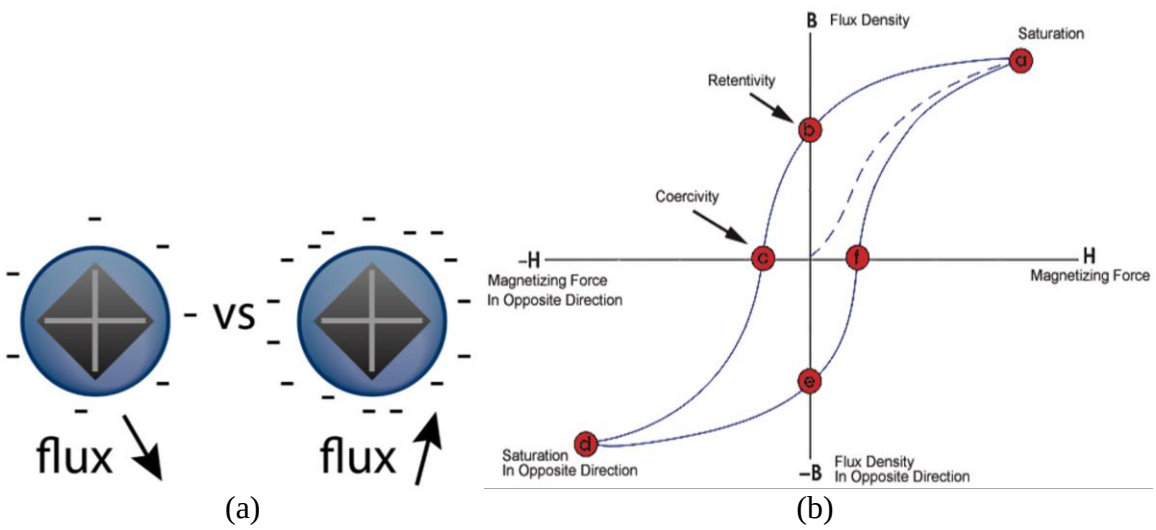

Figure 1.6. (a) Negative surface charge density with change in flux; (b) Schematic of a hysteresis loop caused by the application of a magnetic force.

MENs have also attracted the attention of the biomedical field due to their adaptable particle size, which can go from just a few nanometers to tens of nanometers [89]. This has opened new treatment possibilities since MENs are similar in size to a cell or a virus. Magnetic fields have been used to manipulate MENs to transport drugs, like anticancer drugs, to a desired body, like cancer or tumor [89]. When MENs are attached to a biological entity and then inserted into a human body, an external magnetic field can be utilized to transport the nanoparticles into a region of interest [90]. For example, R. Guduru et al. used MENs for drug delivery to eradicate ovarian cancer cells by controlling the nanoparticle's

intrinsic electric field [91]. K. Yue et al. modeled a non-invasive stimulation of the brain of a patient that suffered from Parkinson's disease by inducing an electric field with a level comparable to that of a healthy patient. This simulation was performed by coupling electric signals in the neural network of the brain to the magnetic field of the MENs [92]. The ME effect has also been capitalized by K. Petcharoen et al. to manufacture nanocomposites with shape memory capabilities [93]. They used MENs to deflect the material in the direction of an induced electric field, and the material was able to recover its original shape when the field was not applied.

Dispersing MENs in epoxy adhesives can be used to non-destructively monitor the effects of mechanical loading and environmental exposure due to changes in the intrinsic properties of the matrix. Figure 1.7a shows how the magnetic signal of plain MENs decreases when dispersed into a polymer. Figure 1.7b depicts a schematic of how this reduction is due to the surface charge neutralization caused by the positive ends of the polymer chains.

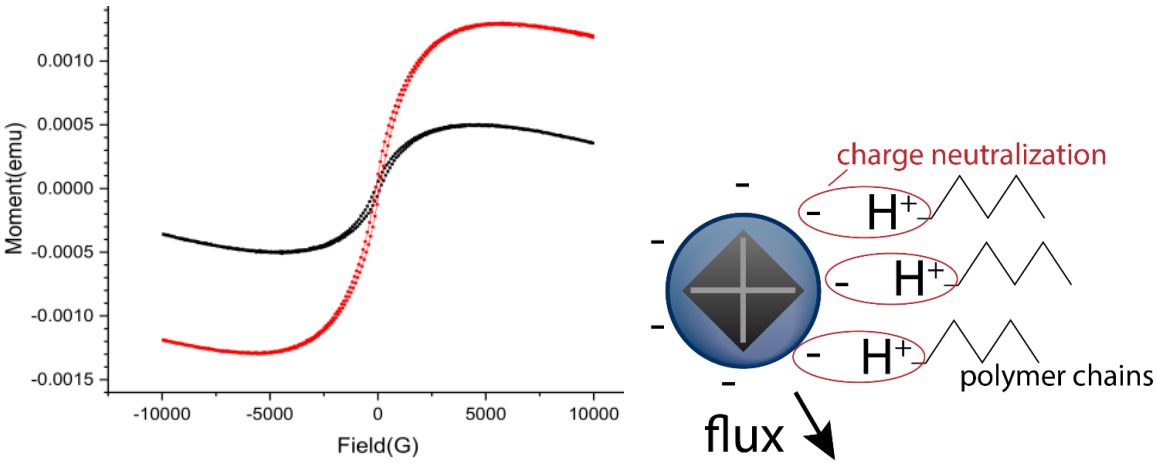

(a) (b)

Figure 1.7. (a) Magnetic response of free MENs vs. polymer coated MENs; (b) Charge neutralization of individual MENs as a function of the polymer coating.

In addition, this method can be used to evaluate the curing process of the adhesive. Changes in the magnetic signatures of the nanoparticles are caused by variations in the inter-particle spacing due to an applied strain or damage on the matrix. Furthermore, MENs not only can be used for non-invasive quality evaluation but also the mechanical strengthening of the adhesive. M. F. Uddin et al. enhanced the ballistic performance of polyurethane by using titanium dioxide nanoparticles [94]. They demonstrated how adding 3 wt% of nanoparticles to the polymer increased the absorbed kinetic energy of the structure by 20 % compared to the plain samples. P. Rosso et al. dispersed a 5 vol% of silica (SiO_2) nanoparticles into an epoxy adhesive (DGEBA), which caused a 20% improvement in the elastic modulus and a 70 % increase in the fracture toughness K_c [95]. However, having an excessive number of nanoparticles can have a detrimental effect on the mechanical properties of the polymer. S. Fu et al. demonstrated how the tensile strength of nylon 6 reached a maximum when containing 5 wt% of silica nanoparticles, but its strength started to decrease when adding higher silica percentages [96]. One of the objectives of this research has been to add MENs into an epoxy adhesive for its non-destructive evaluation while having no adverse effects on the mechanical properties of the polymer.

1.3.2.2 Ultrasonics

Ultrasonics is a popular non-destructive evaluation technique used for examining a variety of materials, such as metals [97], [98], ceramics [99], [100], and polymers [77], [101]. This method is based on the propagation of sound waves and provides high accuracy and sensitivity. As illustrated in Figure 1.8, ultrasonic testing utilizes acoustic waves at frequencies ranging from 20 kHz to 100 MHz. Some of the main advantages of this

technique include its high resolution, ability to detect flaws, and the possibility of in-field testing [79].

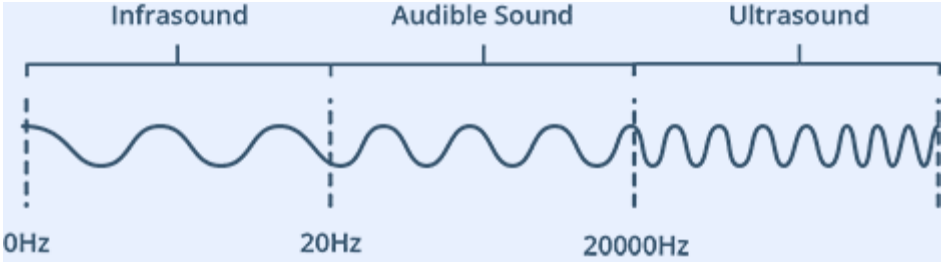

Figure 1.8. Frequency ranges of sound [102].

The velocity and attenuation of ultrasonic waves are highly sensitive to variations in the viscoelastic characteristics of forming macromolecular networks [26]. This sensitivity can be exploited to detect small changes in the adiabatic moduli with high precision. In a material of known density, the longitudinal and shear sound speeds can be utilized to calculate Young's, bulk, and shear moduli [103]. Furthermore, ultrasonics can be utilized to evaluate phase transitions during cure and the physical properties of materials [77], [104].

The ultrasonic pulse-echo method can be used to measure the sound speed of a material and determine its elastic constants, making it suitable for detecting inconsistencies in homogeneous and heterogeneous materials [104] [105]. F. Lionetto et al. demonstrated the effectiveness of this method in monitoring the cure state of thermosetting resins, as well as its superior sensitivity to modulus variations during vitrification compared to differential scanning calorimetry (DSC) [26]. Additionally, ultrasound has been used to non-destructively evaluate the curing mechanics of epoxy resins at different temperatures [26], [77], [106]. Further research into the use of ultrasonics as a non-destructive method is necessary in order to effectively understand how manufacturing variations can affect the

quality of the final product. If successful, this method could be used to tailor the properties of a polymeric material non-destructively for specific applications, while being a cost-effective way to characterize materials and structures. A detailed description of the process of using ultrasonics to analyze the degree of cure and mechanical properties of epoxies is presented in chapter 2.2.4.

1.3.2.3 Fourier transform infrared (FTIR) spectroscopy.

Fourier Transform Infrared (FTIR) spectroscopy is an analytical technique used to identify chemical compounds in materials by measuring the absorption of infrared radiation. This technique has been widely employed in the characterization of organic compounds, as the spectrum of the sample can be compared to the spectra of known materials in online libraries to identify the components of the sample [23]. As FTIR can provide information on the composition, structure, and properties of polymers, it has become an invaluable tool in the polymer industry.

FTIR can be utilized to detect and monitor changes in the structure and properties of polymers and quantify the presence of additives or impurities therein. The technique is also capable of identifying the occurrence of degradation in the polymer [107], [108]. For example, G. V. Salmoira et al. applied FTIR to identify the components of the thermal degradation of liquid and cured photosensitive resin (stereolithography resin Renshape^{TM} 5260) [109]. They increased the temperature of the resin up to 550 ºC and observed the formation of CO_2 and CO related to the absorption bands at 2358 and 2170 cm^{-1} due to the scission of links in the polymer's backbone. They also observed an increased absorption of the 1459 cm^{-1} band, which corresponds to the formation of CH_2 group of the aliphatic products due to the scission of the polymer's main chain.

FTIR is a commonly used technique to quantify the progress of the curing process of epoxies [25], [55]. By taking into account the chemical reactions happening during the curing of an epoxy/amine system (as described in chapter 1.2.1), the development of epoxy group concentrations can be tracked to monitor the process [24], [25] As the epoxy resin is consumed, its spectra intensity is inversely proportional to the degree of cure; meanwhile, the spectra intensity of the hydroxyl groups increases as they are formed during the cure. The procedure for using FTIR to measure the degree of cure is outlined in chapter 2.2.6.

1.3.2.4 Combination of ultrasonics and FTIR

Ultrasonics and FTIR have been independently used to characterize the elastic properties and chemical structure of curing and fully cured polymers. By using these two techniques together, a unique combination of non-destructive evaluation of polymer curing kinetics is obtained. This provides an opportunity to design and customize novel polymeric materials, as well as to establish a correlation between the elastic properties and chemical structure of a material during the curing process and its fully cured mechanical properties. Thus, this novel methodology of combining ultrasonics and FTIR enables researchers and chemists to quickly and cost-effectively develop new materials, while accurately predicting their final properties by monitoring their cure.

Chapter 2 Materials and Methods

2.1 Materials

Magneto-electric nanoparticles (MENs) composed of a piezoelectric and piezomagnetic phase were utilized for the strengthening and non-destructive evaluation of an epoxy adhesive. MENs are synthesized with a core-shell structure, where the shell

constitutes the piezomagnetic phase and the core is the piezoelectric phase. The core was composed of cobalt ferrite ($CoFe_2O_4$) while the shell was made out of barium titanate ($BaTiO_3$).

As a representative two- part epoxy adhesive material, 3M EC-2615 was selected and used. This adhesive is a two-part DEGBA-based resin with an amine hardener. A 2:1 resin (part B) to hardener (part A) ratio by weight was used to manufacture baseline samples following the manufacturer's specifications. The resin and hardener were thoroughly mixed for five minutes. Isopropyl alcohol (IPA) was added to the epoxy adhesive to simulate trapped solvent. The volume percentage of IPA added is described in detail in chapter 3.3. The curing process took place in a laboratory setting that was regulated to a temperature of approximately 21 ± 2 °C and relative humidity of ~44 ± 2.5 %.

A liquid epoxy resin (EPON 828, Hexion) was used for this study. EPON 828 is derived from difunctional bisphenol A/epichlorohydrin and it is known for its versatility due to its good mechanical, adhesive, dielectric, and chemical resistance properties [110], [111]. A liquid curing agent (EPIKURE 3234, Hexion) from the family of unmodified aliphatic amines was used for room-temperature curing. The manufacturer's recommended concentration of the curing agent is 13 phr (parts per 100 resin by weight), which corresponds to a 6.5 to 1 resin-to-curing agent ratio by volume. The resin and hardener were thoroughly mixed for five minutes before being poured into a 3D-printed mold. The curing process took place in a laboratory setting that was regulated to a temperature of approximately 21 ± 2 °C and relative humidity of ~44 ± 2.5 %.

2.2 Methodology

2.2.1 Synthesis of magneto-electric nanoparticles (MENs)

The manufacturing of MENs is divided into two chemical processes: the first one is to synthesize the cobalt ferrite (CoFe2O4) core material and the second one is to synthesize the barium titanate (BaTiO3) shell. Figure 2.1 shows the schematic of the core-shell structured nanoparticle.

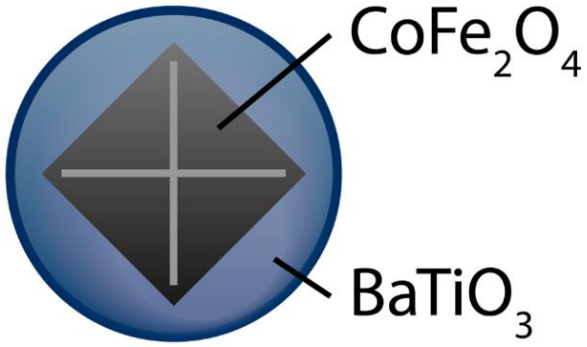

Figure 2.1. The core-shell structure of MENs composed of cobalt ferrite and barium titanate.

Table 2.1 describes in detail the septs on how to obtain cobalt ferrite core, while Table 2.2 contains the procedure to manufacture the barium titanate shell. These steps have to be followed in sequential order and performed in the fume hood to prevent inhalation of any biproducts. Wearing appropriate PPE like gloves, lab coat, and goggles is also necessary.

Table 2.1. Procedure to synthesize the core phase of the MENs.

Step	Description
1	Measure 50 mL of ethanol using a graduated cylinder and pour it into a flask
2	Measure 1.46 g of cobalt (II) nitrate hexahydrate ($Co(NO_3)_3 \cdot 6H_2O$) and pour it into the flask
3	Measure 4.04 g of iron (III) nitrate nonahydrate ($Fe(NO_3)_3 \cdot 9H_2O$) and pour it into the flask
4	Use a magnetic stirrer to mix the solution until the dissolution of the particles
5	Heat the solution in flask #1 to 70°C while magnetically stirring at 500 RPM
6	While the solution in step 5 is being heated up, measure 20 mL of DI water and pour it into a beaker (beaker #1)
7	Measure 2.8 g of sodium hydroxide (NaOH), pour it into beaker #1, and use a sonicator until the particles are dissolved
8	Measure 20 mL of DI water and pour it into another beaker (beaker #2).
9	Measure 4.0 g of polyvinylpyrrolidone (PVP), pour it into beaker #2, and use a sonicator until the particles are dissolved
10	Pour the solution in beaker #1 drop by drop using a pipette into the flask and leave it on the hot plate for 30 minutes at 70°C and 500 RPM
11	After 30 minutes, drop the solution in beaker #2 into the flask using a plastic pipette while stirring. Pour only one or two drops at a time, since doing it faster will cause the solution to boil
12	Once step 11 is complete, leave the solution on the hot plate for 30 minutes at 70°C and stir at 750 RPM.
13	After 30 minutes, increase the temperature to 100°C and the stirring speed to 300 RPM for 12 hours
14	After 12 hours, add 100 mL DI water into the flask and sonicate for ~30 minutes until all the solid is dissolved
15	Then, equally separate the solution into three large beakers and add 200 mL of DI water to each of the beakers
16	Place one of the large beakers on top of a big magnet for ~3 minutes, which will attract the core material to the bottom of the beaker
17	While maintaining the magnet in contact with the bottom of the beaker, pour the remaining DI water into another beaker for disposal
18	Add once again 200 mL to that same beaker and repeat steps 16-18 three times. Perform these steps for each of the three large beakers, which will leave the core material at their bottom.
19	After performing the previous steps three times for each beaker, add 25 mL of ethanol into the beakers
20	Pour the contents of each large beaker (ethanol + core material) into a clean flask and place it on a hot plate at 100°C until the ethanol evaporates
21	Finally, scrape the remaining core material at the bottom of the flask and place it into an enclosed container for storage

Table 2.2. Procedure to synthesize the shell phase of the MENs.

Step	Description
1	Measure 150 mL of ethanol and pour it into a beaker (beaker #1)
2	Measure 5 g of citric acid and put it into beaker #1
3	Using a magnetic stirrer, stir at ~500 RPM until the particles in beaker #1 are dissolved
4	Measure 150 mL of DI water and pour it into a beaker (beaker #2)
5	Measure 1 g of citric acid and put it into beaker #2
6	Place beaker #2 in an ultrasonic sonicator for ~5 minutes until particles dissolve
7	Measure 0.158g of barium carbonate and put it in beaker #2
8	Place beaker #2 once again in a sonicator for ~5 minutes until particles dissolve
9	While magnetically stirring, use a pipette to pour 240 μL of titanium isopropoxide into beaker #1
10	Pour the solution in beaker 2 into beaker 1 and magnetically stir for ~5 minutes
11	Measure 1 g of polyvinylpyrrolidone (PVP) and place into beaker #1 while stirring
12	After the PVP is completely dissolved, place beaker #1 in a table and remove the magnetic stirrer bar
13	Measure 0.097g of core and pour it into beaker #1
14	Place a parafilm on top of beaker #1 and sonicate for 3 hours
15	After sonicating, place beaker #1 in the hot plate at 125 °C and insert a stirring machine for ~8 hours.
16	Scrape out the gel in beaker #1 and place it in a ceramic crucible
17	Place the crucible in a furnace and heat it from 25 °C to 600°C in a period of 2 hours. Then, maintain at 600°C for 5 hours and finally decrease from 600 °C to 25 °C in a period of 10 hours.
18	After the furnace cycle is complete, place the MENs from the crucible into a container for storage

Figure 2.2 contains an image of MENs taken with a transmission electron microscope (TEM). The average size of the nanoparticles was ~30 nm. The cobalt ferrite core can be identified at the center of the nanoparticles, while the barium titanate shell has a lighter tone on the surroundings.

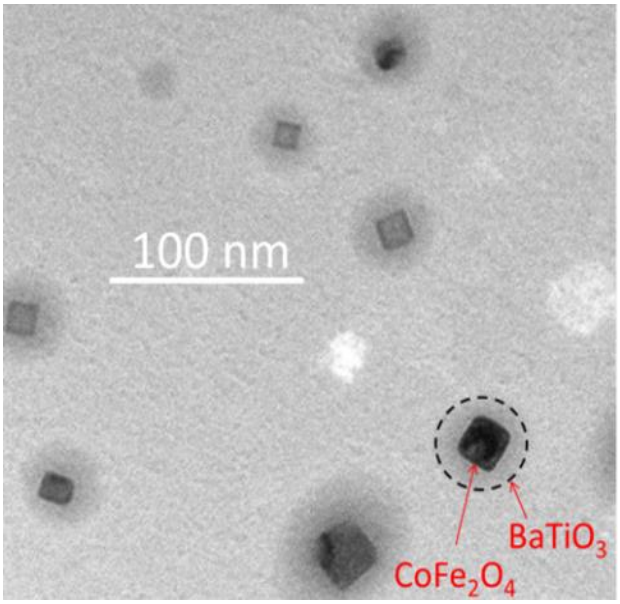

Figure 2.2. TEM image of MENs showing the core-shell structure.

2.2.2 Vibrating sample magnetometry (VSM)

The magnetic properties of the samples were first measured using vibrating sample magnetometry (VSM), which consists of the vibration of a magnetic sample in a uniform magnetic field [112]. This instrument had a sensitivity of 0.01μemu. The difference in magnetic response of plain adhesive samples with respect to samples containing MENs was evaluated. To achieve this, 3M EC-2615 epoxy adhesive samples containing 0 vol% and 1 vol% MENs were manufactured. Samples were cured at room temperature (~22 °C) for 7 days prior to testing. The samples had dimensions of 5 x 5 x 1 in length, width, and thickness, respectively.

To evaluate the effects of environmental exposure on samples containing MENs, samples with the same epoxy adhesive and dimensions were manufactured containing 0, 5, 10, and 15 vol% of MENs. These samples, after being fully cured, were placed in an environmental chamber (Figure 2.3) at 95 % relative humidity and 70 °C for 4 weeks.

Magnetic signatures were measured using VSM prior to and after being exposed environmentally.

Figure 2.3. Environmental chamber located at FIU.

2.2.3 B-H looper testing

A B-H looper setup was used to non-destructively characterize the local properties of adhesive samples. This setup can evaluate the magnetic properties of a sample containing MENs based on the principle of reciprocity, which states that the magnetic flux density B and the applied magnetic field H are influenced by the system's induced and applied voltages, respectively.

From the reciprocity principle, the electromotive force (EMF) or measured signal, ε, in volts is obtained by using equation 2.1 as follows [113]:

$$\varepsilon = \frac{n\Delta\varphi}{\Delta t} = \mu_0 \frac{n\Delta \int H_{img} M(r) dv}{\Delta t} \tag{2.1}$$

Where $\Delta\varphi$ is the change in magnetic flux in volt-seconds, Δt is the change in time in seconds, n is the number of turns in a coil, M(r) represents how the magnetization is distributed throughout the sample, and H_{img} is the normalized reciprocal imaginary field representing the geometry of the B-H setup.

The schematic in Figure 2.4 shows how the B-H looper setup includes a function generator connected to a lock-in amplifier and three coils. The two detection coils (shown in blue) are positioned on either side, and they are connected in series to amplify the magnetic signal from the sample and cancel any background noise. The source coil located in the middle (shown in orange) is connected to the function generator to generate an AC magnetic field. The lock-in amplifier links the detection and source coils and amplifies only the signal at the detection frequency and phase while eliminating all other noise signals.

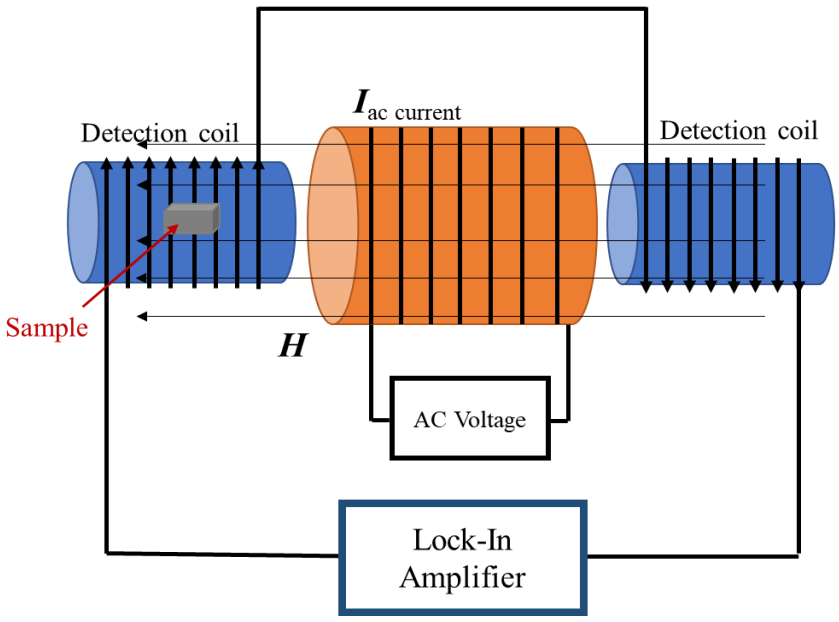

Figure 2.4. Schematic of the B-H looper.

The B-H looper setup was used to monitor the curing process of the 3M epoxy adhesive EC-2615. Figure 2.5a contains a picture of the B-H looper setup and Figure 2.5b depicts how the source coil and detection coils are located on top of the lock-in amplifier. Both coils were wired using a coil winding machine around a 3D-printed base made out of PLA filament. This task could be performed manually, although using the winding machine helped in improving the geometry of the coils. Then, electromagnetic interference (EMI) shielding tape was used to shield the wire against undesirable magnetic signals. Also, the implementation of BNC connectors to each end of the wire ensured an easier and proper connection. The background noise of this design was under 10 µV, which allowed to accurately measure the magnetic signal of adhesive samples containing MENs.

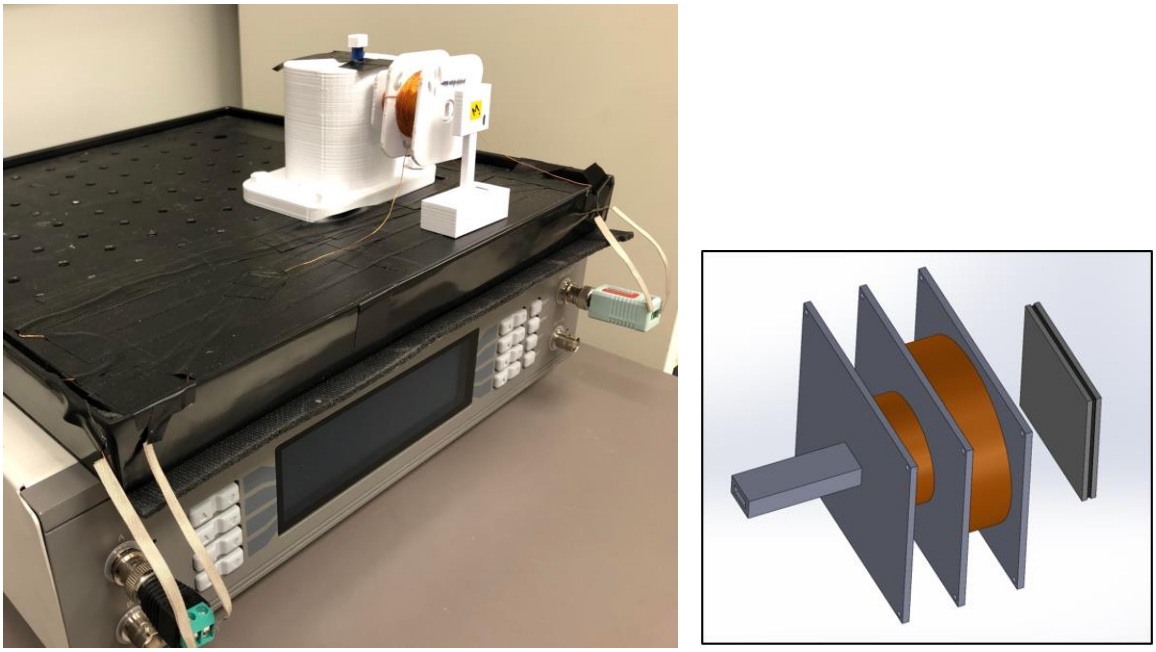

(a) (b)

Figure 2.5. (a) Picture of the B-H looper setup; (b) Schematic of the source and detection coils.

Six adhesive samples (2:1 resin to hardener ratio) containing 5 vol% of MENs were manufactured with dimensions of 8 x 8 x 4 mm in length, width, and thickness, respectively. This percentage was selected to measure a magnetic signal with the B-H looper that was significantly higher than its background noise. Figure 2.6 shows an adhesive sample containing MENs inside a PLA stand, which was used to place the sample next to the B-H looper during testing. Since most of the curing process of this polymer occurs during the initial curing hours, the magnetic signal of the samples was measured every hour during the first 24 hours.

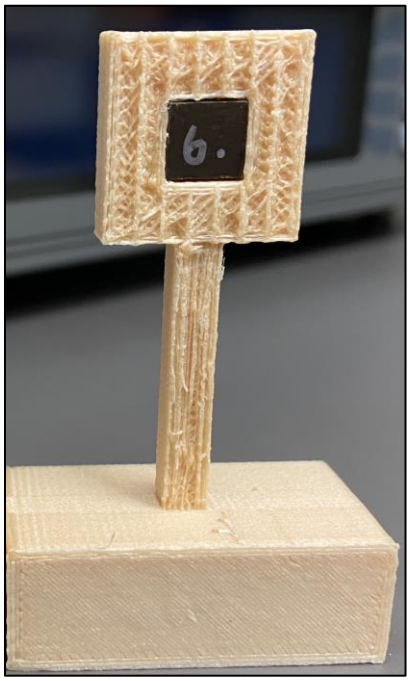

Figure 2.6. Sample stand containing an adhesive sample with 5 vol% MENs.

Tests were conducted by running the B-H looper at 4 V input voltage and 1.3 kHz frequency, which is the critical frequency. This frequency was identified by sweeping the frequency from 100 Hz to 10 kHz with 100 Hz intervals and noting when the signal due to the MENs reached its peak. The inductance of the system, which is affected by the

microenvironment of the sample, was the determining factor of the critical frequency [38]. When a voltage was applied to the B-H looper's source coil and the sample was situated close by, the resulting AC magnetic field generated a magnetic flux in the sample that contained MENs due to the nanoparticles' surface charge density. This magnetic flux was picked up by the detection coils, resulting in a change in signal. The background signal, which includes the noise factor, was recorded prior to placing the sample in the B-H looper and was subtracted from the signal for every measurement.

2.2.4 Ultrasonics

Ultrasonics were utilized to non-destructively measure the sound speed of the adhesive and resin samples during their curing process. This method was also used to obtain the elastic properties of fully cured samples. To achieve this, the resin and hardener components of the epoxies were first measured and thoroughly mixed for three minutes. A detailed description of the sample types manufactured and tested using acoustics is included in chapters 4.3.4 and 5.3.4. Once mixed, they were poured into a PLA 3D-printed mold with the dimensions specified in Figure 2.7. The indents located at each side of the mold were inserted for proper and easier transducer placement.

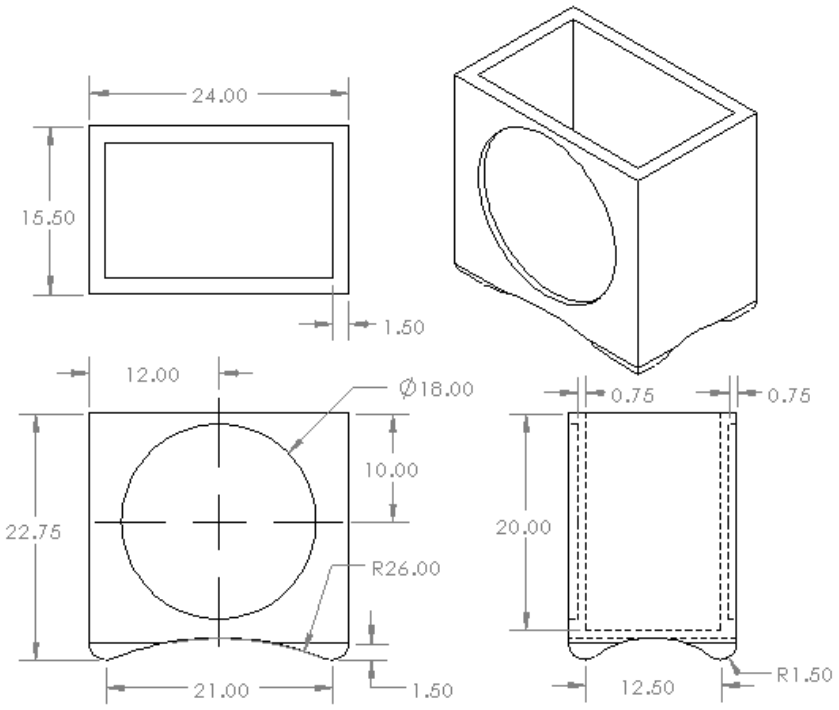

Figure 2.7. Technical drawing containing the dimensions of the PLA 3D printed mold used for ultrasonic testing.

A function generator (AFG31052, Tektronix) was utilized to generate a sine burst of 500 kHz at 10 volts peak-to-peak. This frequency was selected after observation over a range of frequencies as it produced the highest output signal for the polymeric materials evaluated. A Tukey window with a cosine fraction, r, of 0.4 was used to taper the input function consisting of five cycles [114]. This excitation wave is graphed in black in Figure 2.10. The burst was transmitted and detected by transducers placed on each side of the sample. 2.25 MHz transducers (V133-RM and V154-RM, Olympus) were used for evaluating the longitudinal and shear sound speeds, respectively. An ultrasound couplant (Echo Ultrasonics) was used to ensure proper contact between the sample and the transducers. The resulting waveforms were recorded using an oscilloscope (MDO32, Tektronix).

Figure 2.8 contains a schematic of the acoustic setup, which demonstrates how the emitter transducer is connected to the function generator while the receiver is connected to the oscilloscope. These transducers are then placed on the left- and right-hand sides of the sample. The purpose of having a trigger is to synchronize the time scale in both the function generator and the oscilloscope, which is necessary for the proper analysis of the output waveforms to obtain an accurate sound time travel speed in the sample.

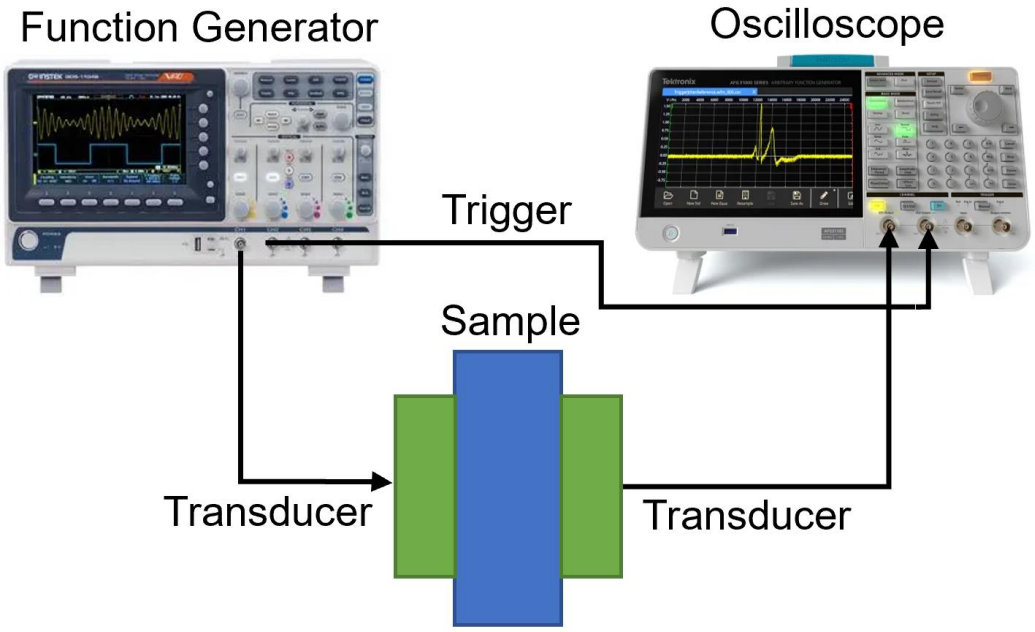

Figure 2.8. Schematic of the ultrasonics setup.

Figure 2.9a shows the acoustic setup mounted at the laboratory, where the function generator is located at the top left and the oscilloscope at the top right corner. A close-up view of how the transducers are placed on each side of the sample is shown. This setup allows to evaluate four samples at a time. This number is limited to the input channels in both the function generator and the oscilloscope.

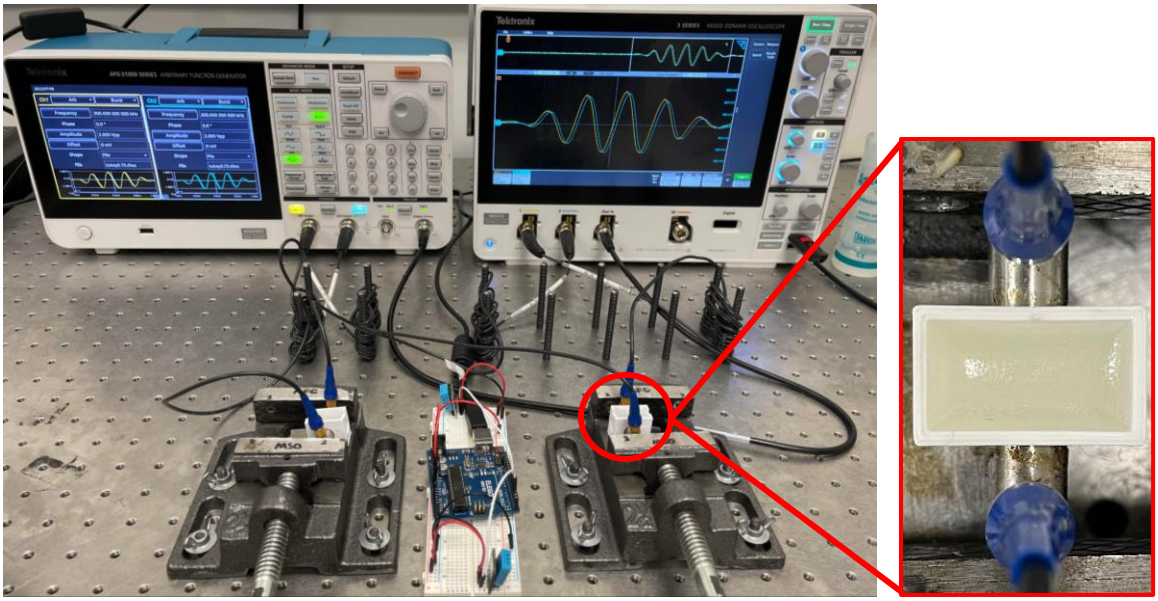

Figure 2.9. Picture of the ultrasonics setup while testing two epoxy resin samples.

For studying the curing processes, the waveforms were autonomously saved every two minutes using the LabVIEW software during the first 48 hours of cure. LabVIEW is a graphical programming software that allows scientists and engineers to combine graphical elements, such as blocks and diagrams, with text-based programming languages to create systems that are easy to understand and modify. They are particularly useful in the areas of data acquisition, data processing, and process control, as they allow users to perform these tasks autonomously and rapidly. LabVIEW has a variety of tools and libraries to easily connect and interact with laboratory instruments.

To accurately calculate the sound travel time in the sample at any point during the curing process, the cross-correlation function is used to measure the similarity of two signals as a function of the displacement relative to one another. The cross-correlation of two arbitrary functions, *g(t)* and *h(t)* is defined as follows [115]:

$$Corr(g,h) = \int_{-\infty}^{+\infty} g(\tau + t)h(\tau)d\tau \qquad (2.2)$$

Where *t* is the lag between the two functions. An example of the cross-correlation (blue) between the excitation waveform (black) and the output waveform (red) of a fully cured adhesive sample are graphed in Figure 2.10. The lag between the two functions, i.e., the sound time travel in the sample, is the x-coordinate of where the highest peak of the cross-correlation is located. It can be observed how the highest peak in the cross-correlation corresponds to the point in time where the beginning of the output waveform is located.

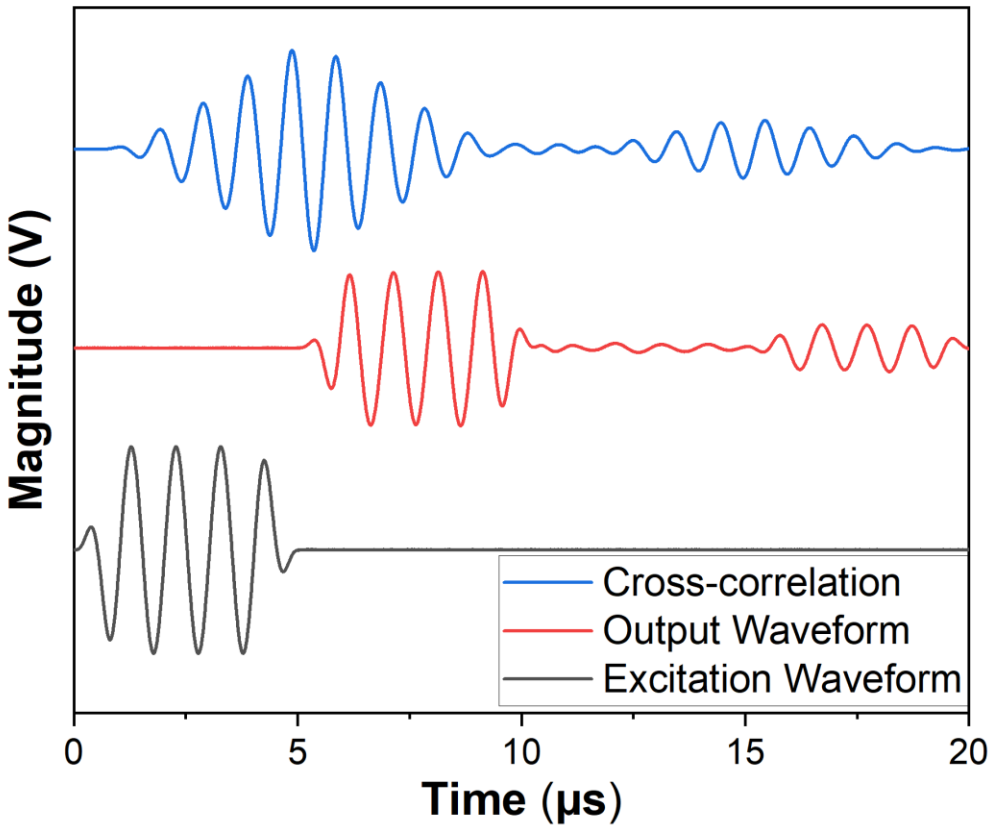

Figure 2.10. Graph of the excitation waveform, output waveform, and cross-correlation waveform.

The travel time obtained from the cross-correlation of the output waveform includes the delay produced by the transducers, the 3D-printed mold, and the polymeric material inside the mold. However, only the sound speed through the polymer is of interest. To

calculate the delay introduced by the other components of the system, the recently described testing procedure is performed for a system composed of just the transducers, and a system composed of the transducers and a 100% infill 3D printed cube. Equation 2.3 is implemented to calculate the delay produced by just the polymeric material in the system:

$$t_p = t_s - \frac{1}{\frac{d_m}{t_{m+t} - t_t}} - t_t \tag{2.3}$$

where t_p is the time delay from the polymeric material of interest, t_s is the time delay of the whole system, t_{m+t} is the time delay of the system composed of the transducer and the 100% infill 3D printed cube, d_m is the thickness of the 3D-printed cube, and t_t is the time delay of the system composed of just the transducers.

After the time of flight corresponding to the polymeric material is obtained, equation 2.4 is used to calculate the sound speed in the material:

$$c = \frac{d}{t_p} \tag{2.4}$$

where d is the thickness of just the polymer part of the whole system, and t_p is the sound travel time in the polymer obtained from equation 2.3. The law of propagation of uncertainty was used to obtain the error associated with the velocity calculations [116]. This method accounts for the uncertainty associated with the resolution of the oscilloscope to plot the output waveforms (9 ns), which were used to obtain the sound travel time, and the uncertainty associated with the digital micrometer that was used to evaluate the thickness of the sample (0.01 mm).

The elastic properties of an isotropic material can be obtained using ultrasonics if its density, longitudinal speed, and shear speed are known [77], [117]. The densities of the sample were obtained using a pycnometer (AccuPyc II 1340, Micromeritics). However, since the epoxies used are a dispersive medium, the sound travel speed is dependent on the frequency utilized. Thus, the cross-correlation method along with a frequency sweep method similar to the one performed by C. Pantea et al. [104] were used to accurately determine the longitudinal and shear sound travel times in the samples. For the longitudinal travel time, a frequency sweep from 0.9 to 2.3 MHz with a 0.1 MHz step was used, while for the shear travel time, a range from 0.5 to 1 MHz was used with the same step size. Different frequency ranges were implemented to obtain the longitudinal and shear travel times since a minimum amount of signal was required to perform a correct measurement, but the magnitude of the output signal varied for each frequency and wave type. Thus, the ranges of frequencies selected depended on having a minimum magnitude of the output signal to perform a proper cross-correlation.

In this method, a total of five peaks of the cross-correlation waveform were used: one corresponding to the overlap between the excitation, two to the left side of the overlap, and two to the right side of the overlap. The time travel times (time delays) for each of the frequencies and cycles were plotted versus the inverse of frequency. After plotting and extrapolating the linear fits to a frequency of infinity, the intercept of each of the cycles where the inverse of the frequency equals zero provides the sound travel time in the sample. The plots for the longitudinal and shear sound travel time vs. the inverse of the frequency of a fully cured baseline 3M EC-2615 epoxy adhesive are given in Figure 2.11a and Figure

2.11b, respectively. Then, equation 2.3 is used to calculate the longitudinal and shear sound speed using the sample's thickness.

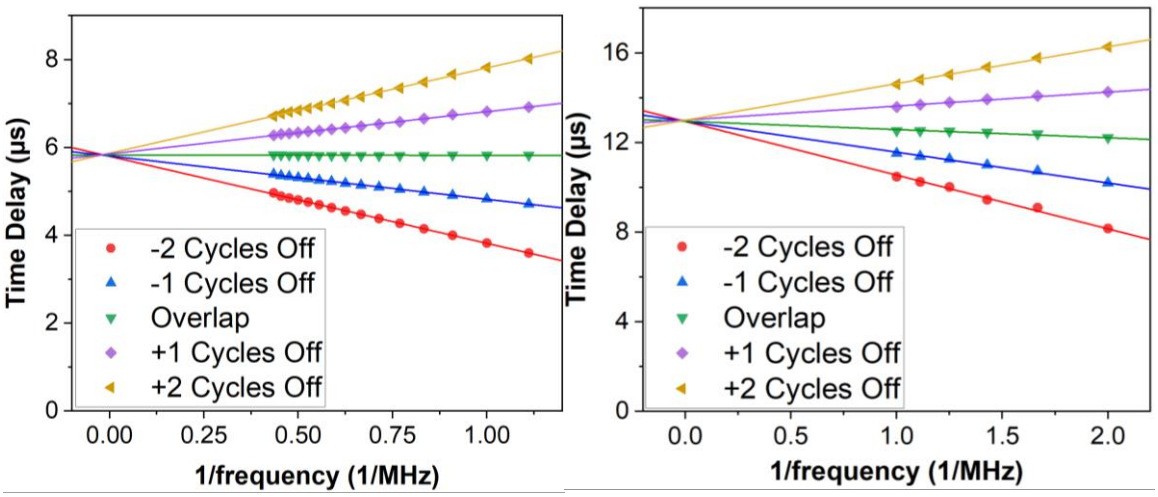

Figure 2.11. (a) Longitudinal and (b) shear sound travel time vs. the inverse of the frequency of a fully cured baseline 3M EC-2615 epoxy adhesive.

In the case of homogeneous isotropic materials, once the longitudinal and shear sound speeds have been calculated and the density of the material is obtained, equations 2.5 and 2.6 can be used to determine the Youngs modulus and Poisson's ratio, respectively [103]:

$$E = \rho c_s^2 \left(\frac{c_l^2 - 2c_s^2}{2c_l^2 - 2c_s^2}\right) \tag{2.5}$$

$$v = \frac{c_l^2 - 2c_s^2}{2c_l^2 - 2c_s^2} \tag{2.6}$$

where ρ is the density of the material, c_l is the longitudinal speed in, and c_s is the shear speed, E is Young's modulus, and v is Poisson's ratio. These formulas can also be applied to evaluate the elastic properties of polymeric materials during their curing process. 2.2.5 Modeling

As manufacturing processes and structural geometries become more and more complex, following the traditional way of iterating the design until a desired outcome is obtained becomes too expensive [118]. Thus, optimized models that predict processes with the aid of numerical simulation methods are essential to reduce manufacturing costs. In addition, polymers with anisotropic behavior and the determination of their material properties based on cross-linking make the prediction of the final product difficult if not impossible [118].

For this application, modeling helps to better understand numerically the curing processes of each sample type and how they differ from one another. When a great amount of data on a material is obtained, modeling allows for predicting if improper manufacturing was performed and how the process would influence the final properties of the structure. This can be very favorable during in-situ analysis since a part can be deemed safe or unsafe before waiting for the whole manufacturing process to be completed.

The degree of conversion, $\alpha(t)$, ranges from 0 to 1 and can be expressed using the Hill equation as shown in equation 2.7 [119]:

$$\alpha = 1 - \frac{1}{(\frac{t}{\tau})^{\theta}} \tag{2.7}$$

where t is cure time in seconds, θ is the shape parameter constant, and τ is the time constant defined as $\tau = \theta/k$, where k is the rate constant. The time constant τ is an important parameter of the distribution since it represents when the degree of conversion $\alpha = 0.5$. A generalize reduced gradient (GRG) algorithm was used to minimize the sum of the errors squared between the normalized experimental sound speed and modeled data by fitting different θ and k parameters.

2.2.6 Fourier transform infrared spectroscopy

FTIR was performed on a Nicolet iS50 (Thermo Scientific), which is displayed in Figure 2.12, using a DTGS KBr detector and OMNIC software. Scans were taken from 4000 to 400 cm^{-1} with a resolution of 0.482 cm^{-1}. Sixteen scans were used and the spectra were graphed in absorbance mode. The sample was placed on a golden gate diamond top plate (Specac) equipped with a KRS-5 lens. The lens was cleaned using ethanol followed by DI water before each sample. When analyzing fully cured adhesive samples, the specimen was made sure to have good contact with the detector's surface to obtain a proper amount of signal. To achieve this, a torque-limited knob was utilized to apply pressure on the samples during testing.

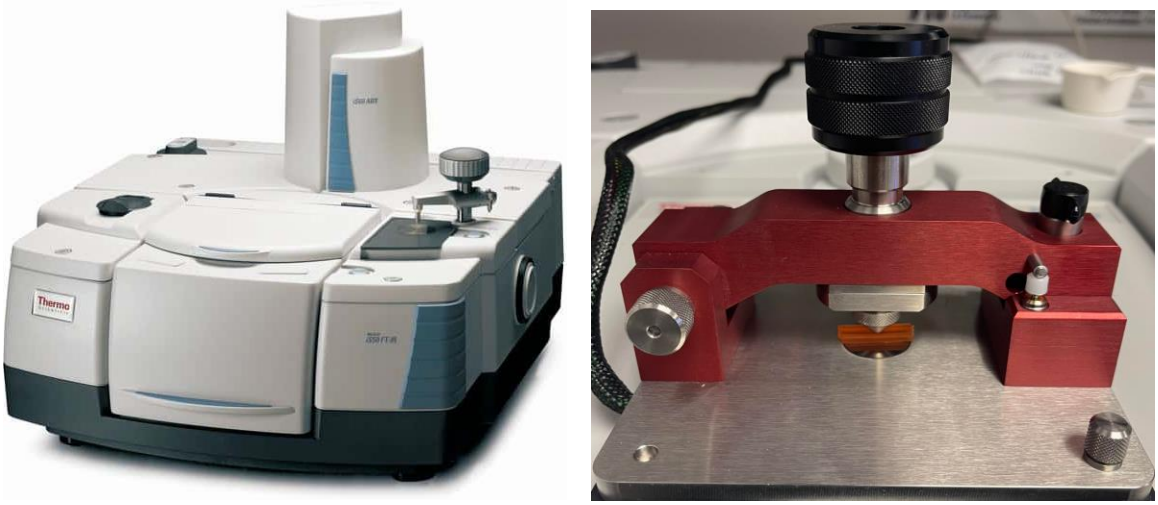

(a) (b)

Figure 2.12. (a) Nicolet iS50 FTIR from Thermo Scientific; (b) picture of an epoxy resin sample being tested on the FTIR.

When performing FTIR analysis during the cure of EPON 828 epoxy resin sample, 100 µL of material was poured on top of the crystal after the resin and hardener had been thoroughly mixed. The images in Figure 2.13 portray an EPON 828 sample being tested in the FTIR during cure. Testing was performed using the same parameters as described

above, although this time spectra were taken every two minutes during the first 24 hours of cure. A background scan was completed before testing each sample.

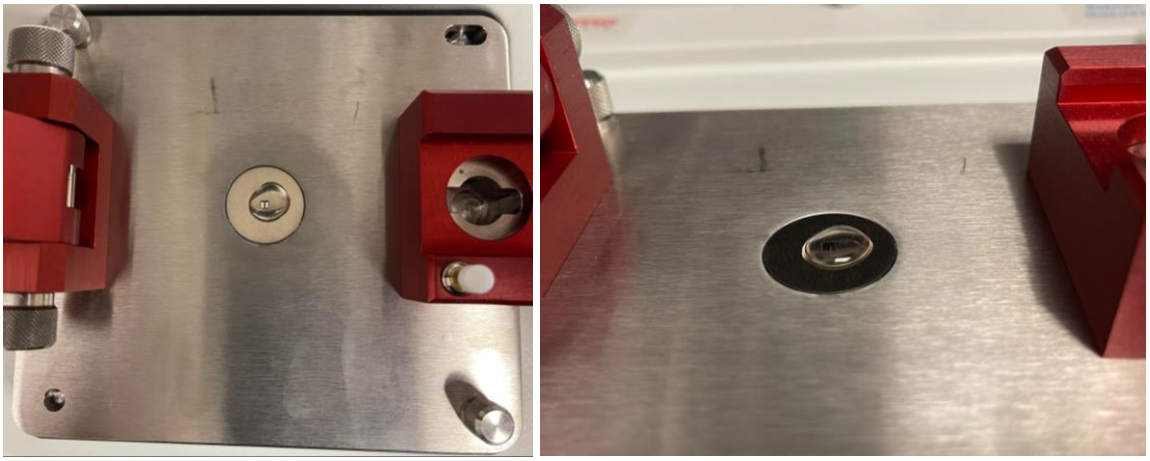

(a) (b)

Figure 2.13. (a) Top and (b) side view of an epoxy resin sample being tested on the FTIR during cure.

The intensity of an FTIR spectrum is higher in solid samples compared to liquid samples because vibrations in solids are typically more intense than those in liquids. This is due to the fact that the molecules in solids are closer together, allowing for stronger interactions and more efficient energy transfer. The molecules in liquids are less tightly packed, resulting in weaker interactions and less energy transfer. Thus, to take into account the change in intensity of the baseline FTIR spectra as the polymer cures, the intensities of the analyzed peaks were normalized with respect to the wavenumber 1034 cm^{-1} using equation 2.8. This peak corresponds to the phenyl group and it remains chemically unmodified during cure. The degree of conversion, α, of any given peak intensity can be calculated using equation 2.9, where α goes from 0 to 1 when the intensity of the peak increases during cure and from 1 to 0 where the intensity decreases during cure.

$$I_{peak\ norm}(t) = \frac{I_{peak}(t)}{I_{1034}(t)} \tag{2.8}$$

$$\alpha\,(t) = 1 - \frac{\frac{I_{peak}(t)}{I_{1034}(t)}}{\frac{I_{peak}(0)}{I_{1034}(0)}} \tag{2.9}$$

2.2.7 Thermal Analysis

Thermal analysis was performed using a Q600 SDT (TA Instruments), which is shown in Figure 2.14. 3M EC-2615 epoxy adhesive samples (2:1 resin to hardener ratio) containing 5 wt% MENs were tested during their initial 24 curing hours with one-hour intervals. These tests were used to evaluate how the glass transition temperature of the epoxy adhesive behaves during the curing process to corroborate the magnetic signatures obtained with the B-H looper. The tests were run from room temperature (~23 °C) to 500 °C at a heating rate of 5 °C/min. Argon gas was used as a purge gas. The weight of the samples ranged between 11 and 12 µg.

Figure 2.14. Q600 SDT from TA Instruments.

Thermal testing was also used to analyze how residual IPA affected the thermal stability of the 3M EC-2615 epoxy adhesive. Testing was performed on fully cured adhesive samples (2:1 resin to hardener ratio) containing 0, 2, 4, and 6 wt. % IPA. The tests

were run from room temperature (~23 °C) to 450 °C at a heating rate of 5 °C/min. Argon gas was used as a purge gas. The weight of the samples ranged between 9.0 and 9.5 µg.

The effect of varying EPON 828 resin to EPIKURE 3234 hardener ratio on thermal stability was also investigated. Testing was performed on fully cured epoxy resin samples containing 1:0.6, 1:1, and 1:1.4 resin-to-hardener ratios. The tests were run from room temperature (~23 °C) to 500 °C at a heating rate of 5 °C/min. Argon gas was used as a purge gas. The weight of the samples ranged between 8.5 and 9.0 µg.

2.2.8 Mechanical testing

2.2.8.1 Tensile testing

Standard ASTM D638-03 was followed to obtain the tensile strength of the dogbone adhesive and resin samples [120]. The size of sample type I in the standard was adapted to reduce the amount of material volume used per sample. The dimensions were reduced to have the final values shown in Figure 2.15. The total length of the sample was 165 mm while its thickness was 7 mm. The width at the center of the sample and the grips was 13 and 19 mm, respectively. The samples were manufactured by casting the adhesive and resin into PLA 3D-printed molds. The epoxy was thoroughly mixed for three minutes prior to casting. A mold release agent was added to the mold for easy removal of the cured polymers. A detailed description of the sample types manufactured and tested is included in Chapter 3.3.

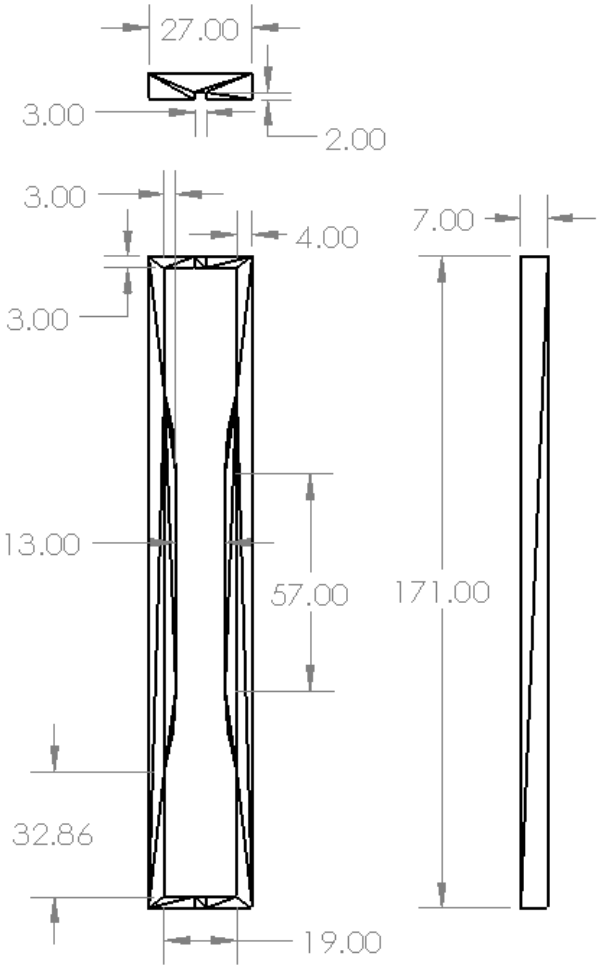

Figure 2.15. The mold used to manufacture dogbone tensile samples following standard ASTM D638-03.

A tensile tester from MTS (Criterion Model 43), shown in Figure 2.16a, was used to test the samples at a displacement rate of 5 mm/min. Testing was run until complete failure of the samples occurred. Figure 2.16b displays how the dogbone samples were placed in the MTS prior to testing. It was made sure that the samples had the same amount of gripped area at each side and that they were at a vertical position to apply the load perpendicular to the cross-sectional area. Load-displacement curves were recorded for each test. The maximum load was used to calculate the peak tensile stress, in MPa, of the material using equation 2.10 as follows [121]:

$$\sigma = \frac{F}{A} \tag{2.10}$$

where F is the maximum load in Newtons and A is the cross-sectional area in mm^2. The width and thickness of the samples used to calculate the cross-sectional area were measured using a caliper prior to performing the tests.

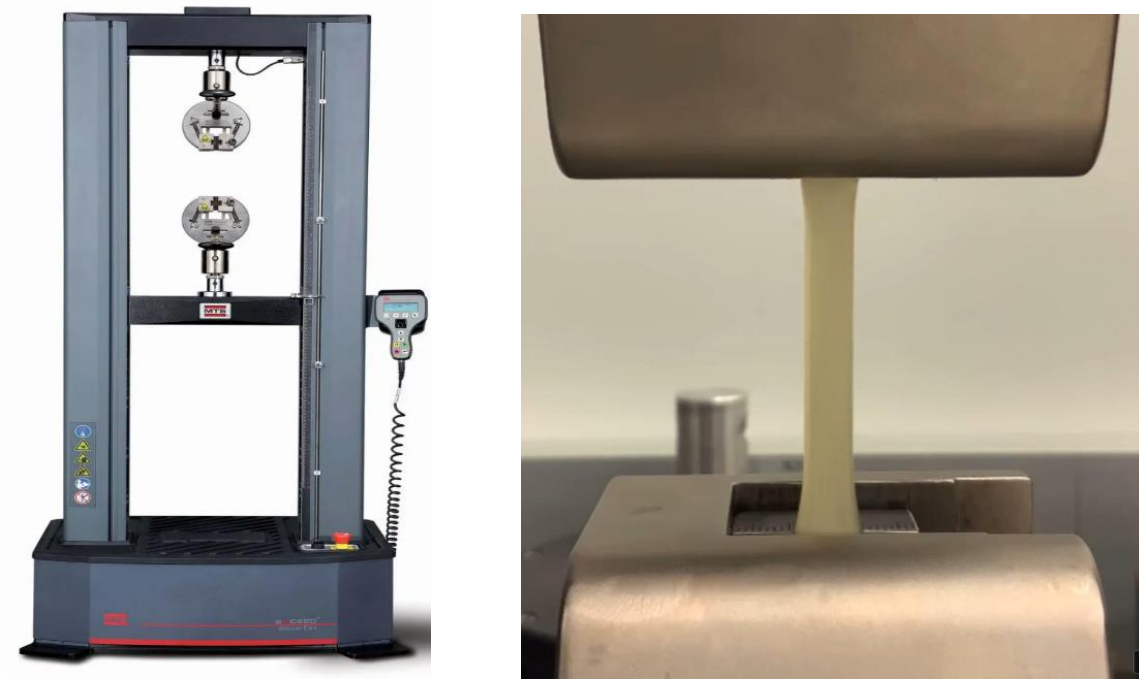

(a) (b)

Figure 2.16. (a) Picture of the MTS Criterion Model 43 used for tensile and lap-shear testing; (b) Picture of an epoxy adhesive sample placed in the MTS grippers prior to testing.

2.2.8.2 Single lap-shear

Lap shear testing was performed to characterize the bonding properties under a shear load of the 3M EC-2615 epoxy adhesive when joining carbon fiber-reinforced plastics (CFRP). Samples were manufactured and tested following standard ASTM D5868-01 [122]. First, a hand layup process was performed to manufacture carbon fiber panels. A

unidirectional carbon fiber prepreg material (T800H, Toray) was cut to prepare a 12-layer square panel with a side of 12 inches. The 12 layers that formed the panel were oriented in the same direction, and special care was taken to prevent misalignment. Figure 2.17a contains a picture of how the prepreg was cut, while Figure 2.17b shows how a peel ply was put on both sides of the panel before curing it in the autoclave (American Autoclave Co.). The peel ply protects the panels from contamination and allows them to have a surface texture that enhances mechanical interlocking during bonding. Due to the size of the autoclave, shown in Figure 2.19b, only two panels were manufactured per curing cycle.

(a) (b)

Figure 2.17. (a) Picture of prepreg laminates being cut to the desired dimensions; (b) Carbon fiber panel containing 10 layers and covered by a peel ply.

Both panels were placed on an aluminum plate that was covered by a release film, which prevents any excess resin to bond to the plate. Then, a breather ply was added on top of the plates to absorb any excess resin from the laminate and allows for air and volatiles to escape during the curing process in the autoclave. Vacuum ports were placed at each side of the aluminum plate; two were used to pull a vacuum while the other two were used to monitor the vacuum levels during cure. Finally, a vacuum bag covered the

whole aluminum plate, which was pasted to it using vacuum tape. Figure 2.18 contains a schematic of the described setup, while Figure 2.19a shows a picture of the final setup before being inserted into the autoclave for curing. The laminates were cured at a temperature of 350 ºF and a pressure of 30 psi in accordance with the manufacturer's specifications.

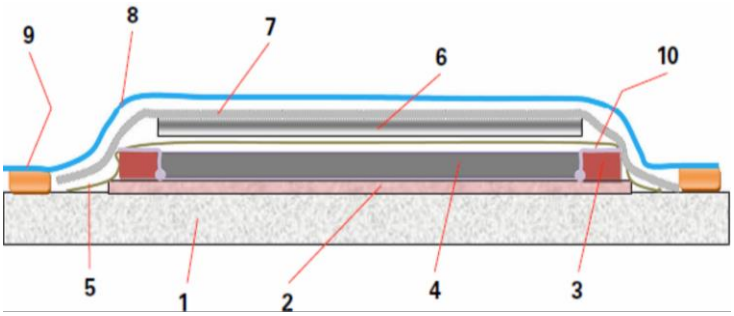

Number	Description
1	Aluminum plate
2	Release film
3	Silicon edge dams
4	Laminate
5	Release film
6	Caul plate
7	Breather ply
8	Vacuum bag
9	Vacuum tape
10	Glass yarn string

Figure 2.18. Schematic of the setup materials used to cure carbon fiber panels in the autoclave.

(a) (b)

Figure 2.19. (a) Picture of the final setup containing two panels before being inserted into the autoclave for curing; (b) picture of the autoclave from American Autoclave Co. used.

After curing, the panels were cut using a table saw prior to being bonded with the epoxy adhesive. Standard ASTM D5868-01 recommends the samples to be 7 inches in length by 1 inch in width and a total bonded area of 1”x1”. Figure 2.20a contains a schematic of the sample dimensions while Figure 2.20b shows how the sample was placed on the MTS machine, in which the samples were tested with a loading rate of 13mm/min. The specimens were left curing for seven days prior to testing. Load-displacement curves were recorded for each tested specimen. A detailed description of the sample types manufactured and tested is included in Chapter 3.3.

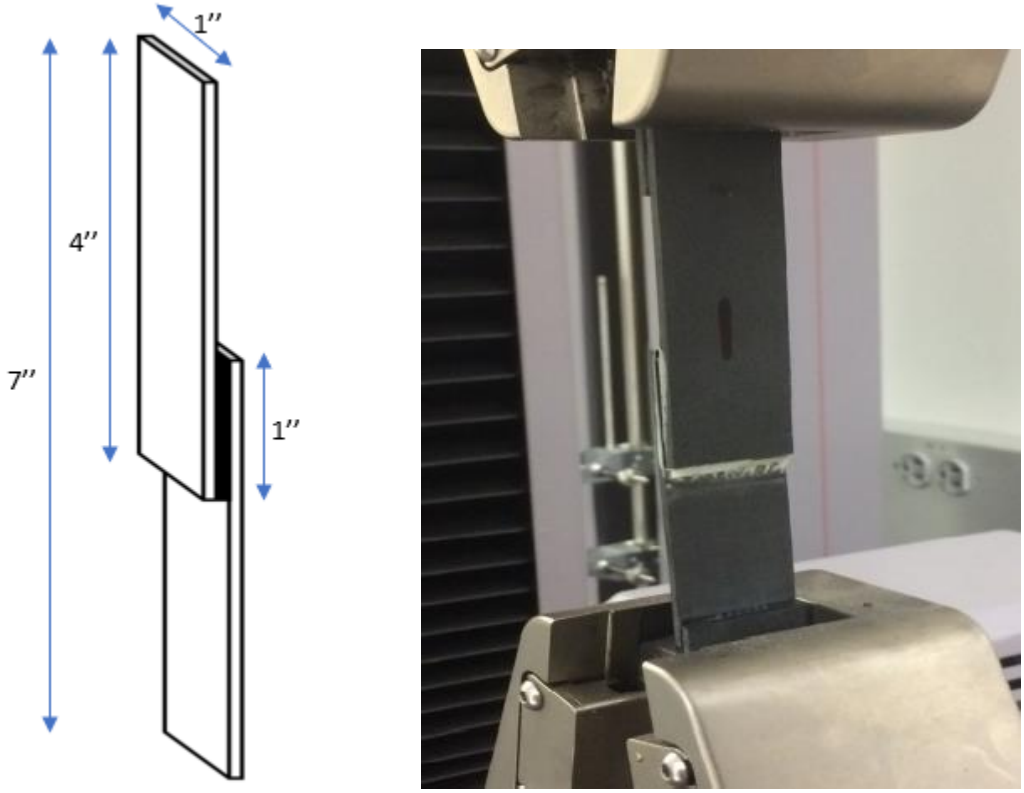

(a) (b)

Figure 2.20. (a) Schematic of the lap-shear sample dimensions following standard ASTM D5868-01; (b) Lap-shear sample placed in the MTS grippers prior to testing.

2.2.8.3 End-notched flexure (ENF)

End-notched flexure (ENF) testing was performed conforming to ASTM D7905/7905M [123] to evaluate the Mode II (sliding/shear mode) fracture toughness of an adhesively bonded joint. ENF samples were made with reinforced carbon fiber panels that were manufactured as described in Chapter 3.3. Samples were bonded with 3M EC 2615 epoxy adhesive that contained no MENs and 1 vol% MENs. An MTI Instruments SEM 1000 micro load frame was used in a three-point bend configuration. Testing was performed at a fixed displacement rate of 0.5 mm/min. The supporting span was 50 mm, while the sample was 120 mm in length and 3.5 mm in thickness and contained a 25 mm pre-crack. A detailed description of the sample types manufactured and tested is included in Chapter 3.3. Figure 2.21 shows a schematic of the three-point bending test obtained from the ASTM D7905/7905M standard [123].

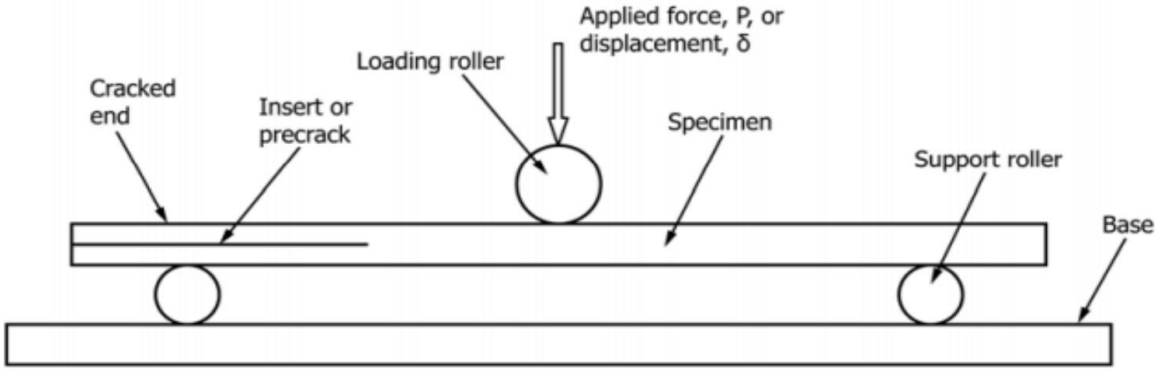

Figure 2.21. Schematic of the three-point bending test obtained from the ASTM D7905/7905M standard [123].

To obtain the mode II critical energy release rate, G_{IIC}, in kJ/m^2 of the ENF samples, equation 2.11 was used as follows [38]:

$$G_{II} = \frac{9a^2P\delta}{2\beta(2l^3+3a^3)} \quad (2.111)$$

Where a is the pre-crack in meters, P is the load in kN, δ is the displacement of the pre-crack, β is the width of the ENF samples in meters, and l is the distance between the two bottom points from the three-point bend test fixture which is fixed at 0.0165 m.

In situ ENF testing was performed within the chamber of a JEOL JIB-4500 SEM/FIB under vacuum at a pressure of 1.4×10^{-4} Pa or below after Au coating the sample for 30 seconds. Recording real-time imaging of how the crack propagates through the sample allows for a visual understanding of how fracture occurs and develops during testing. Figure 2.22a contains the apparatus utilized to perform the ENF testing, while Figure 2.22b shows the apparatus inside the SEM/FIB chamber.

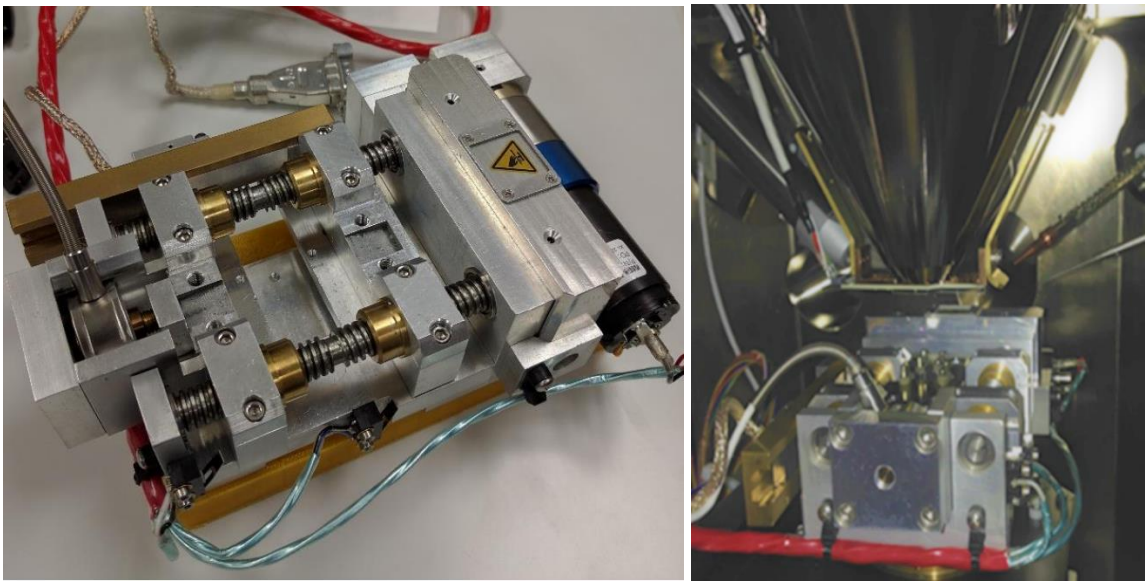

(a) (b)

Figure 2.22. Picture of the MTI Instruments SEM 1000 micro load frame; (b) load frame inside the FIB/SEM chamber prior to testing.

Chapter 3 Multifunctional MENs Doped Adhesives: Strengthening, Bond Quality Evaluation, And Variations in Magnetic Signal with Environmental Exposure

3.1 Abstract

Adhesive bonding of polymer matrix composites offers various advantages over traditional fasteners such as a uniform stress state, reduced weight, and delay of composite delamination. However, adhesive bonding has limited implementation due to challenges in the prediction of durability. This work introduces a new method to monitor an adhesively bonded composite joint by dispersing magneto-electric nanoparticles (MENs) into the polymer precursor and monitoring changes in their surface charge density by evaluating the output magnetic signal under an applied magnetic field. Real-time monitoring of the curing process of a polymer adhesive was performed and corroborated via thermal analysis and mechanical testing. Lap shear and end notch flexure testing showed that adding 1 vol % MENs led to a ~23 % increase in shear strength and a ~12 % increase in mode II critical energy release rates compared to the undoped adhesive. Adding 5 vol % MENs also increased the adhesive's peak tensile stress by ~8 %. Strengthening mechanisms of the doped adhesive were monitored using *in situ* electron microscopy. A correlation between water ingression and a change in the magnetic moment was observed. Results show the MENs potential as a structural health monitoring tool for a wide range of materials and applications.

3.2 Introduction

Polymer matrix composites (PMCs) have shown improved properties over traditional structural materials, especially weight-normalized properties such as specific strength and stiffness [124]. While known for some time, the implementation of PMCs as

structural materials have been limited by complications in joining complex geometries [125]. Currently, the bonding of composite panels is completed primarily through the use of mechanical fasteners [40]. However, while their use can create a robust joint with the potential to compartmentalize crack growth, the process of drilling holes in a laminate remains a consistent challenge. For example, drilling in a PMC can create edge effects, leading to delamination and interlaminar failure, and also create locations of stress concentrations [34]. Furthermore, traditional mechanical fasteners are mainly manufactured from high-density metals, adding significant weight and complexity (possible issues with corrosion, etc.) [34]. Over-design of the composite panel is often necessary to compensate for these factors, leading to a loss in overall efficiency [40].

One solution that could mitigate the issues associated with mechanical fasteners is to use adhesively bonded composite joints (ABCJs). Adhesive bonds offer the potential to join complex geometries at a fraction of the weight, simplifying a very challenging problem. The implementation of this type of bond also allows for an improved distribution, eliminates the corrosion occurring in metallic fasteners, and reduces the number of parts of the structure. While the potential is vast, the current Federal Aviation Administration certification requires a demonstration that every bond used on a primary structure maintains integrity over the expected aircraft life cycle [126]. The motivation behind this restriction is that, unlike mechanical fasteners, adhesive bonds cannot act to delay damage propagation, potentially leading to large-scale catastrophic failure [127] [6]. Therefore, to increase the scope of PMC usage, a robust and exhaustive structural health monitoring (SHM) tool must be developed to evaluate the quality of ABCJs without reliance on the initiation of damage in the bond [127]. The method should advance beyond the current

structural health monitoring methods (such as E/M impedance and wave propagation approach [128], acoustic and ultrasonic methods [129], and terrestrial laser scanning [130]) that are limited in resolution and scope and rely on damage initiation.

In this work, the dispersal and integration of magneto-electric nanoparticles (MENs) into an adhesive resin were used to monitor the quality of a polymer adhesive when exposed to an accelerated temperature and moisture environment. Monitoring was achieved through a coupling of magnetostriction and piezoelectricity in the MENs [131]. This consists in having an electric polarization when a magnetic field is applied, while obtaining magnetic polarization when an electric field is applied. A schematic of this relationship is shown in Figure 3.1. As a result, the dipole surface charge density of the particle induced an electric field, which caused a change of magnetization that was detected using standard magnetometry techniques [132]. Variation in the obtained magnetic moment was associated with the history of environmental exposure of the bond. The integration of MENs also provided a multifunctional effect, leading to improved shear, tensile, and flexural performance over the unfilled adhesive. Additionally, the strengthening of the adhesive due to doping was investigated using in-situ microscopy and a nanocomposite toughening model. The changes in the surface charge density of MENs were also used to nondestructively evaluate the curing process of the adhesive. In the past, MENs have been used for optical and magnetic applications [133], [134] and as materials for biomedicine and drug delivery [135], [136], but this is the first study to investigate their potential as a multifunctional SHM tool. Future applications of this work could lead to SHM techniques that can evaluate loading history and damage state (without reliance on

damage initiation) for a broad range of materials, loading types, geometries, magnitudes, and applications.

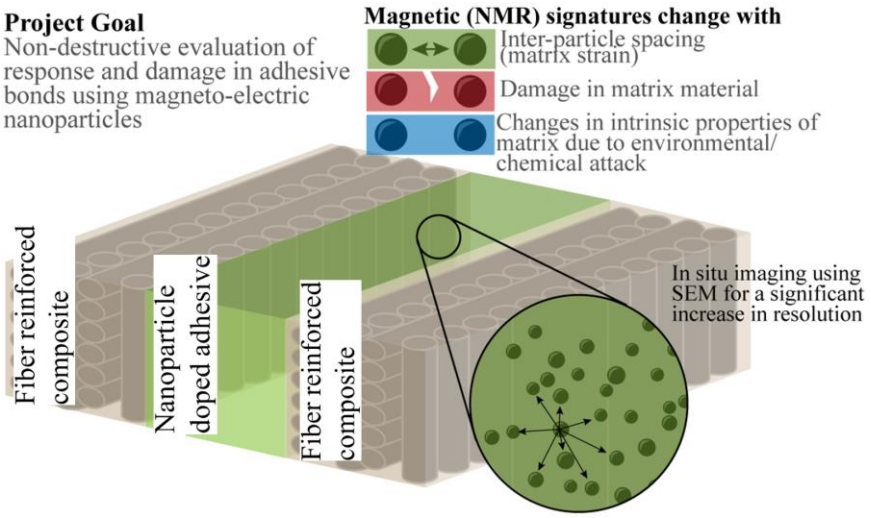

Figure 3.1. Possible sample loading history influences on output magnetic signal of MENs doped adhesives.

3.3 Materials and Methods

The carbon fiber composite material selected to manufacture the lap shear and end notch flexure (ENF) samples was a unidirectional prepreg material (T800H) from Toray. Following ASTM D5868-01 [122] and ASTM D7905/7905M [123] standards for the manufacturing process, the lap shear specimens had a 12-layer layup process and the end notch flexure specimens had a 10-layer layup process, respectively. A polyester peel ply was placed on both sides of the prepreg layups in order to prepare the surface for bonding. An autoclave from American Company Co. was used to cure the prepreg layup at a temperature of 177 °C and a pressure of 30 psi for 1 hour. The lap shear specimens were cut to a size of 25.4 mm by 177.8 mm with a bonded area of 25.4 mm by 25.4 mm, while ENF specimens were manufactured to be 35 mm by 10 mm. The carbon fiber panels were bonded together using 3M's Scotch-Weld two-part epoxy adhesive EC 2615 B/A. A 2:1

resin-to-hardener ratio was used. For the doped adhesive, MENs, synthesized to consist of a cobalt ferrite ($CoFe_2O_4$) core and a barium titanate ($BaTiO_3$) shell nanoparticles with a median diameter of ~30 nm [19], were hand mixed into the hardener component of the epoxy at a 1% volume concentration prior to curing. The fabrication and characterization of the MENs used in this study have also been discussed previously [135], [136]. Both ENF and lap shear specimens were placed under a vacuum during the adhesive cure in order to minimize void content. Then, the same epoxy adhesive was used to manufacture the tensile testing dogbone samples.

The lap shear specimens were tested using the ASTM D5868-01 standard [122]. A tensile tester from MTS (Criterion Model 43) was used to test the samples with a loading rate of 13 mm/min. The dogbone tensile testing samples were tested at a rate of 5 mm/min using the same MTS instrument using standard ASTM D638-03 [120]. ENF testing was performed conforming to ASTM D7905/7905M [19] using an MTI Instruments SEM 1000 micro load frame in a three-point bend configuration. Testing was performed at a fixed displacement rate of 0.5 mm/min. The supporting span was 50 mm, while the sample was 120 mm in length and 3.5 mm in thickness and contained a 25 mm pre-crack. *In situ* ENF testing was performed within the chamber of a JEOL JIB-4500 SEM/FIB under vacuum at a pressure of 1.4×10^{-4} Pa or below after Au coating the sample for 30 seconds. Uncertainty measurements were obtained using the law of propagation of uncertainty [116]. To obtain the mode II critical energy release rate, G_{IIC}, in kJ/m^2 of the ENF samples, equation 3.1 was used as follows [38]:

$$G_{II} = \frac{9a^2 P\delta}{2\beta(2l^3+3a^3)} \tag{3.1}$$

Where a is the pre-crack in meters, P is the load in kN, δ is the displacement of the pre-crack, β is the width of the ENF samples in meters, and l is the distance between the two bottom points from the three-point bend test fixture which is fixed at 0.0165 m.

To study the curing process of the 3M epoxy adhesive, three 8 x 8 x 4 mm samples were manufactured containing 5 vol % of MENs. This volume percentage was used since the manufacturing process with the resources available was time-consuming, but a higher than the previous 1 % used for the lap shear and ENF samples was utilized to obtain a higher signal using the B-H looper setup. The curing and testing process took place in a laboratory environment at room temperature (~22 °C). Signal measurements during the curing process were taken every two hours using the B-H looper setup, which is described later in this section.

Using the same adhesive, samples measuring 5 x 5 x 1 mm and containing 0, 5, 10, and 15 vol % of MENs were placed in an environmental chamber at 95 % relative humidity and at an elevated temperature of 70 °C. The magnetic signatures were taken prior to environmental exposure. After a four-week time period, the samples were removed and again scanned. All magnetic signatures were taken using a vibrating samples magnetometer which has a sensitivity of 0.01 μemu [137].

The adhesive's glass transition temperature was obtained using a Q600 SDT from TA instruments to determine its evolution as a function of the curing time during the first 24 hours of curing. The tests were run from room temperature (~22 °C) until 250 °C at a heating rate of 5 °C/min. Argon gas was used for this testing.

To monitor the local physical properties of adhesives nondestructively and noninvasively, the magnetic properties of MENs dispersed into these materials were

evaluated using a B-H looper setup. In specific, this setup was used to characterize the local properties of adhesive samples, adhesively bonded composite panels, and bonded mini-DCB (double cantilever beam) samples. The Principle of Reciprocity states that local values of the magnetic fields B and H are reflected by the system's induced and applied voltages, respectively.

The application of other techniques like vibrating sample magnetometry (VSM) is limited since the sample needs to be attached to a piezo-actuator, thus requiring specific sample preparation. On the other hand, the B-H looper setup allows for the evaluation of the sample's surface without physically damaging it. This setup takes advantage of the magneto-electric effect to noninvasively evaluate magnetic signature differences at a microenvironment level.

From the reciprocity principle, electromotive force (EMF) or measured signal, ε, in volts is obtained by using equation 3.2 as follows [113]:

$$\varepsilon = \frac{n\Delta\varphi}{\Delta t} = \mu_0 \frac{n\Delta \int H_{img} M(r) dv}{\Delta t} \tag{3.2}$$

Where $\Delta\varphi$ is the change in magnetic flux in volt-seconds, Δt is the change in time in seconds, n is the number of turns in a coil, M(r) represents how the magnetization is distributed throughout the sample, and H_{img} is the normalized reciprocal imaginary field representing the geometry of the B-H setup.

It can be seen in the B-H looper setup in Figure 3.2 how this setup consists of a function generator equipped with a lock-in amplifier and three different coils. Two detection coils are located on either side (shown in blue) with the purpose of acquiring a balanced detection. To amplify the magnetic signal from the sample and to cancel any

background noise, these two detection coils were connected in series. The source coil located in the middle (shown in orange) is connected to the function generator to generate an AC magnetic field. The lock-in amplifier connects the detection and source coils and was used to amplify only the signal at the detection frequency and phase and cancel out all the noise signals at all the other frequencies. The sensitivity of the setup was reduced down to the microvolt level and it is limited by the inductance of the whole setup, which is frequency dependent. Fortunately, this is not a fundamental limit and we can further improve it in the future by increasing the number of balancing coils and optimizing the geometry of the coils through numerical simulations.

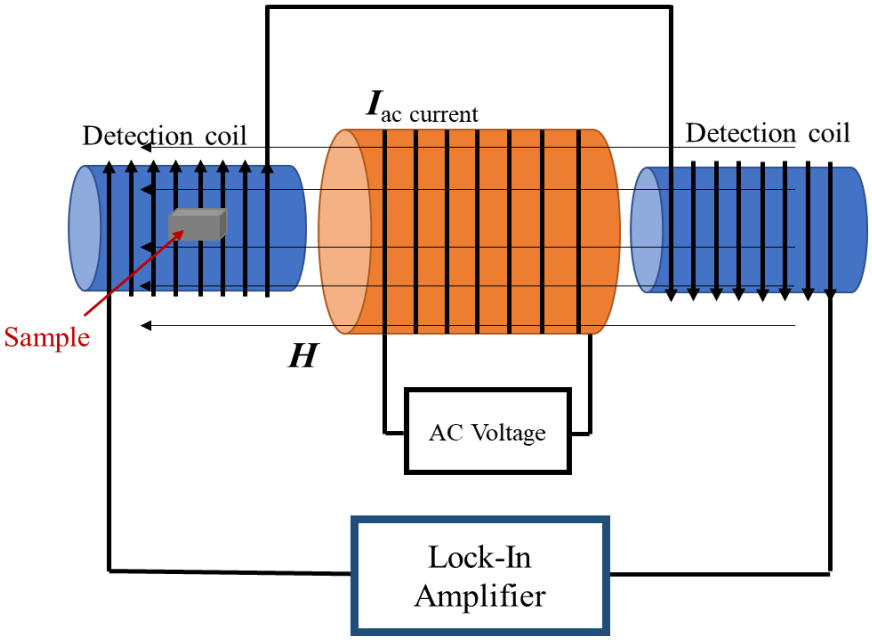

Figure 3.2. B-H looper setup diagram.

To test the curing process using the B-H looper of the adhesive containing MENs, an input voltage of 4 V and a frequency of 1.3 kHz were utilized, which is the critical frequency. To determine this frequency, the frequency was swept from 100 Hz to 10 kHz, and the value at which the signal due to the MENs reached its maximum was recorded.

This frequency value was characterized by the net inductance of the whole system, which is influenced by the sample's microenvironment [38]. Thus, the inductance is partially determined by the magnetic dynamics of the MENs dispersed in the sample. The critical frequency value slightly increases when the applied field is further increased via the source voltage.

When a voltage was applied to the source coil of the B-H looper and the sample was placed next to the coils, the AC magnetic field generated caused a magnetic flux in the sample containing MENs due to the surface charge density of the nanoparticles. This magnetic flux was perceived by the detection coils, causing a change in signal. The background signal, which includes the noise factor, prior to putting the sample was subtracted from the recorded signal for every measurement.

3.4 Results

3.4.1 Magnetic Moment on MENs Doped Adhesive

The influence of surface charge on the magnitude of the magnetic moment generated during VSM is shown in Figure 3.3a for MENs with and without a polymer coating. Results show a 60 % decrease in the magnitude of the magnetic moment when MENs contained a polymer coating as compared to the free particles. Figure 3.3b shows the difference in VSM signal generated from undoped and doped (1 vol % MENs) cure polymer adhesive (EC 2615 B/A, 3M). The doping of the adhesive resulted in an approximate 500% increase in the magnetic moment from approximately 10 μemu to 50 μemu.

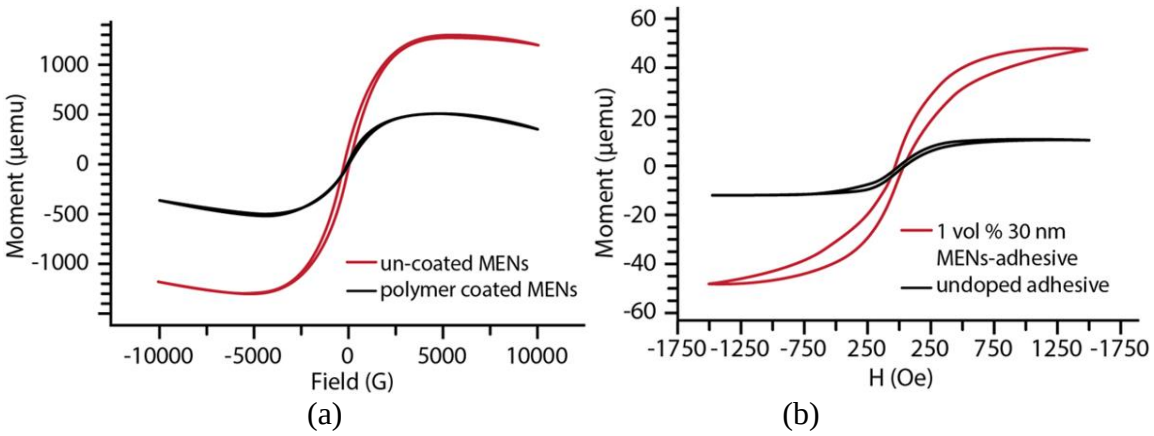

Figure 3.3. (a) Magnetic response of free MENs vs. polymer coated MENs; (b) the influence of MENs doping on the magnetic signal on a polymer adhesive.

The sensing capability of the MENs particles predominantly comes from variations in surface charge density based on loading history [138]. For the uncoated and coated individual particles, Figure 4a shows the possible mechanism for a decrease in surface charge and, as a result, magnetic moment. As a MEN is coated with polymer chains, free H+ atoms in the chains act to neutralize the surface charge [136], increasing bond strength between the particle and the polymer as well as lowering the measured magnetic moment, as shown in Figure 3.3a. Then, Figure 3.3b shows how adding the nanoparticles into the adhesive causes the magnetic properties of the material to increase.

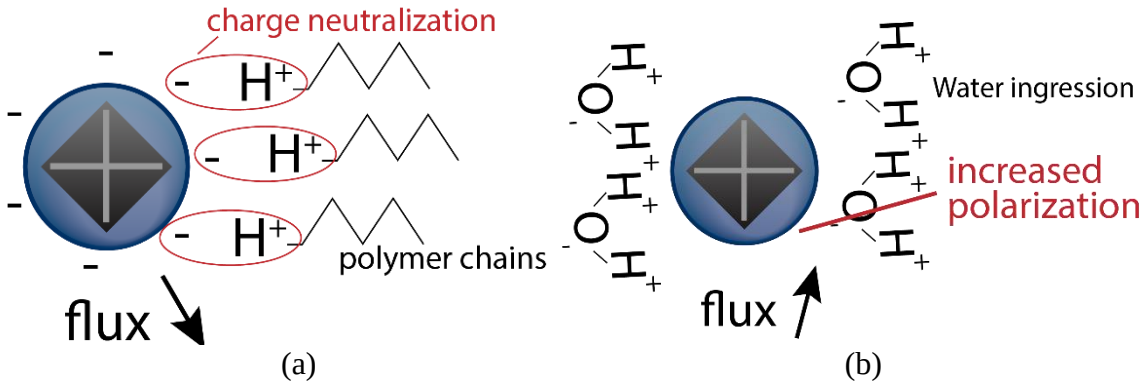

Figure 3.4. (a) Charge neutralization of individual MENs as a function of polymer coating; (b) Polarization of MENs as a function of water ingression.

3.4.2 Monitoring of the Curing Process Using the B-H Looper

The BH looper was used to evaluate the magnetic signal of adhesive samples containing 5 % MENs to monitor their curing process. The initial magnetic signal (at curing hour zero) of the three samples was measured. Subsequent measurements were recorded and the percentage increase with respect to the initial signal was obtained. The average percentage increase of the three samples was calculated and graphed in red in Figure 5. It can be observed that there is an increasing trend in magnetic signal during the first curing hours, which starts converging after approximately eight hours of curing time.

To confirm the magnetic signal results obtained with the BH looper, tensile testing was performed on undoped adhesive to study if a similar type of convergence was observed on the adhesive's mechanical properties. The peak stress with respect to curing time is plotted in Figure 3.5 in blue. A very similar trend is appreciated, in which there is a rapid increase in tensile strength during the first curing hours and then it starts converging at around eight hours of curing time until reaching ~41 MPa. This trend was also confirmed by the progression of the adhesive's glass transition temperature (plotted in black) as it cured, which converged at ~137 ºC.

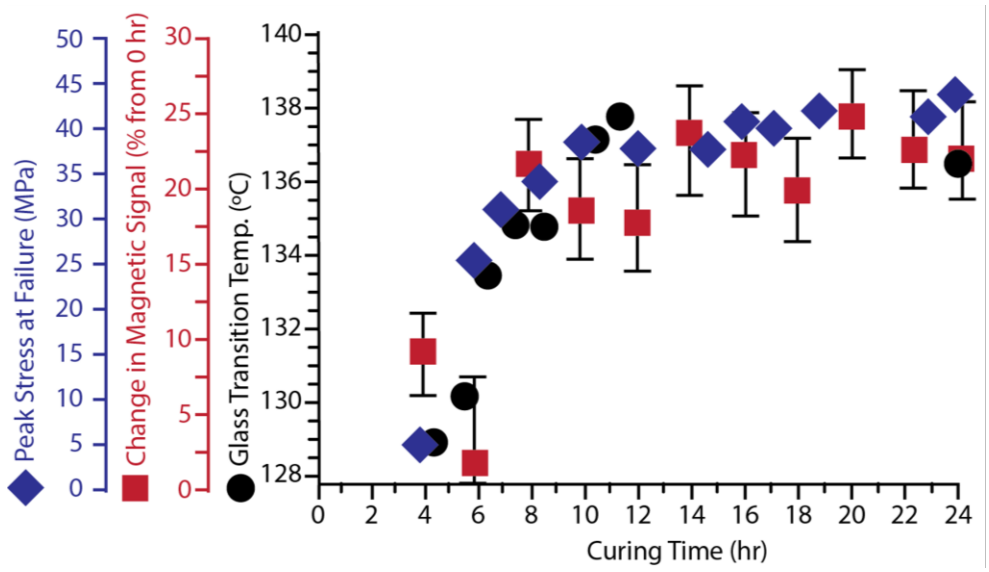

Figure 3.5. Undoped adhesive peak stress (blue), change in magnetic signal (red), and glass transition temperature (black) with respect to adhesive curing time.

3.4.3 Single Lap Shear

For the single lap shear, Figure 3.6 shows the relationship between displacement and peak stress at failure for each undoped and doped (1 vol % MENs addition) sample. The average shear strength for each condition was 25.01 ± 2.45 MPa and 30.79 ± 2.16 MPa, respectively, signifying an increase of 23 % for the doped adhesive. This increase in bond strength is significant as the primary application of the addition of MENs is for the sensing aspects and any gains in bond quality are secondary. These samples experienced cohesive failure, and the addition of the nanoparticles did not seem to impact the type of failure in lap shear testing.

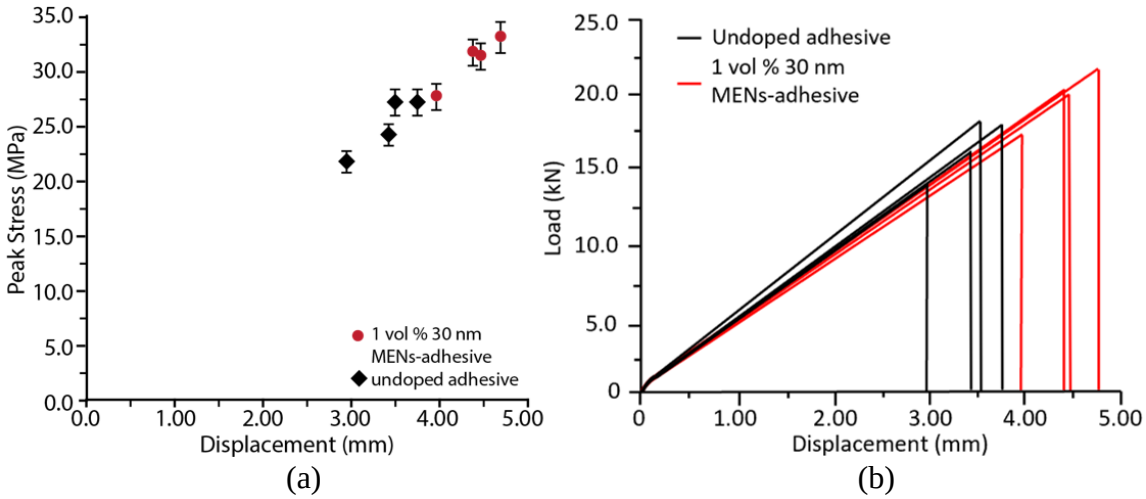

Figure 3.6. (a) Peak stress of undoped and doped adhesives for single lap shear samples; (b) load-displacement curves for undoped (black) and doped (red) samples.

3.4.4 End Notch Flexure (ENF)

Regarding the ENF samples, Figure 3.7 shows the relationship between displacement and mode II critical energy release rate G_{IIC} at failure for each sample that was doped and undoped. The average G_{IIC} value for each condition was 503 ± 46 J/m^2 and 564 ± 37 J/m^2, respectively, showing an increase of 12 % for the doped adhesive. The strengthening of adhesive bonds with the addition of hard ceramic nanoparticles (such as Al_2O_3, ZnO, and TiO_2) has been well documented [81], [82], [138]–[141]. These samples experienced cohesive failure, and the addition of the nanoparticles did not seem to impact the type of failure in lap shear testing. This study shows how adhesive joints containing MENs had an increase in mechanical performance over undoped joints. The increase in critical energy release rate can be modeled using the formulation discussed in Johnsen, et al. [141] in which the G_C of a particle-toughened polymer adhesive can be determined using the G_C of the adhesive (values obtained from ENF testing above) plus the change in energy required for plastic zone growth. This energy can be obtained from the mechanical

properties of the ceramic (E_{MENs} = 50 GPa [142]), the volume fraction of the nanoparticle (1 vol %) and voids, and the plastic zone radius of the unmodified polymer. Based on these inputs, the range of expected critical energy release rate as a function of MENs addition was calculated to be between 546 J/m^2 to 553 J/m^2, which slightly under-predicts the experimental G_{IIC} values found with the ENF testing (average of 564 J/m^2).

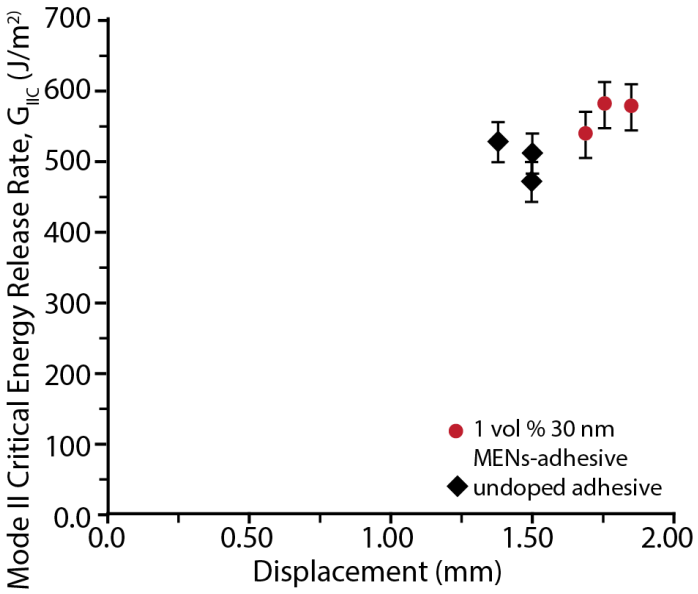

Figure 3.7. G_{IIC} of undoped and doped adhesives with 1 vol % of MENs.

In addition, a JEOL JIB-4500 Dual Beam FIB-SEM was used to take in situ images of the failure of one doped ENF sample, which are included in Figure 8. Imaging shows localized shear loading, plastic zone evolution, and failure of the ABCJ in the crack tip region. As indicated by the blue arrows, localized damage is seen to occur outside of the plastic zone in the form of visible microcracking resulting from the distribution of loading away from the pre-crack. In addition, the red arrows identify the initial formation of microvoid clusters in the high-shear region. The fracture surfaces of the failed specimen show similar plastic zone development in the failure and crack tip regions for plain samples

and samples containing MENs. The most likely toughening mechanisms, in this case, are stress shielding of the crack tip and localized stress transfer to the stiffer nanoparticle [143].

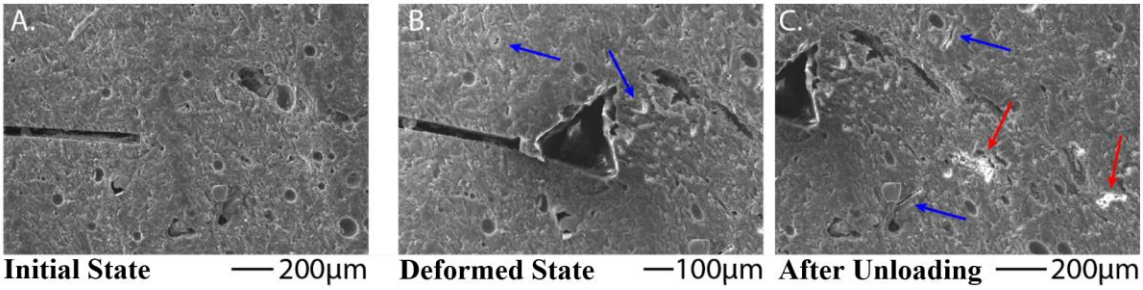

Figure 3.8. In situ images of an ENF specimen of (a) the crack tip region prior to loading; (b) and (c) the deformed crack tip region.

3.4.5 Tensile Testing

Table 3.1 displays the peak tensile stress on undoped and doped samples. It can be appreciated how dispersing 5 vol % MENs into the 3M adhesive increased its maximum tensile stress compared to the undoped samples, which was 39.5 ± 1.76 MPa and 36.6 ± 1.28 MPa respectively. This signifies approximately an 8 % increase, confirming that adding MENs into the epoxy adhesive does not negatively affect its mechanical properties.

Table 3.1. Maximum tensile stress in undoped and doped adhesives with 5 vol% of MENs.

Sample Type / Sample #	**Peak Tensile Stress (MPa)**					**STD Dev**	**Avg Stress (MPa)**
	1	2	3	4	5		
Baseline (2:1 ratio)	38.09	36.61	36.10	38.44	35.00	1.28	**36.85**
(5 vol % MENs	38.18	36.32	42.56	40.58	43.84	2.76	**40.30**

3.4.6 Environmental Exposure

VSM scans were completed in individual cured adhesive resin samples (non-bonded) with concentrations of 5, 10, and 15 vol % MENs before and after environmental exposure, with the results shown in Figure 3.9. Magnetic signatures before and after environmental exposure of (a) 0 vol % concentration; (b) 5 vol % concentration; (c) 10 vol % concentration; (d) 15 vol % concentration. Before exposure, the doped adhesives showed

an increasing magnetic moment with increased concentration (3.7 x 10^{-5} emu for 5 vol % MENs, 10.2 x 10^{-5} emu for 10.2 vol % MENs, and 15.5 x 10^{-5} emu for 15 vol % MENS). After exposure, the signal saturated and was consistent over varying MENs concentrations (magnitude approximately 15.0 x 10^{-5} emu).

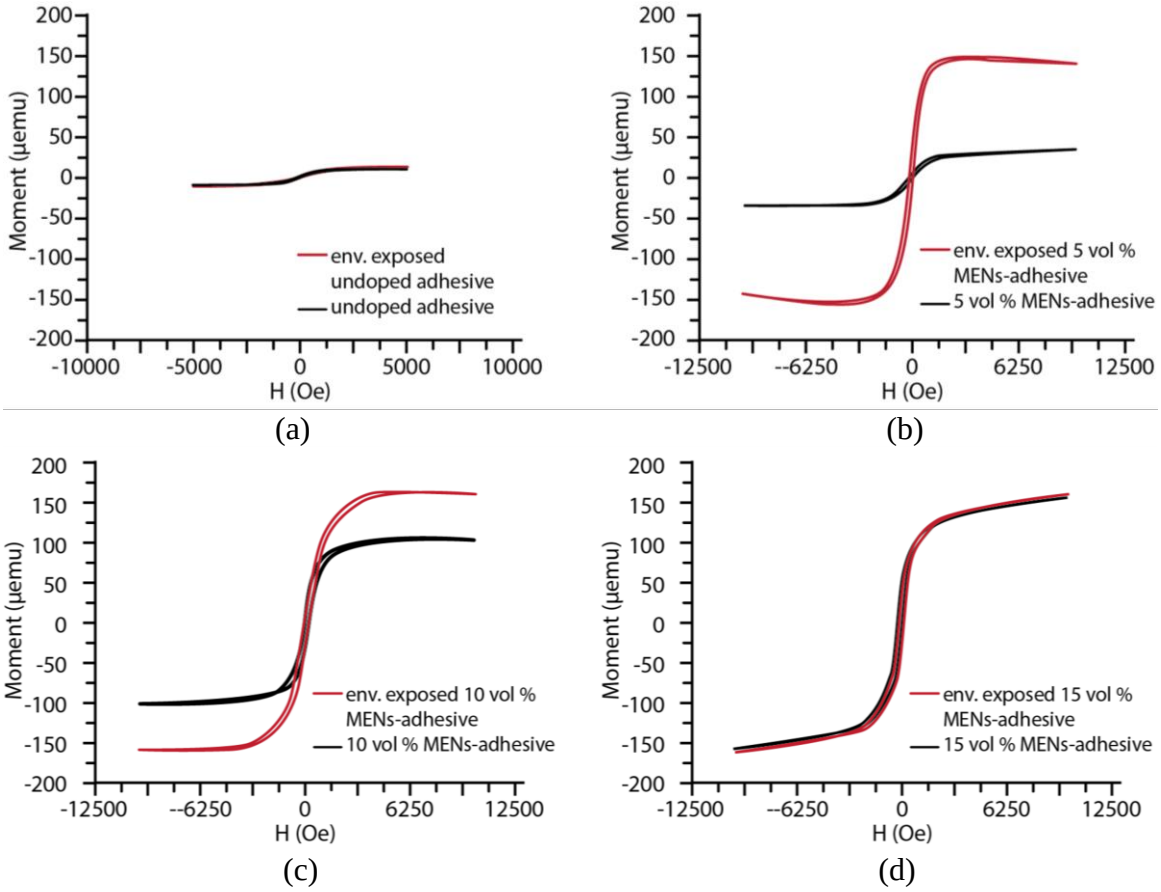

Figure 3.9. Magnetic signatures before and after environmental exposure of (a) 0 vol % concentration; (b) 5 vol % concentration; (c) 10 vol % concentration; (d) 15 vol % concentration.

As illustrated in Figure 4b, water ingression has the opposite effect on the magnetic moment. This can occur since the polarization of the surface charge of MENs can experience an increase due to the ingression of polar H_2O molecules. As the concentration of MENs is increased, the magnetic moment can result from both the increased amount of

magnetic material, along with the agglomeration of MENs resulting in a higher percentage of MENs with uncoated free surfaces. After exposure, the saturation point of the magnetic moment was most likely the result of water ingression being a surface area-dominated phenomenon.

3.5 Discussion

Using MENs to nondestructively evaluate adhesives using magnetic signals can aid with the widespread implementation of adhesive bonding. It has been shown how this method detects magnetic changes that are affected by variations in the sample's microenvironment, which allows to measure changes in the material at a very localized level. Correlating the curing process of the doped polymer adhesive with the strength of the output magnetic signal, and corroborating it with thermal analysis and tensile testing, shows the potential of this method to nondestructively evaluate materials not only during their lifetime but also during their manufacturing process. In addition, being able to measure changes in the surface charge density of the MENs allows for the analysis of materials that undergo harsh environmental conditions which cause the ingression of water molecules that polarize the surface of MENs.

Ideally, for each particular material, a baseline calibration curve would have to be obtained. Knowing how MENs behave in each material and how the magnetic signal evolves during the curing process will help to know when a specific sample is not curing ideally. This would help observe whether a sample was incorrectly manufactured or if the curing parameters are not correct. Future studies will focus on obtaining calibration curves for common adhesives used in the aerospace industry and then determine when specific samples are undergoing a curing process that deviated from the baseline.

It is important to highlight that the tensile, lap shear, and end notch flexure testing show enhancement in the mechanical properties of the adhesive bond when dispersing MENs into the adhesive. This means that the addition of these nanoparticles into the adhesive does not negatively influence the integrity of the adhesive bond when a low volume percentage is added. This is necessary so that MENs can successfully be used in industries like aerospace or automotive where the integrity of the bonds is of primary importance.

3.6 Conclusions

VSM and the B-H looper setup were used to nondestructively evaluate an adhesive resin doped with magneto-electric nanoparticles. These setups were used to obtain changes in surface charge density in the nanoparticles of ABCJs with respect to curing time and varying history of environmental exposure. There was a strong correlation between the magnetic signal obtained during the curing process of the doped adhesive and its mechanical and thermal properties. There is also a relationship between increased levels of exposure and an increase in the measured magnetic moment (up to a saturation point). Also, mechanical property evaluation revealed an increase in the shear strength, mode II critical energy release rate (G_{IIC}), and tensile strength of MENs doped adhesive. With further refinement and development, this technique has the potential to become a non-destructive evaluation tool for damage and quality inspection, both in an in-field and manufacturing setting.

Chapter 4 Assessment and Non-Destructive Evaluation of The Influence of Residual Solvent on a Two-Part Epoxy-Based Adhesive Using Ultrasonics

4.1 Abstract

Polymers are increasingly being used in higher demanding applications due to their ability to tailor the properties of structures while allowing for weight and cost reduction. Solvents play an important role in the manufacture of polymeric structures since they allow for a reduction in the polymer's viscosity or assist with the dispersion of fillers into the polymer matrix. However, the incorrect removal of the solvent affects both the physical and chemical properties of polymeric materials. The presence of residual solvent can also negatively affect the curing kinetics and the final quality of polymers. Destructive testing is mainly performed to characterize the properties of these materials. However, this type of testing involves using lab-type equipment that cannot be taken in-field to perform in situ testing and requires specific sample preparation. Here, a method is presented to non-destructively evaluate the curing process and final viscoelastic properties of polymeric materials using ultrasonics. In this study, changes in longitudinal sound speed were detected during the curing of an aerospace epoxy adhesive as a result of variations in polymer chemistry. To simulate the presence of a residual solvent, samples containing different weight percentages of isopropyl alcohol were manufactured and tested using ultrasonics. Thermogravimetric analysis was used to show changes in the decomposition of the adhesive due to the presence of IPA within the polymer structure. Adding 2, 4, and 6 wt.% of IPA decreased the adhesive's lap shear strength by 40, 58, and 71%, respectively. Ultrasonics were used to show how the solvent influenced the curing process and the final sound speed of the adhesive. Young's modulus and Poisson's ratio were determined using

both the longitudinal and shear sound speeds of the adhesive. Using ultrasonics has the potential to non-invasively characterize the quality of polymers in both in-field and manufacturing settings, ensuring their reliability during use in demanding applications.

4.2 Introduction

The manufacturing conditions of polymeric materials are critical since they determine the resulting polymer structure, and as an outcome, their final properties and performance characteristics [144]–[147]. Therefore, it is important to monitor polymers during the fabrication process to enhance our understanding of their relationship to the final quality of the manufactured parts. Ensuring polymers have the required characteristics will help improve their reliability when used in primary structures in fields such as aerospace, automotive, biomedical, electrochemical, etc.

When manufacturing polymers, solvents play an important role since they allow for a reduction in the polymer's viscosity during a coating process or assist with the dispersion of fillers into the polymer matrix [21], [46], [47]. This inevitably raises the concern of improperly removing the solvent from the polymer before obtaining its final structure. It has been shown that the incorrect removal of the solvent affects both the physical and chemical properties of polymers [48]–[51]. For example, J. Trinidad et al. showed that the presence of solvent in sodium dodecyl sulfate decorated graphene hybrid electrically conductive adhesives significantly decreased their lap shear strength due to the presence of voids and bubble formation [53]. N. Othman et al. experienced a decrease in tensile strength and hardness of 17 and 9%, respectively, when adding 16 wt.% of acetone in an epoxy resin [21]. Their study also showed that having this amount of acetone caused a decline in the epoxy's adhesion strength from 13 MPa to 4.9 MPa, which signifies a

reduction of ~62%. In addition, K. Qiu et al. demonstrated that residual solvent content in an epoxy resin affected its curing mechanics and decreased its crosslinking density. This lowered the glass transition temperature (Tg) of the resin by ~8.5 ◦C when they added 5 wt.% of cellular nanocrystals as a filler due to a decrease in the homogeneity of the material [54]. Since having residual solvent can negatively affect the properties of a polymeric material, it is important to have a precise evaluation method to determine if the solvent is present in the final structure.

Destructive testing, which involves using lab-type instrumentation that requires specific sample preparation and geometry, is mainly performed to characterize the mechanical properties of materials [70]–[76], [148]. It has also been used to characterize the curing kinetics of polymeric materials. Tests include dynamic mechanical analysis (DMA), differential scanning calorimetry (DSC), thermogravimetric analysis (TGA), tensile testing, lap shear testing, etc. However, this type of equipment cannot be taken in-field to perform in situ testing. Therefore, it has become essential to develop a non-destructive in situ method to evaluate the degree of reaction and the viscoelastic properties of polymers during curing and after they have been manufactured [77], [149].

Acoustics, consisting of the propagation of sound waves, have been used as a non-destructive evaluation method for different types of materials such as metals [97], [98], ceramics [99], [100], and polymers [77], [101], due to their accuracy and sensitivity. Ultrasonics, which involve the use of acoustic waves at high frequencies (20 kHz–100 MHz), can be used to detect small changes in adiabatic moduli with high precision. Therefore, ultrasonics can be implemented to evaluate phase transitions during curing and the physical properties of materials [77], [104]. For example, the ultrasonic pulse-echo

method can be implemented to measure the sound speed of a material with a short pulse of ultrasound generated by a transducer, from which elastic constants of the material can be determined [104]. F. Lionetto et al. used ultrasonics to monitor the cure state of thermosetting resins and showed how ultrasonic wave propagation was more sensitive to variations in moduli during the vitrification stage of the curing process compared to DSC [26]. This method has also been used to non-destructively evaluate the curing mechanics of epoxy resins at different temperatures [26], [77], [106]. However, a deeper understanding of the use of ultrasonics as a non-destructive method is needed to effectively understand the curing mechanics of resins and adhesives under different parameters that can affect the quality of the final product.

As an example, in the aerospace industry, epoxy and film adhesives are used to substitute mechanical fasteners for joining carbon fiber composites. This methodology has been proposed as a result of an adhesive bond's potential for increased strength, weight reduction, and improved stress distribution [33], [124], [150]. On the other hand, the Federal Aviation Administration (FAA) is concerned about the performance of adhesive bonds after aging during their life cycle [151]. In addition, failures associated with weak bonds, bondline voids, and contamination remain critical issues in today's adhesion community [152]. Manufacturing parameters, such as temperature and pressure, are difficult to precisely control and unwanted fluctuations can have an impact on the curing process and final product [153]. In addition, the usage of a mold release or other chemicals throughout the manufacturing process can lead to potential contamination and reduction in performance [154], [155]. As mentioned, the presence of residual solvent on an epoxy adhesive can considerably decrease its adhesive strength [21].

The focus of this paper is to detect changes in sound speed in an aerospace epoxy adhesive during the curing process as a result of residual solvent concentration. In this study, varying amounts of isopropyl alcohol (IPA) were added to the adhesive to simulate trapped solvent. Since the addition of IPA affects the crosslinking density and mobility of the adhesive, TGA was performed to analyze the decomposition of each of the sample types and to confirm the presence of different weight percentages of IPA in the adhesive samples. Fourier transform infrared (FTIR) spectroscopy was performed to investigate the effects on the chemical structure of the samples as a function of solvent concentration. Lap shear testing was used to evaluate the effects of IPA on the mechanical and adhesion properties of the adhesive under a shear load. We hypothesize that the sending and receiving of ultrasonic waves have the ability to detect the presence of this solvent and to determine how it influences the curing process of the adhesive. This curing process was modeled to better understand how variations in trapped solvent affect the curing mechanics of the material. Comprehending these effects can improve future techniques designed to use ultrasonics as an in situ, non-destructive quality control method during the manufacturing process. In addition, measuring the sound speed of fully cured samples that have been properly manufactured can serve as an in-field quality control method during the lifetime of polymeric materials.

4.3 Materials and methods

In this study, a two-part epoxy adhesive (EC 2615 B/A, 3M) was selected and used as a representative material. This adhesive is a two-part DEGBA-based resin with an amine hardener. A 2:1 resin-(part B)-to-hardener-(part A) ratio was used as recommended by the manufacturer. To simulate the effect of the trapped solvent, adhesive samples with 2, 4,

and 6 weight percentages (wt.%) of isopropyl alcohol (IPA) were manufactured. IPA was selected since it is a commonly used solvent for manufacturing polymeric materials and structures [156]–[159]. The curing and testing took place in a monitored laboratory environment at room temperature (~23 ± 2 ◦C) and ~44 ± 2.5% relative humidity.

4.3.1 Thermal analysis (TGA)

Thermal analysis was performed using a Q600 SDT (TA Instruments, New Castle, DE, USA) on fully cured adhesive samples containing 0, 2, 4, and 6 wt.% IPA. The tests were run from room temperature (~23 ◦C) to 450 ◦C at a heating rate of 5 ◦C/min. Argon gas was used as a purge gas. The weight of the samples ranged between 9 and 9.5 µg.

4.3.2 Fourier transform infrared (FTIR)

FTIR spectroscopy was performed on a Nicolet iS50 spectrometer (Thermo Fisher Scientific, Waltham, MA, USA) from 3600 to 400 cm^{-1} with a resolution of 0.482 cm^{-1}. A DTGS KBr detector and OMNIC software were utilized. Sixteen scans were used and the spectra were graphed in absorbance mode. The lens was cleaned using ethanol and a background scan was completed before testing each sample. In addition to the samples analyzed by TGA, FTIR spectroscopy was also performed on the IPA used to simulate the residual solvent

4.3.3 Single lap-shear

Lap shear testing was performed on carbon fiber composite samples bonded using adhesive manufactured with 0, 2, 4, and 6 wt.% IPA. The ASTM D5868-01 [160] standard was followed for the manufacture and testing of the lap shear samples. Four specimens per sample type were manufactured and tested. An autoclave (American Autoclave Co., Jasper, TX, USA) was used to cure the prepreg layup at a temperature of 177 ◦C and a pressure of

30 psi for 1 hour. A polyester peel ply was placed on both sides of the prepreg layups in order to prepare the surface for bonding. The lap shear specimens were cut to a size of 25.4 mm by 177.8 mm with a bonded area of 25.4 mm by 25.4 mm. A tensile tester from MTS (Criterion Model 43) was used to test the samples with a loading rate of 13 mm/min.

4.3.4 Ultrasonics: cure process

Ultrasonics were utilized to non-destructively measure the sound speed of the adhesive during its curing process. To perform this testing during the adhesive's curing process, the adhesive was first mixed and then placed in a PLA 3D-printed mold. The mold had dimensions of 20 mm in height, 22 mm in width, and 12.5 mm in thickness. The mold's wall thickness was 1.5 mm, except for the locations where the transducers were placed, which had a thickness of 0.5 mm. A function generator (AFG31052; Tektronix, Beaverton, OR, USA) was utilized to generate a sine burst of 500 kHz at 10 volts peak-to-peak. This frequency was selected after observation over a range of frequencies as it produced the highest output signal for this particular adhesive material. A Tukey window with a cosine fraction, r, of 0.4 was used to taper the input function consisting of five cycles [114]. The burst was transmitted and detected by transducers placed on each side of the sample. Transducers (V133-RM and V154-RM, Olympus, Center Valley, PA, USA) of 2.25 MHz were used for evaluating the longitudinal and shear sound speeds, respectively. An ultrasonic couplant (Echo Ultrasonics, Bellingham, WA, USA) was used to ensure proper contact between the sample and the transducers. The resulting waveforms were recorded every two minutes using an oscilloscope (MDO32; Tektronix, Beaverton, OR, USA). **Error! Reference source not found.**a shows a diagram of the ultrasonics setup, where the sample is depicted in blue and the transducers, in green. The output waveforms were then

used along with the excitation waveform to calculate the sound travel time across the sample utilizing the cross-correlation method [104]. It is important to mention that the delays introduced to this travel time by the transducers and the PLA mold, where the adhesive was placed, were accounted for prior to using equation 4.1 to calculate the sound speed in the material:

$$c = \frac{d}{t} \tag{4.1}$$

where *d* is the thickness of the sample and *t* is the sound travel time. The law of propagation of uncertainty was used to obtain the error associated with the velocity calculations [116]. This method accounts for the uncertainty associated with the resolution of the oscilloscope to plot the output waveforms (9 ns), which were used to obtain the sound travel time, and the uncertainty associated with the digital micrometer that was used to evaluate the thickness of the sample (0.01 mm).

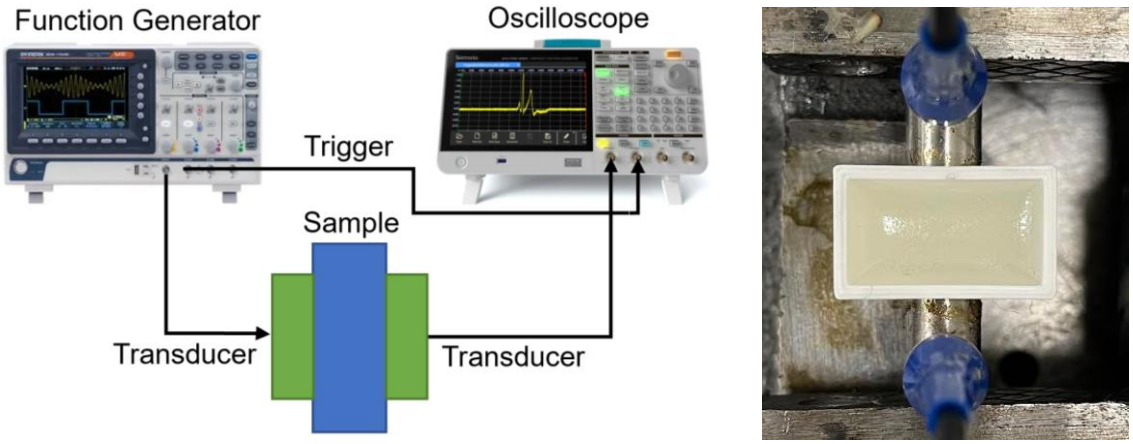

(a) (b)

Figure 4. 1. (a) Diagram of the ultrasonics instrumentation and sample setup; (b) picture of an adhesive sample while being tested during curing.

4.3.5 Cure process modeling

The Hill equation was used to model the curing process for each of the samples.

This was used to help to better understand how variations in trapped solvent affected the curing mechanics of the adhesive and to allow for future predictions of material quality. The degree of conversion, $\alpha(t)$, ranges from 0 to 1 and can be expressed using the Hill equation as shown in equation 4.2 [119]:

$$\alpha = 1 - \frac{1}{(\frac{t}{\tau})^{\theta}} \tag{4.2}$$

where t is the curing time in seconds, θ is the shape parameter constant, and τ is the time constant defined as $\tau = \theta/k$, where k is the rate constant. The time constant τ is an important parameter of the distribution since it represents when the degree of conversion $\alpha = 0.5$. A generalized reduced gradient (GRG) algorithm was used to minimize the sum of the errors squared between the experimental and modeled data by fitting different θ and k parameters.

4.3.6 Ultrasonics: elastic properties

The elastic properties of an isotropic material can be obtained using ultrasonics if its density, longitudinal speed, and shear speed are known [77], [117]. The density of a baseline sample (2:1 resin-to-hardener ratio) was obtained using a pycnometer from Micromeritics (AccuPyc II 1340). Using the ultrasonics setup previously mentioned in this section along with the cross-correlation method, a frequency sweep similar to the one performed by C. Pantea et al. [104] was used to accurately determine the longitudinal and shear sound travel times in the adhesive sample. For the longitudinal travel time, a frequency sweep from 0.9 to 2.3 MHz with a 0.1 MHz step was used, while for the shear travel time, a range from 0.5 to 1 MHz was used with the same step size. Different frequency ranges were used to obtain the longitudinal and shear travel times since a

minimum amount of signal was required to perform an accurate measurement, but the magnitude of the output signal varied for each frequency and wave type. For homogenous isotropic materials. For homogenous isotropic materials, equations 4.3 and 4.4 can be used to determine Young's modulus and Poisson's ratio, respectively [103]:

$$E = \rho c_s^2 \left(\frac{3c_l^2 - 4c_s^2}{c_l^2 - c_s^2} \right) \tag{4.3}$$

$$v = \frac{c_l^2 - 2c_s^2}{2c_l^2 - 2c_s^2} \tag{4.4}$$

where ρ is the density of the material, c_l is the longitudinal speed in, and c_s is the shear speed, E is Young's modulus, and v is Poisson's ratio.

To compare it with destructive testing, the Young's modulus of the adhesive was also determined using tensile testing. Three tensile testing dogbone samples were manufactured and tested following ASTM D638-03 [120]. The MTS tensile tester previously mentioned was used to test the dogbone samples at a loading rate of 5 mm/min. The size of sample type I in the standard was adapted to reduce the amount of material volume used per sample. The dimensions were reduced to have a total length of 87 mm while the thickness was 4.68 mm. The width at the center of the sample and at the grips was 6.84 and 10 mm, respectively. The samples were manufactured by casting the adhesive into a PLA 3D-printed mold.

4.4 Results

4.4.1 Thermal analysis

TGA was performed on the adhesive samples to analyze their thermal decomposition to demonstrate differences in their chemical composition due to the

presence of IPA in the studied samples. It can be observed in Figure 4.2a how the samples containing IPA started decomposing earlier than the baseline sample (0% IPA) at ~100 ◦C, which is most likely due to the solvent causing a decrease in their crosslinking density and an increase in their chain mobility. Similar behavior was observed by N. Othman et al. with 16 wt.% of acetone in an epoxy resin [21]. Figure 4.2b, which is an augmented version of what is located inside the dashed rectangle in Figure 4.2a, demonstrates how this behavior was more accentuated with increasing IPA content. All the samples experienced a sharp decrease in weight percentages with a similar onset temperature (~320 ºC). The adhesive samples containing 0, 2, 4, and 6 wt.% of IPA experienced a weight loss of around 2.3, 3.8, 4.8, and 6.2%, respectively.

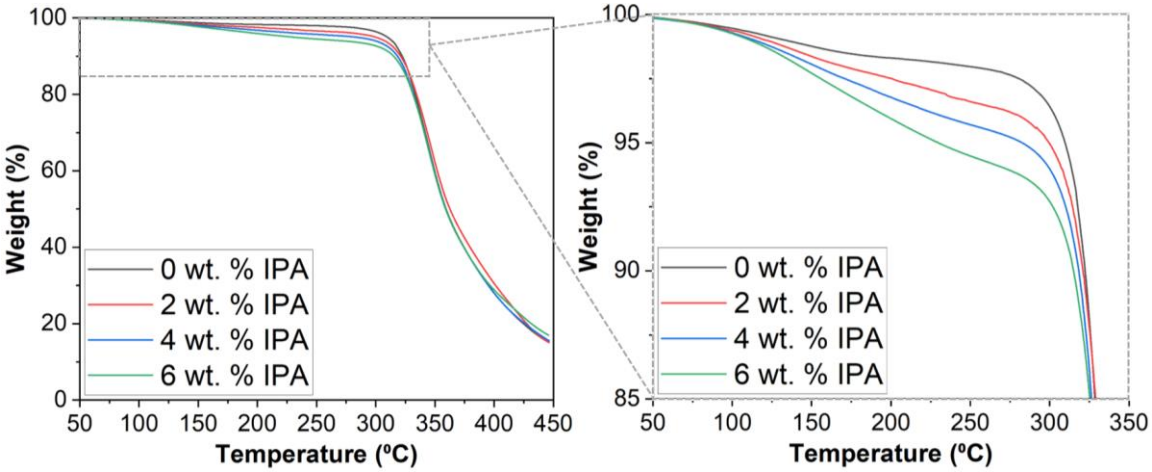

Figure 4.2. TGA of adhesive samples containing 0, 2, 4, and 6 wt. % of IPA (a) from 0 to 450 ºC; (b) from 50 to 350 ºC located inside the dashed rectangle of Figure 4.1a.

4.4.2 Fourier transform infrared (FTIR)

The FTIR spectra for the analyzed samples are shown in Figure 4.3. The region between 400 and 1600 cm^{-1} contains the fingerprint region for these materials and special attention was given to the area between 900 and 1000 cm^{-1} since one of the characteristic

peaks of IPA is located at 950 cm^{-1} [161]. As observed in the spectra of the adhesive samples containing IPA, a peak is present at that wavenumber, indicating the presence of this solvent within the adhesive's structure. On the other hand, this peak is not visible in the adhesive sample that contained no IPA. Having solvent within the structure of the adhesive may have altered the crosslinking process and caused a reduction in the molecular weight of some of the polymer chains [162].

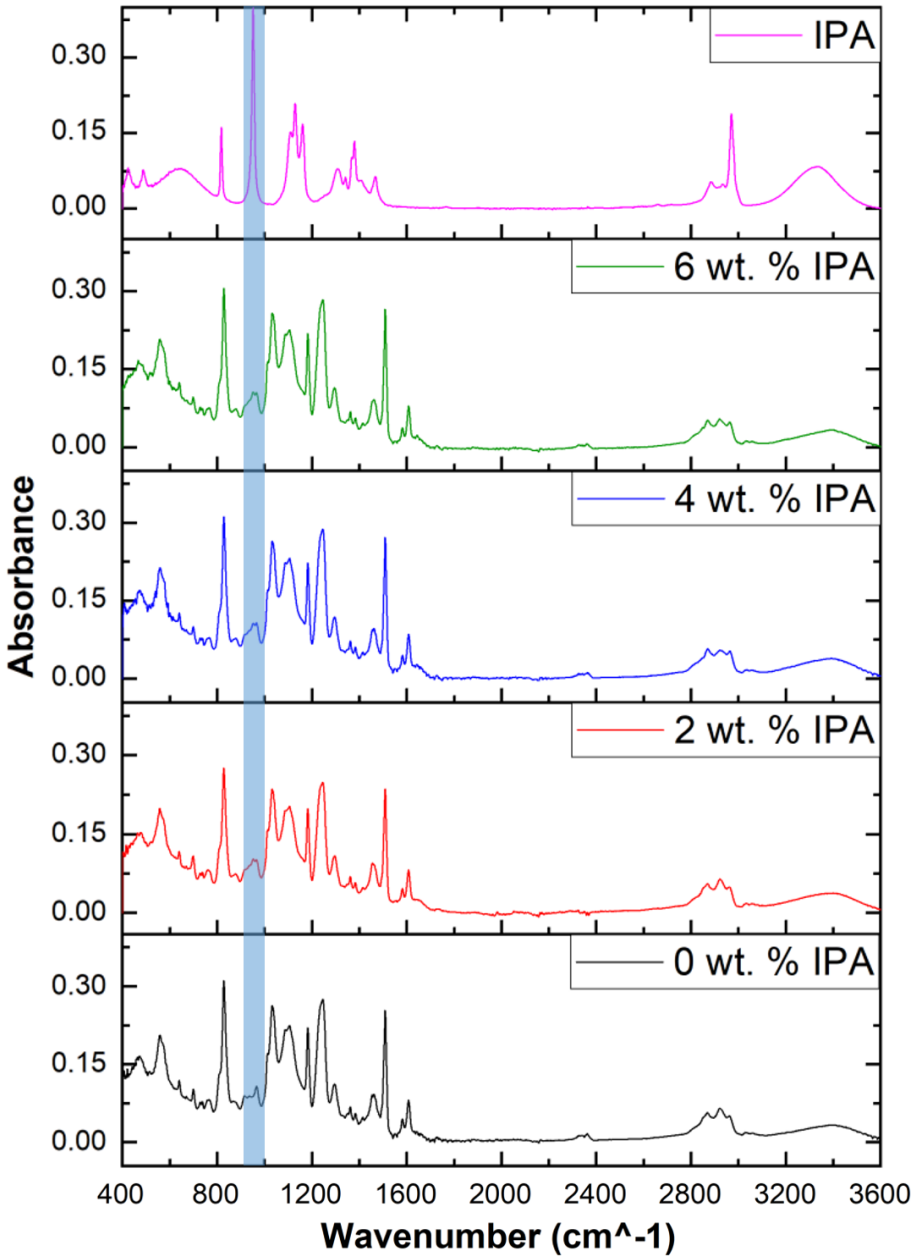

Figure 4.3. FTIR spectra for IPA and for cured adhesive samples containing 0, 2, 4, 6 wt. % IPA.

4.4.3 Single lap-shear

The resultant peak lap shear stresses for each of the specimens are recorded in. The average lap shear stress for the samples without IPA content was 21.18 MPa, which is consistent with what has been previously observed [82]. The samples containing IPA

experienced a considerable reduction in strength. The average lap shear stresses for the samples containing 2, 4, and 6 wt.% were 12.62 (−40.42%), 8.92 (−57.88%), and 6.07 MPa (−71.35%), respectively. These results show that even the presence of a small quantity of trapped solvent in the two-part epoxy adhesive considerably influenced its adhesion properties to the point where catastrophic failure could occur.

Table 4.1. Maximum lap-shear stress of samples containing 0, 2, 4, and 6 wt.% IPA.

Sample Type / Sample #	**Peak Lap-Shear Stress (MPa)**					
	1	2	3	4	**STD Dev**	**Avg Stress (MPa)**
0 wt. % IPA	21.37	17.63	25.55	-	3.46	**21.18**
2 wt. % IPA	13.02	15.29	11.21	10.96	2.00	**12.62 (− 40.42 %)**
4 wt. % IPA	8.81	6.96	10.73	8.18	1.68	**8.92 (− 57.88 %)**
6 wt. % IPA	6.65	6.91	5.16	5.56	0.84	**6.07 (− 71.34 %)**

The load–displacement curves of the specimens #1 in Table 4.1 for each sample type are shown in Figure 4.4a. The presence of IPA not only lowered the maximum load, but it also decreased the displacement required for failure to occur. This displacement ranged from 3.26 mm for the sample without IPA content down to 0.88 mm for the sample containing 6 wt.% IPA. As seen in Figure 4.4b, all the sample types experienced the same failure mechanism where the samples failed at the adhesive–substrate interface. No visual differences on the failure surfaces between each sample type were observed, which accentuates the need for a non-destructive evaluation method for this type of material.

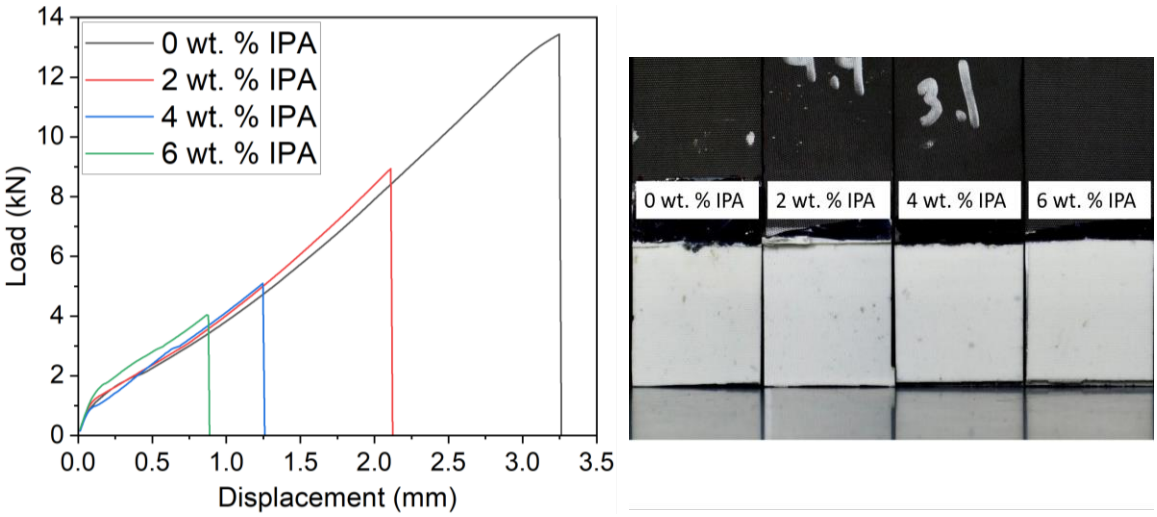

(a) (b)

Figure 4.4. (a) Load-displacement curves of the specimens #1 in Table 2 for each sample type; (b) failure surfaces for the specimens represented in the load-displacement curves in Figure 4.3a.

4.4.4 Monitoring the sound travel speed during the curing process using ultrasonics

The longitudinal sound speed was first evaluated in three adhesive baseline samples during their curing process. The samples were fabricated and tested simultaneously to determine the repeatability of the analysis technique. It can be observed in Figure 4.5 that the sound speed of the three samples behaved very similarly, where a sharp increase in sound speed occurs during the first four hours of curing, followed by a convergence until the sample is fully cured. After four days of curing, the final sound speeds for the first, second, and third baseline samples were 2319 (±47) m/s, 2317 (±46) m/s, and 2320 (±47) m/s, respectively. The difference between the samples with the highest and lowest sound speeds was ~0.13%.

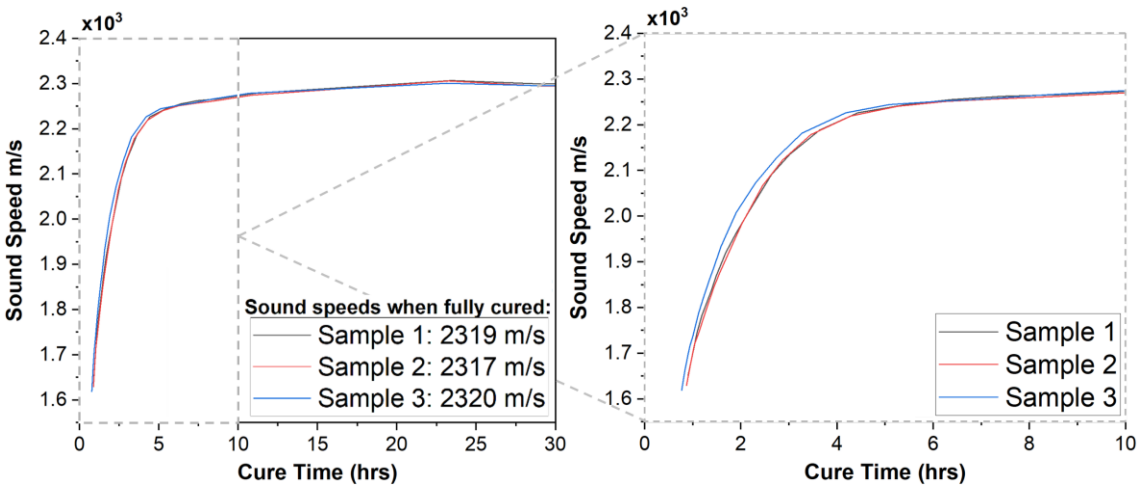

Figure 4.5. Sound speed with respect to cure time of three adhesive baseline samples during (a) the first 30 curing hours; (b**)** the first 10 curing hours located in the dashed rectangle in Figure 4.4a.

After adding 2, 4, and 6 wt.% of IPA to the adhesive samples to simulate a trapped solvent, their sound speed was also evaluated during the curing process. Figure 4.6 shows how, unlike as previously seen with the baseline samples, the curing process differs for each sample. The sound speed of the sample with no IPA content started converging at a lower cure time while adding IPA delayed the convergence process. To give some perspective, the curve onset of the sample with 0 wt.% IPA occurred at 1.89 curing hours, while the onset for the samples with 2, 4, and 6 wt.% IPA occurred at 2.77, 3.34, and 3.99 curing hours, respectively. This shows a difference of approximately 2.1 h between the baseline sample without IPA and the sample containing 6 wt.% IPA. In addition, the sound speeds after four curing days for the samples with 0, 2, 4, and 6 wt.% of IPA were 2322 (±47), 2369 (±49), 2354 (±48), and 2351 (±48) m/s, respectively. This shows how IPA content not only affected the curing mechanics of the adhesive but also its final sound speed.

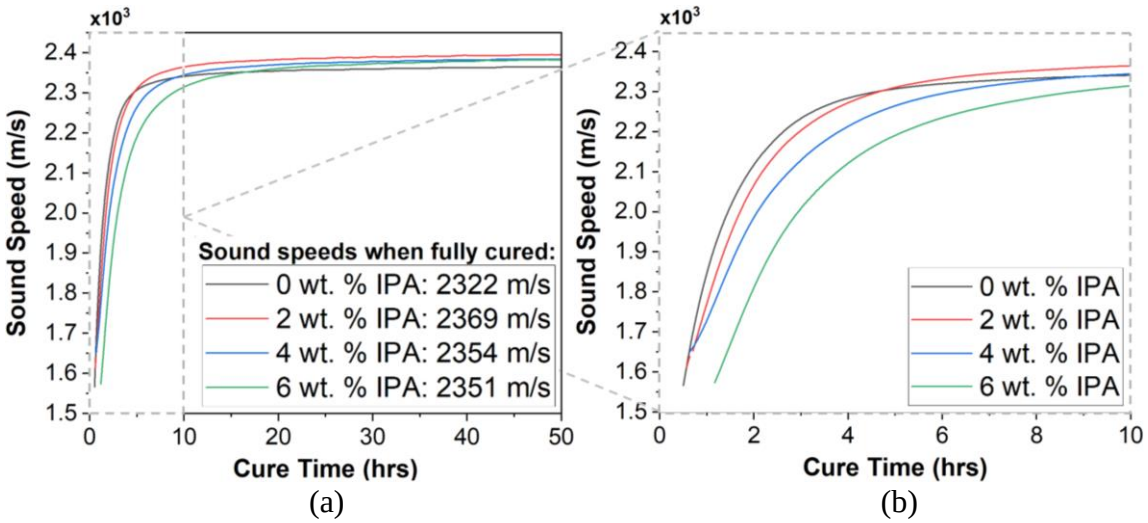

Figure 4.6. The sound speed with respect to cure time of adhesive samples containing 0, 2, 4, and 6 wt. % of IPA during (a) the first 30 curing hours; (b**)** the first 10 curing hours located in the dashed rectangle in Figure 5a.

4.4.5 Cure modeling using the Hill equation

To numerically understand how trapped solvent affected the cure kinetics of the adhesive, the Hill equation was used to model the curing process for each of the samples. First, to better visualize the curing process, the curves shown in Figure 4.6a were normalized and plotted in Figure 4.7a. This graph represents the degree of conversion α of the adhesive, which ranged from zero (at the beginning of curing) to one (when the adhesive was fully cured). As previously seen in Figure 4.6b, it is also clear in Figure 4.7a how increasing IPA content delayed the converging process. Figure 4.7b compares the experimental and theoretical curves of the baseline adhesive sample containing no IPA. The Hill model gives a good estimate of the curing kinetics of the adhesive.

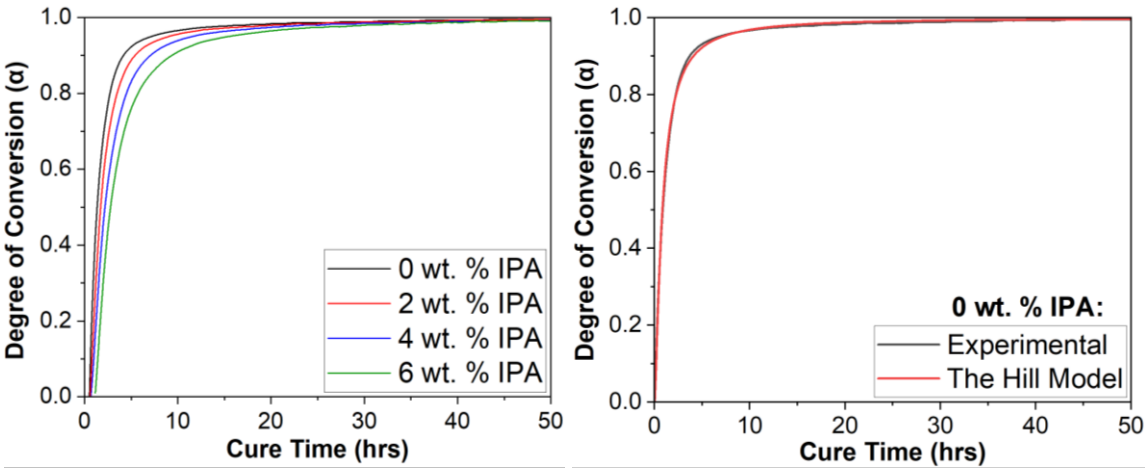

(a) (b)

Figure 4.7. Degree of conversion with respect to cure time of (a) adhesive samples containing 0, 2, 4, and 6 wt. % of IPA; (b) experimental and model using the Hill equation of the 0 wt. % IPA sample.

The values for the rate constant k and the shape parameter θ obtained for each sample type after fitting the experimental data to the Hill equation using a GRG algorithm are summarized in Table 4.2. As expected, the rate constant decreased with increasing IPA content, although the decreasing rate decayed with increasing solvent content. On the other hand, the shape parameter for all the samples ranged between 1.35 to 1.48 and no particular trend was observed. The sum of errors (between the experimental and theoretical values) squared was small, meaning that the modeling resembled the experimental results.

Table 4.2. Rate constant k and shape parameter θ of the Hill equation model for each sample type.

Sample	$\boldsymbol{k}$ $(*\ \mathbf{10^{-4}})$	$\boldsymbol{\theta}$	**Sum of Error Sq**
0 wt. % IPA	4.63	1.37	0.0352
2 wt. % IPA	3.48	1.46	0.0262
4 wt. % IPA	2.66	1.48	0.0224
6 wt. % IPA	2.34	1.35	0.0244

4.4.6 Young's modulus using ultrasonics

The density of the adhesive baseline sample was found to be 1.113 g/cm^3 . This experimental value is slightly under the theoretical density of 1.133 g/cm^3 obtained using

the mass fractions of the resin and hardener components and their corresponding densities. This could have been caused by the presence of porosity introduced during the mixing process.

Figure 4.8 shows the longitudinal and shear time delays after performing the cross-correlation between the excitation and output signals versus the inverse of the frequency. Similar to the method used by C. Pantea et al. [104], a total of five peaks of the cross-correlation were used: one corresponding to the overlap between the excitation; two to the left side of the overlap; and two to the right side of the overlap. After plotting and extrapolating the linear fits to a frequency of infinity, the intercept of each of the cycles where the inverse of the frequency equaled zero provided the sound travel time in the sample. After taking into account the transducers and mold delay, the longitudinal travel time ranged from 4.881 to 4.951 μs, which resulted in a sound speed of 2271 ± 18 m/s. For the shear travel time, the time delay ranged from 11.240 to 11.293 μs, which resulted in a sound speed of 983 ± 21 m/s. Using these longitudinal and shear sound speeds in the adhesive, Young's modulus and Poisson's ratio were calculated using Equations (4.3) and (4.4), respectively. The Young's modulus was determined to be 2.963 ± 0.133 GPa, while the Poisson's ratio was calculated to be 0.385 ± 0.005.

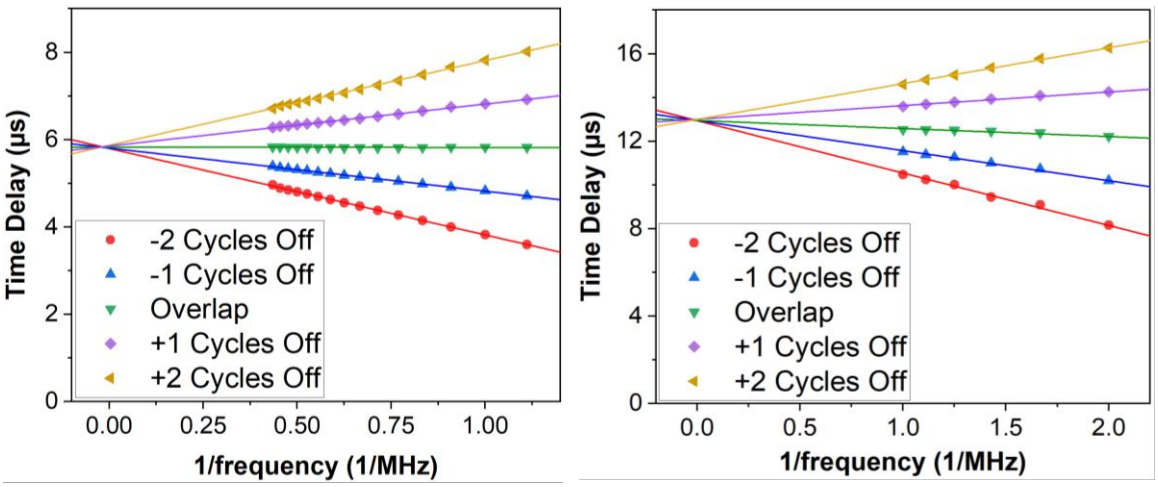

Figure 4.8. **(**a) The longitudinal time delay between the excitation and output signal vs 1/frequency; (b) the shear time delay between the excitation and output signal vs 1/frequency.

The average Young's modulus obtained using tensile testing was 2.906 ± 0.073 GPa. This represents a difference of 1.92% with respect to the value determined using ultrasonics. This demonstrates the capability of ultrasonics as a non-destructive evaluation tool for measuring the elastic properties of an epoxy adhesive. ºC

4.5 Discussion

The presence of residual solvent in polymeric materials can considerably affect their curing process and chemical structure, thus altering their mechanical properties as well. In samples designed to observe this phenomenon, TGA confirmed that the presence of varying weight percentages of IPA in the adhesive affected its decomposition. Figure 2 shows how a higher wt.% of IPA caused higher weight loss from 100–320 °C, which is due to the IPA likely influencing the curing process of the adhesive [21], [162]. This affected its chemical structure by possibly increasing the presence of lower molecular weight chains, which underwent thermal degradation earlier. FTIR also verified the

presence of IPA within the structure of the adhesive which may have affected the crosslinking process during curing. Similar behavior was observed by M. Loos et al. when they investigated the effect of acetone on the properties of an epoxy resin [162].

Lap shear testing showed that the presence of trapped solvent in an adhesive can heavily decrease its adhesion properties. This is consistent with the results reported by C. Yi et al., in which they showed how the addition of 14 vol. % of xylene solvent into an epoxy adhesive decreased its adhesion strength by 35% [163]. They also reported that the samples with this same amount of solvent experienced a decrease of 60% in their tensile strength compared to the pristine resin samples. Figure 4b demonstrates that adhesive failure was obtained but no major visual changes in the failure surfaces occurred for the different sample types. This emphasizes the need for a non-destructive evaluation method since performing destructive testing to obtain the properties of adhesives is time-consuming and costly. Ultrasonics can help in performing in situ testing during the manufacturing process, and, as shown in Section 4.4.6, in obtaining the elastic properties of polymers if their density is known.

It was demonstrated that ultrasonics can be used to monitor the curing process of an epoxy adhesive by evaluating changes in sound speed due to variations in its chemical structure. The first test shown in Figure 4.5 of three different baseline adhesive samples shows that the ultrasonics setup could repeatedly be used to monitor the kinetics of polymer curing. This helped determine that the fluctuations in the curing behavior of the samples containing residual solvent (Figure 4.6) were due to the IPA preventing an ideal curing rate of the adhesive. Previous work has shown that the tensile strength of this adhesive with respect to cure time starts converging between curing hours 8 and 10 [81], [164], meaning

that the sound speed is more sensitive than tensile strength to the gelation process and early crosslinking between the polymer chains of the curing adhesive. Repeated laboratory testing reflected that both the mixing technique and the adhesive's temperature could influence its curing process. In addition, evaluating the sound speed in fully cured adhesives that are manufactured properly can serve as an in-field quality control method during the lifetime of those materials. The evaluation of the elastic properties of the epoxy adhesive using ultrasonics was corroborated with tensile testing values, validating this non-destructive evaluation method.

Modeling the curing process using the Hill equation helped in achieving a better numerical comprehension of how the curing rate of the adhesive was affected by the trapped solvent. This model can predict how improper manufacturing influences the properties of materials by correlating the rate constant k and shape parameter θ to the strength of the polymer. A decreasing trend was observed for the rate constant although no variation was found for the shape parameter. Further analysis will be performed to correlate k and θ to the types of chemical reactions occurring during the curing process and how those influence the final mechanical properties of the polymer, which, to the authors' knowledge, is a work that has yet to be performed. If a specific curing mechanism is associated with the final structure of the polymer, in situ analysis during the curing process could also determine if a part is safe or unsafe to use before waiting for the whole manufacturing process to be completed.

4.6 Conclusions

Solvents are commonly used during the manufacture of polymeric materials, which raises concerns about their proper removal. The influence of residual solvent on the curing

process of an epoxy adhesive was studied. It was observed that the presence of IPA in the adhesive can have a significant impact on its physical and chemical properties. FTIR confirmed the presence of IPA within the polymer structure, while TGA showed that the solvent caused an increased and faster decomposition at lower temperatures. Catastrophic consequences can occur due to the considerable decrease in the adhesion properties of the epoxy, as revealed by the lap shear test. This suggests the need for the development of a non-destructive method for evaluating the curing process and viscoelastic properties of polymers. Ultrasonics have shown promising results for becoming a tool for polymer quality evaluation in both manufacturing and in-field settings.

Chapter 5 Coupling Ultrasonics and FTIR to Non-destructively Characterize Changes in Cure Kinetics, Chemical Structure, and Thermal Properties of an Epoxy as a Function of Varying Stoichiometry.

5.1 Abstract

Epoxy resins are thermosets with increasing demand in high-performance applications as a lightweight and cost-effective alternative. However, controlling and monitoring the manufacturing parameters, which can impact the curing process of the polymer and its final quality, is a difficult task. To address this issue, destructive testing is typically performed for quality control and material characterization, which involves expensive lab-type equipment and instrument-specific sample preparation. Moreover, this type of testing cannot be taken in-field to perform an in-situ evaluation. To overcome these issues, this work presents a novel method to non-destructively evaluate the curing kinetics and viscoelastic properties of epoxy resin in real time due to variations in the manufacturing process, combining ultrasonics and Fourier Transform Infrared Spectroscopy. Samples with a different amine-to-epoxy ratios were manufactured and

tested, and thermogravimetric analysis revealed that deviations from the manufacturer's recommended ratio decreased the thermal stability of the system. Furthermore, changes in longitudinal sound speed were detected during the resin's curing process, resulting from variations in the polymer's chemical structure. The longitudinal and shear sound speeds were used to calculate the viscoelastic properties of the material, including Young's modulus and Poisson's ratio. Finally, the curing kinetics were modeled using the Hill equation to better understand numerically the effect of varying stoichiometry in the curing process. This approach has the potential to non-destructively characterize the properties of polymers in both an in-field and manufacturing setting, aiding in the tailoring process and ensuring their reliability in demanding applications.

5.2 Introduction

Epoxy-amine resins are widely used in the manufacture of composites, coatings, and adhesives due to their excellent mechanical, thermal, and electrical properties [111], [165] [28]. This type of polymer is very versatile since its final properties can be tailored for specific applications by changing its chemistry, i.e., the resin to hardener stoichiometry. For example, having excess amine in the epoxy can cause an increase in fracture toughness while decreasing the fatigue crack propagation [6], [58]. On the other hand, this can also reduce the glass transition temperature and allow higher moisture ingression, among other deteriorating properties [20], [59]. Finding the optimal stoichiometry depends on the final properties of interest for each application.

The chemistry of the polymer also affects its curing process. When the epoxy and hardener are mixed and curing starts, microgel particles form containing low molecular weight. Then, these chains start linking together until they comprise the continuous phase.

At this point of the cure, vitrification happens, where the reaction rate drops and further crosslinking is diffusion/mobility dependent [28], [29]. However, some uncrosslinked molecules are not able to come together and react, preventing a complete cure. This will only occur if the epoxy's temperature is raised to its glass transition temperature Tg [60]. Preventing the presence of unreacted amine can be achieved by using excess epoxy [61]. However, altering the curing process causes a variation in microstructure due to the changes in crosslinking density and molecular weight [13], [25], [61]. K. Frank et al. showed how having a 25 % excess epoxy in a system containing diglycidyl ethers of bisphenol-A (DGEBA) cured with 3,3'-diaminodiphenylsulfone (DDS) caused a decrease in crosslinking density of more than 50 % [55]. Similarly, F. Meyer et al. decreased the amine content in a DGEBA/DDS epoxy-amine resin system by 25 %, which caused an increase in molecular weight from 265 to 596 amu due to an increase in crosslinking density [62]. Understanding how the epoxy chemistry network relates to stoichiometry is not only needed to tailor the material's properties but also to optimize the use of fillers and other additives in the resin [63].

As a consequence of varying chemical structure, the mechanical and thermal properties of epoxies are influenced by the epoxy/amine stoichiometry [19], [61]. J. Szabelski et al. tested the adhesive joint strength of an Epidian 57/PAC epoxy resin cured at 25 ºC for seven days [65]. They showed how the joint strength decreased from 27.10 MPa to 23.49 and 13.65 MPa with – 30 % and + 30% of PAC hardener content, respectively. They also demonstrated that both curing and testing at increased temperatures enhance joint strength when having a reduced amount of hardener. The higher temperature increased mobility which allowed for all the epoxy molecules to diffuse and bond with the

hardener. M. A. Andres et al. demonstrated how amine-rich mixtures experienced increased flexural strength and ductility, while the epoxy-rich counterpart showed a more brittle behavior with a decreased strength [31]. This is corroborated by S. Pandini et al. and J. R. M. D'Almeida et al., who obtained a brittle to ductile transition with increasing hardener amount and observed plastic deformation in hardener-rich formulations [66], [67]. Considerable changes in glass transition temperature (T_g) occur with varying epoxy/amine stoichiometry. H. Wang et al. obtained a decrease in T_g from 87.2 to 73.7 ºC of a bisphenol A epoxy resin with a diamine curing agent when using 20 % less epoxy due to a reduction in cross-linking density [68]. F. Bignotti et al. also observed a reduction in T_g when using excess amounts of both epoxy and hardener, obtaining the highest glass transition temperature when using the recommended epoxy/hardener ratio by the manufacturer [19]. This shows how T_g can be used to find the optimum stoichiometry for enhanced thermal properties.

Destructive testing, including differential scanning calorimetry (DSC), thermogravimetric analysis (TGA), dynamic mechanical analysis (DMA), or tensile testing, is used to determine the thermal and mechanical properties of polymers [81], [82], [113], [166]–[168]. DSC is also implemented to evaluate the cure kinetics of polymers for different curing parameters [11], [169]. The main three downsides of destructive testing are that it requires lab-type equipment that cannot be taken in-field, it is invasive, and requires specific sample preparation and geometry. Thus, it is important to develop a non-destructive evaluation method that can characterize the cure kinetics and elastic properties of polymers under different manufacturing conditions [77].

Ultrasonics involves using acoustic waves at frequencies higher than 20 kHz and can be used to evaluate the phase transitions during cure and the physical properties of materials due to its high precision [77], [115]. In previous work, ultrasonics were utilized to non-destructively characterize the influence of residual solvent in the curing mechanics and viscoelastic properties of an epoxy adhesive. The effect of temperature on the cure kinetics of epoxy resins has also been investigated using ultrasonics [26], [77], [106]. However, a deeper understanding of how this method correlates to the chemical structure and final properties of polymers due to varying manufacturing parameters is needed. Since Fourier transform infrared spectroscopy (FTIR) non-destructively characterizes the chemical structure of a polymer, combining this method with ultrasonics can help investigate in-situ how varying stoichiometric formulations affect the chemical structure of polymers. Correlating how changes in chemical structure influence the cure kinetics and final mechanical and thermal properties of a polymer will allow to optimize the resin-to-hardener ratio for each specific application.

The focus of this paper is to detect changes in the cure kinetics and in the final properties of an epoxy resin using ultrasonics and FTIR as a result of varying stoichiometry. In this study, a resin was manufactured and tested with different amine-to-epoxy ratios. Since modifying the chemical structure affects the crosslinking density and mobility of the resin, TGA was performed to analyze the thermal stability of each of the sample types. We hypothesize that the sending and receiving of ultrasonic waves have the ability to detect how the change in stoichiometry influences the curing process of the resin. This curing process was modeled to better understand how variations in stoichiometry affect the curing mechanics of the material. Correlating FTIR and ultrasonics creates a

unique methodology to perform in-situ, non-destructive quality control method in the manufacturing process.

5.3 Materials and Methods

5.3.1 Materials and Sample Preparation

A liquid epoxy resin (EPON 828, Hexion) was used for this study. EPON 828 is derived from difunctional bisphenol A/epichlorohydrin and it is known for its versatility due to its good mechanical, adhesive, dielectric, and chemical resistance properties [111], [165]. A liquid curing agent (EPIKURE 3234, Hexion) from the family of unmodified aliphatic amines was used for room-temperature curing. The recommended manufacturer concentration of the curing agent is 13 phr (parts per 100 resin by weight), which corresponds to a 6.5 to 1 resin-to-curing agent ratio by volume. Samples with an amine-to-epoxy ratio, r, of 0.6, 1, and 1.4 were manufactured, where r = 1 is the recommended ratio. The samples with r = 0.6 and r = 1.4 have -40% and +40% of amine content, respectively. The resin and hardener were thoroughly mixed for five minutes before being poured into the printed mold. The curing and testing were conducted in a laboratory setting that was regulated to a temperature of approximately 21 ± 2 °C and relative humidity of ~44 ± 2.5 %.

5.3.2 Thermal Analysis (TGA)

Thermal analysis was performed using a Q600 SDT (TA Instruments) on resin samples with r = 0.6, 1, and 1.4. The tests were conducted by heating the samples from room temperature (~21 °C) to 600 °C at a rate of 5 °C/min, while argon gas was used as a purging agent. The weight of the samples ranged between 9 and 9.5 mg.

5.3.3 Fourier Transform Infrared (FTIR)

A Nicolet iS50 (Thermo Scientific) spectrometer was used to conduct FTIR. Scans were taken from 4000 to 400 cm^{-1} with a resolution of 0.482 cm^{-1}. Sixteen scans were used and the spectra were graphed in absorbance mode. Resin samples with r = 0.6, 1, and 1.4 were tested during the cure. Spectra were collected every 2 minutes. The samples were placed on a golden gate diamond top plate (Specac) equipped with a KRS-5 lens. The lens was cleaned using ethanol followed by DI water before each sample.

5.3.4 Ultrasonics: Curing Process and Elastic Properties

To non-destructively evaluate the sound speed of the resin during cure, the resin was first mixed and poured into a resin 3D printed mold using Form Labs rigid 10k resin. Add new mold dimensions. A function generator (AFG31052, Tektronix) was used to generate a sine burst at 10 volts peak-to-peak with a frequency of 500 kHz. This frequency for the excitation waveform was selected since it gave the strongest output signal for this sample size and material. A Tukey window with a cosine fraction, r, of 0.4 was used to taper the input function consisting of five cycles [114]. Transducers placed at opposite sides of the filled mold transmitted and detected the signal. 2.25 MHz transducers (V133-RM and V154-RM, Olympus) were used for evaluating the longitudinal and shear sound speeds, respectively. To ensure adequate contact and signal transmission between the sample and the transducers, an ultrasound couplant (Echo Ultrasonics) was utilized. An oscilloscope (MDO32, Tektronix) was used to record the resulting waveforms every two minutes during the curing process.

The excitation waveform along with the output waveforms were then used to obtain the longitudinal and shear sound travel time across the sample utilizing the cross-correlation method [170]. Using the same method from previous work, the sound speed in

each of the samples was calculated from the travel time and thickness of the samples using equation X as follows:

$$c = \frac{d}{t} \tag{5.1}$$

where d is the thickness of the sample and t is the sound travel time. The thickness was measured using a digital micrometer once the samples were fully cured. To account for the uncertainty resulting from the oscilloscope's and micrometer's resolution (9 ns and 0.01 mm, respectively), the law of propagation of uncertainty was employed to calculate the error related to the velocity computations [116].

Since the epoxy resin used is a dispersive medium, the sound travel speed is dependent on the frequency utilized. Thus, to accurately determine the longitudinal and shear sound travel times, the cross-correlation method along with a frequency sweep method similar to the one performed by C. Pantea et al. [104]. A frequency sweep ranged from 0.9 to 2.3 MHz with a 0.1 MHz step. In the case of homogeneous isotropic materials, once the longitudinal and shear sound speeds have been calculated and the density of the material is obtained, equations 5.2 and 5.3 can be used to determine the Youngs modulus and Poisson's ratio, respectively [103]:

$$E = \rho c_s^2 \frac{c_l^2 - 2c_s^2}{2c_l^2 - 2c_s^2} \tag{5.2}$$

$$v = \frac{c_l^2 - 2c_s^2}{2c_l^2 - 2c_s^2} \tag{5.3}$$

where ρ is the density of the material, c_l is the longitudinal speed in, and c_s is the shear speed, E is Young's modulus, and v is Poisson's ratio. The density of the samples was obtained using Archimedes' method.

5.3.5 Cure process modeling

The Hill equation was used to model the curing process for each sample. This was used to better understand how variations in stoichiometry affect the curing mechanics of the resin and to allow for future predictions of material quality. The degree of conversion, α(*t*), ranges from 0 to 1 and can be expressed using the Hill equation as shown in equation 5.4 [119]:

$$\alpha = 1 - \frac{1}{(\frac{t}{\tau})^{\theta}} \tag{5.4}$$

where *t* is cure time in seconds, θ is the shape parameter constant, and τ is the time constant defined as $\tau = \theta/k$, where *k* is the rate constant. The time constant τ is an important parameter of the distribution since it represents when the degree of conversion α = 0.5. A generalized reduced gradient (GRG) algorithm was used to minimize the sum of the errors squared between the experimental and modeled data by fitting different θ and *k* parameters.

5.4 Results and Discussion

5.4.1 Thermal Analysis (TGA)

Since thermal stability is highly dependent on the chemical structure of the polymer, TGA was performed on fully cured samples to demonstrate how the varying stoichiometry affected the decomposition of the epoxy resin. It can be observed in Figure 5.1 how the samples containing either excess resin or hardener experienced an increased decomposition at the 250-325 ºC temperature range. The system with excess resin (r = 0.6) had the most weight loss in the aforementioned temperature range. H. Wang et al. describe a very similar decomposition behavior when mixing bisphenol A epoxy resin with a diamine curing agent, in which decreasing the amine/resin ratio caused an increase in

thermal instability due to a reduction in cross-linking density [68]. The increased weight loss at lower temperatures could have also been caused by the presence of lower molecular weight chains, which undergo thermal degradation earlier. However, the sample with the most excess amount of curing agent (r = 1.4) became the least thermally stable at temperatures higher than 325 ºC. The system with the recommended stoichiometry (r = 1) was the most stable from room temperature until 325 ºC, which correlates with companies using thermal analysis to optimize the amine/epoxy ratio.

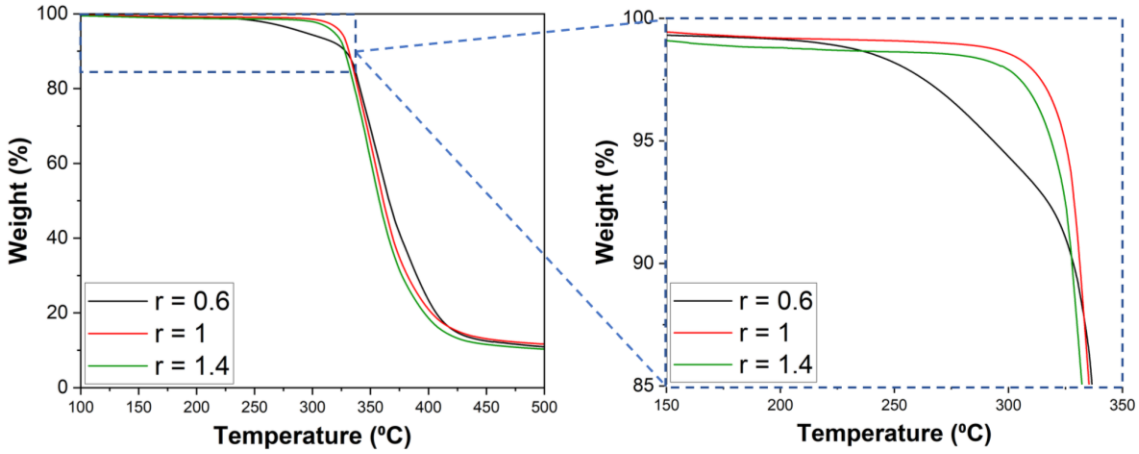

Figure 5.1. TGA of resin samples containing r = 0.6, 1, and 1.4 (a) from 0 to 500 ºC; (b) from 150 to 350 ºC located inside the dashed rectangle of Figure 5.1a.

This thermal analysis demonstrates how varying the amine/resin stoichiometry affects the chemical structure of the cured polymer. Increasing the resin amount possibly increases the presence of lower molecular weight chains, which undergo thermal degradation earlier. The presence of unbonded amines due to an excess amount of curing agent also induces lower thermal stability.

5.4.2 FTIR

Since the molecular structure of the resin changes during cure, FTIR is able to

monitor the cure kinetics. The spectra at 0, 0.5, 2.5, 5, and 22 curing hours of the r = 1 sample are displayed in Figure 5.2. It can be observed how the peak located at 913 cm^{-1}, corresponding to the epoxy groups, decreases in intensity as the cure proceeds due to epoxy consumption. Note that the epoxy is not fully consumed since the reaction cannot be fully completed due to the decreased mobility/diffusion at vitrification, which prevents the epoxy and amine molecules from finding each other and bond. The temperature of the resin would have to be increased above its glass transition temperature to further complete the reaction.

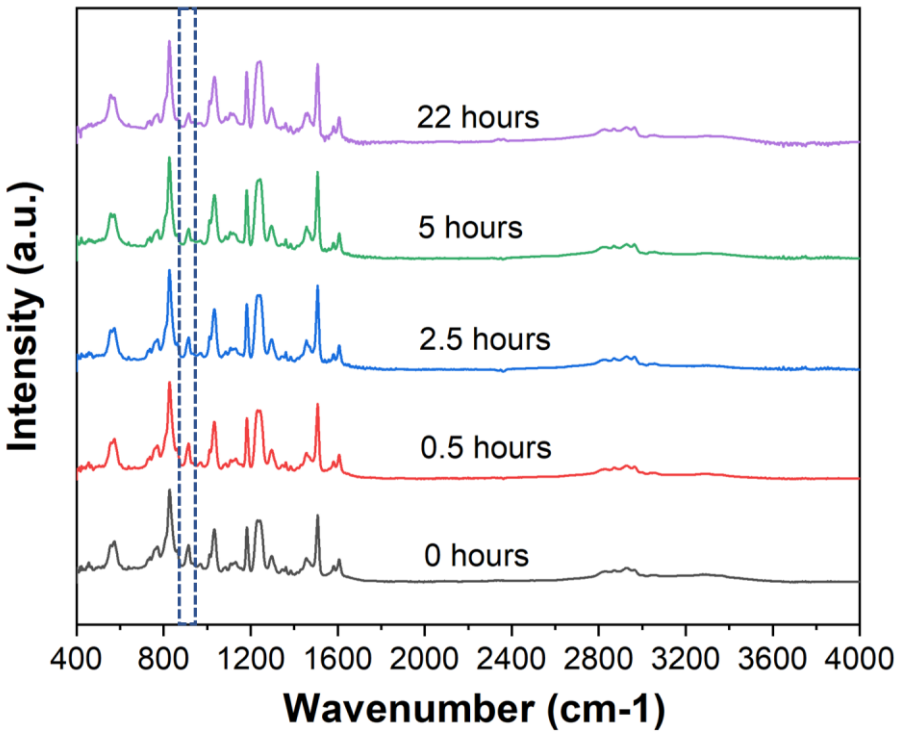

Figure 5.2. FTIR spectra of the r = 1 sample at different curing times.

The FTIR spectra between 875 and 950 cm^{-1} of fully cured samples are shown in Figure 5.3a. They exhibit how the 913 cm^{-1} peak corresponding to the epoxy group

decreases in intensity with an increasing amount of hardener present in the sample. The sample with 40% excess hardener (r = 1.4) experiences the highest epoxy consumption. This trend is also observed in Figure 5.3b, which contains the intensity of the epoxy group peaks during cure. To allow for a better visual comparison, the intensities were shifted so that their initial points at cure time 0 were coincident.

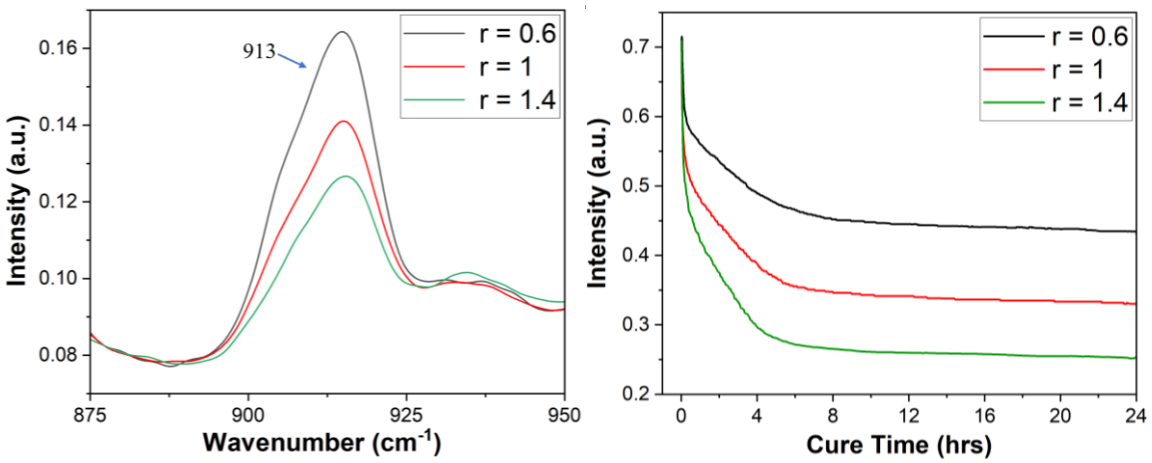

Figure 5.3. (a) FTIR spectra of the three different ratios between 875 and 950 wavenumbers; (b) intensity of the epoxy group peak (913 cm^{-1}) of the three ratios during cure.

To quantify the rate at which the epoxy was being consumed for each of the sample types, the intensities of the 913 cm^{-1} peaks were normalized with respect to the intensity of the 1034 cm^{-1} peak. This peak is associated with the phenyl band and is taken to be chemically unmodified during the curing process. The degree of conversion α of the r = 0.6, 1, and 1.4 resin samples are plotted in Figure 5.4. It can be observed how the epoxy of the amine-rich system (r = 1.4 sample) is consumed at a faster rate compared to the other samples. Similarly, the epoxy-rich system (r = 0.6) shows a slower cure. The onsets of the curves were evaluated to be 5.44, 4.89, and 4.53 hours for the r = 0.6, 1, and 1.4 samples,

respectively. This clearly demonstrates that the amine-to-epoxy ratio influences the cure kinetics of the epoxy resin.

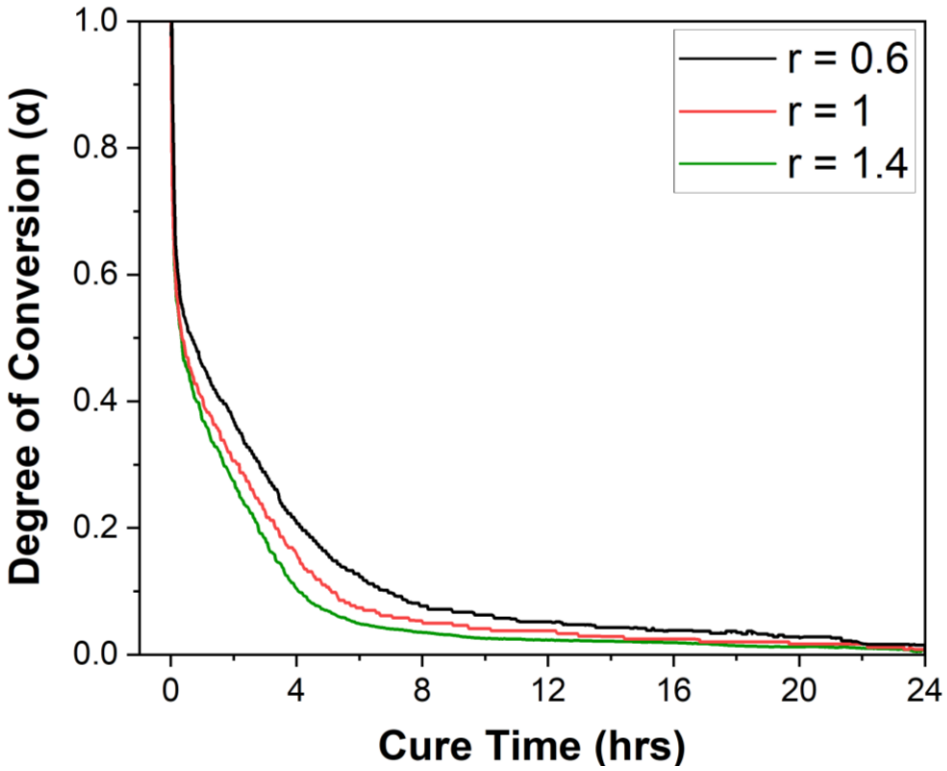

Figure 5.4. Degree of conversion of the intensity of peak 913 cm^{-1}.

5.4.3 Ultrasonics

The longitudinal sound speed was evaluated in the four sample types during the curing process. Figure 5.5a shows how the curing process differs for each sample due to the varying stoichiometry. The epoxy resin cured at a faster rate with an increasing amount of curing agent. The curve onsets for the r = 0.6, 1, and 1.4 samples were 5.36, 4.88, and 4.34 hours, respectively. This shows a similar trend to the one observed with FTIR, especially regarding the r = 1 and 1.4 samples, although ultrasonics converged at an earlier time for the r = 0.6 sample. The excess amount of amine reduces the diffusion required for

the epoxy and amine molecules to find each other and bond, thus speeding up the curing process. This also allows for almost a complete reaction of the epoxy molecules present. Experimentally, achieving a complete consumption of the epoxy molecules will most likely not occur. When vitrification occurs, the diffusion/mobility drops, which impedes a full reaction to happen.

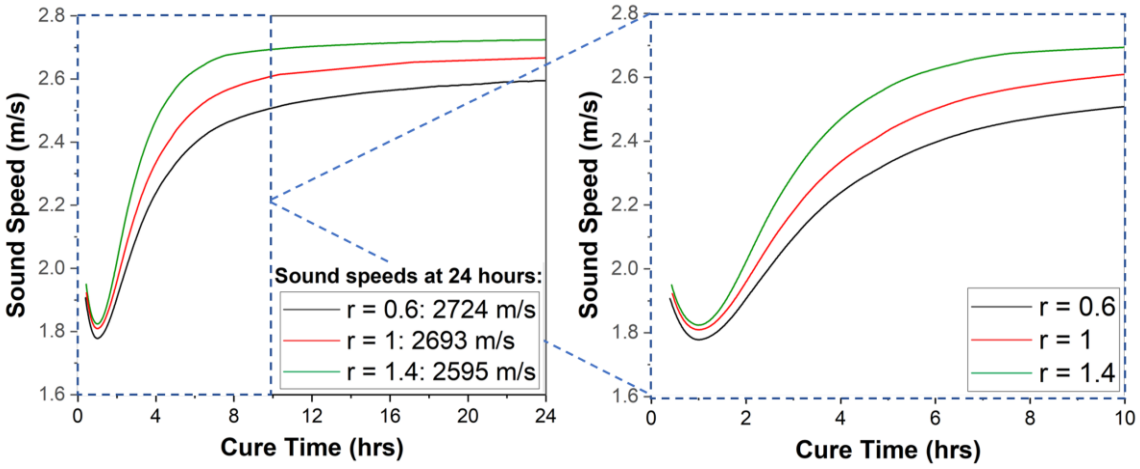

(a) (b)

Figure 5.5. The sound speed with respect to the cure time of resin samples with r = 0.6, 1, and 1.4 during (a) the first 24 curing hours; (b) the first 10 curing hours located in the dashed rectangle in Figure 5.2a.

The sound speed in the samples at 24 curing hours indicates that the viscoelastic properties are also affected by the change in chemical structure, where the stiffness of the epoxy increased with amine content. The longitudinal sound speeds for the r = 0.6, 1, and 1.4 samples were 2595 (± 46), 2667 (± 47), and 2724 (± 51) m/s, respectively. This shows how the system's stoichiometry not only affects the curing mechanics of the resin but also its mechanical properties, which has been proven by various researchers [31], [171].

Since sound speed increases as the reaction and cross-linking proceeds, it has an inverse relationship with the FTIR intensity of the epoxy group peak 913 cm^{-1}. It is appreciated in the plot in Figure 5.6 how the sound speed increases as the epoxy group is

consumed as the reaction proceeds. Both the sound speed and the FTIR intensity of the 913 cm^{-1} peak start converging when the vitrification phase occurs and the reaction rate decreases.

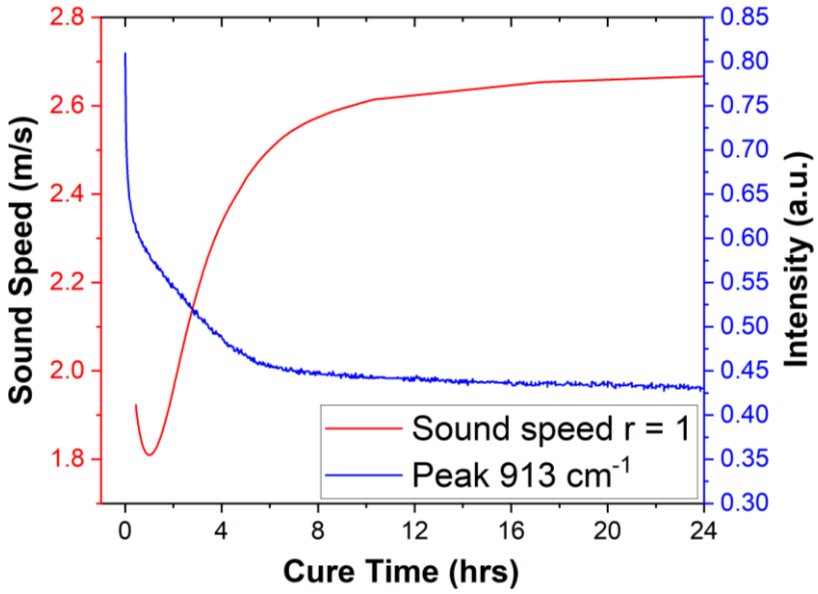

Figure 5.6. Sound speed and FTIR intensity of the epoxy group during cure for r = 1.

To further correlate the sound speed and the chemical structure of the resin during cure, the FTIR intensity of the peak 1106 cm^{-1}, which corresponds to the C-H aromatic stretching, and the sound speed were plotted and compared in Figure 5.7. The intensity of the C-H aromatic stretching closely follows the trend of the sound speed during cure, which is related to the mechanical properties of the polymer. This trend is observed for all the sample types. During the first curing hour, both the sound speed and the 1106 cm^{-1} peak intensity decrease. This can be due to the relaxation of the polymer chains caused by the increase in temperature of the material, which induces a decrease in viscosity. Then, as the reaction proceeds, cross-linking between the polymer chains occurs. This causes both an increase in sound speed and in C-H aromatic stretching, which may be due to the

intensification of the interaction between the polymer chains. Finally, the sound speed and intensity converge after the gel point and during the vitrification stage.

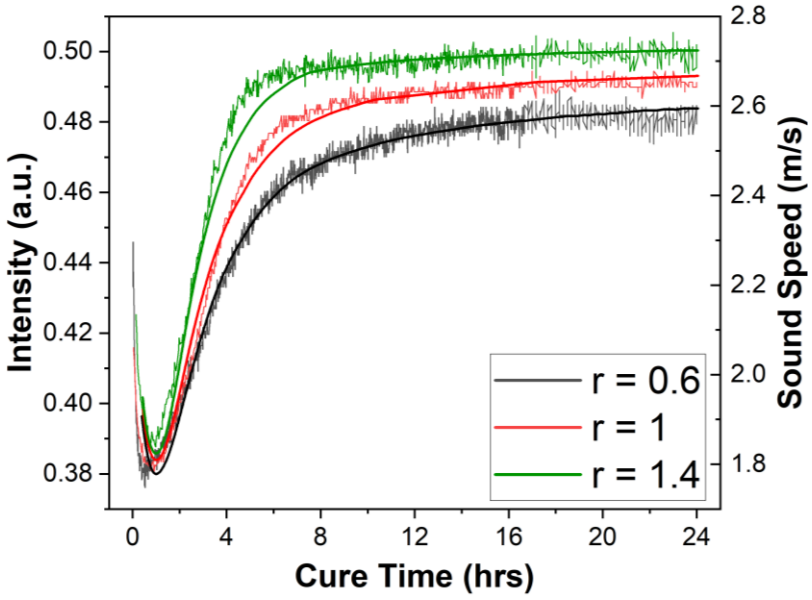

Figure 5.7. FTIR intensity of peak 1106 cm^{-1} and sound speed during cure for each of the sample types.

5.4.4 Modeling

To numerically understand how varying stoichiometry affects the cure kinetics of the epoxy resin, the Hill equation was used to model the curing process for each of the samples. The longitudinal sound speed curves in Figure 5.5a were normalized and plotted in Figure 5.8a. This graph represents the degree of conversion α of the resin, which ranges from 0 (uncured) to 1 (cured). Normalization accentuates what was portrayed in Figure 5.5b, where an increasing amount of curing agent reduces the time needed for the convergence to begin. Figure 5.8b compares the experimental and theoretical curves of the resin sample with r = 1. The Hill model gives a good estimate of the curing kinetics of the epoxy resin.

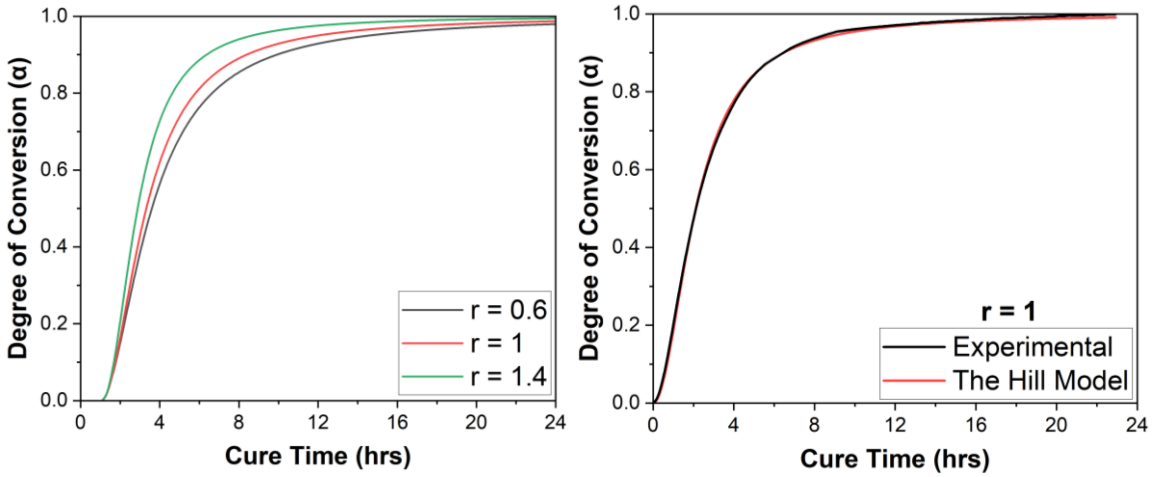

Figure 5.8. Degree of conversion with respect to cure time of (a) resin samples with r = 0.6, 1, and 1.4 ; (b) experimental and model using the Hill equation of the r = 1 sample.

Table 5.1 summarizes the rate constant *k* and the shape parameter θ values for each sample type after fitting the experimental data to the Hill equation. As expected, the rate constant k increased with raising amine content, going from $1.92 * 10^{-4}$ to $3.12 * 10^{-4}$ for the sample r = 0.6 and r = 1.4, respectively. The shape parameter θ appears to have a linear increasing relationship proportional to the amine content. A higher θ represents a more accentuated sigmoidal "S" shape. The sum of errors (between experimental and theoretical values) squared was small, meaning that the modeling resembled the experimental results. This model helps predict how the manufacturing process influences the curing behavior of the final properties of the structure, which is very advantageous during in-situ evaluation.

Table 5.1. Rate constant *k* and shape parameter θ of the Hill equation model for each sample type.

Sample (r)	$k\ (* 10^{-4})$	θ	***Sum of Error Sq***
0.6	1.92	1.76	0.121
1	2.30	1.87	0.070
1.2	2.58	1.96	0.045
1.4	3.12	2.05	0.048

5.4.5 Elastic Properties

Table 5.2 summarizes the longitudinal and shear sound speeds of the tested samples. As reported previously, the longitudinal sound speed increases with amine content. However, the baseline (r = 1) sample had the fastest shear speed. After using the densities to calculate Young's modulus and Poisson's ratio of the polymers using equations 5.2 and 5.3, the highest Young's modulus had a value of 4.285 ± 0.131 GPa, corresponding to the r = 1 sample. The resin with the least amount of amine had the lowest Young's modulus with a value of 4.285 ± 0.131 GPa. Using ultrasonics is an effective way to non-destructively evaluate the elastic properties of curing and fully cured epoxy resins. These results demonstrate that ultrasonics can serve as a quality control method during the manufacturing process, and that it could be used for structural health monitoring while the part is being utilized.

Table 5.2. Longitudinal and shear sound speeds used to calculate the elastic properties.

Sample (r)	Longitudinal Speed (m/s)	Shear Speed (m/s)	Density (g/cm^3)	Young's Modulus (GPa)	Poisson's Ratio
0.6	2318 ± 14	1164 ± 21	1.1885	4.285 ± 0.131	0.332 ± 0.005
1	2341 ± 12	1195 ± 24	1.1882	4.491 ± 0.157	0.324 ± 0.005
1.4	2412 ± 15	1182 ± 20	1.1842	4.440 ± 0.124	0.342 ± 0.004

5.5 Conclusions

Epoxy resins are highly versatile thermosets, exhibiting a wide range of properties that can be tailored through the modification of their manufacturing process. Varying the ratio of epoxy to curing agent is a common approach to altering the mechanical properties of the material. However, it has been found that this alteration of the system's stoichiometry can affect not only the final properties of the material but also its curing process. To this end, the influence of the amine-to-epoxy ratio was studied using a range of analytical

techniques. TGA revealed that the sample with the stoichiometry recommended by the manufacturer was the most thermally stable. Furthermore, FTIR confirmed that changing the chemical composition of the polymer affected its curing kinetics. Ultrasonics has also demonstrated its potential to become a useful tool for the evaluation of polymer quality in both a manufacturing and in-field setting. This unique combination of techniques can be employed as a non-destructive method to assess the curing process and viscoelastic properties of polymers.

Chapter 6 Conclusion and Future Work

The use of tailored polymers in highly demanding applications has been shown to be advantageous, reducing both the weight and cost of structures. This has attracted considerable attention from both industry and research communities. It has been established that the manufacturing process of polymeric materials is integral, as it defines the structure of the polymer and thus, its final properties and performance. It is essential to monitor the polymer during fabrication in order to gain a better understanding of the effects of the cure kinetics and the quality of the manufactured parts. Non-destructive testing is a cost-effective way to evaluate the properties of the polymer during fabrication and post-manufacture without damaging the samples, making it suitable for in-field examinations. This type of testing can be used to characterize the cure kinetics, the chemical structure, and the viscoelastic properties of epoxies. Thus, non-destructive testing offers a reliable and accurate alternative to destructive testing when it comes to assessing the properties of polymers. This article presents the successful use of three non-destructive evaluation methods, including magneto-electric nanoparticles (MENs), ultrasonics, and Fourier transform infrared spectroscopy. The key outcomes of this work are the following:

1. Successfully synthesized and dispersed magneto-electric nanoparticles (MENs) to an aerospace epoxy adhesive to perform non-destructive testing by monitoring changes in the nanoparticles' surface charge density by evaluating output magnetic signal under an applied magnetic field.
2. Increased both the tensile and shear strength of an epoxy adhesive by dispersing up to 5 vol% of MENs.
3. Developed an ultrasonic setup to monitor changes in longitudinal and shear sound speeds during the cure of an epoxy adhesive containing IPA as residual solvent. Used LabVIEW software to create a graphical program to autonomously perform the data acquisition.
4. Used the acoustics setup to detect changes in the cure kinetics of an epoxy resin as a result of varying stoichiometry (i.e., amine to epoxy ratio)
5. Modeled the curing kinetics using the Hill equation to better understand numerically the curing processes of polymers and allow for future predictions during the tailoring process. The rate constant k and the shape parameter θ were correlated to the residual solvent content and the stoichiometry of the system.
6. Correlated the longitudinal and shear sound speeds to the viscoelastic properties of the polymeric materials. It was proven that varying chemical structure affects the mechanical properties of the epoxies during cure and after they have been manufactured.
7. Used FTIR to monitor changes in the chemical structure of an epoxy resin during the curing process. FTIR was correlated with ultrasonics,

implementing a unique combination of these two non-destructive evaluation methods to characterize the curing kinetics of polymers.

The work presented in this dissertation can be adopted to design new polymeric materials, which will aid in achieving their widespread implementation in highly demanding applications.

The focus in the future will be put on the ultrasonics method since it was determined to be the most feasible and accurate of the two methods presented. First, the curing kinetics of polymeric materials will be investigated as a function of the curing temperature. This will help understand if the quality of the material is maintained under different curing temperatures, especially when these cannot be easily controlled. It will also aid in determining how the properties are affected by different temperature cycles during the cure. Temperatures both higher and lower than room temperature will be investigated. Ultrasonics measurements will be correlated with FTIR to further understand the structure of the material under different curing rates affected by temperature. The goal will be to optimize the temperature cycles during cure to obtain the desired properties of the material.

Another focus will be the investigation of the influence of fillers in both the curing kinetics and the final properties of the polymer. Fillers include boron nanotubes, carbon nanotubes, 3D-structured foams, and diverse types of nanoparticles. Fillers are usually introduced into the polymer to enhance properties like thermal, electrical, and mechanical.

References

[1] A. Bandyopadhyay, P. K. Valavala, T. C. Clancy, K. E. Wise, and G. M. Odegard, "Molecular modeling of crosslinked epoxy polymers: The effect of crosslink density on thermomechanical properties," *Polymer (Guildf)*, vol. 52, no. 11, pp. 2445–2452, May 2011, doi: 10.1016/j.polymer.2011.03.052.

[2] C. Li and A. Strachan, "Molecular simulations of crosslinking process of thermosetting polymers," *Polymer (Guildf)*, vol. 51, no. 25, pp. 6058–6070, Nov. 2010, doi: 10.1016/j.polymer.2010.10.033.

[3] S. A. Bidstrup and J. Simpson', "The Effect of Stoichiometry on Chain Segment and Ion Mobility in Partially Polymerized Epoxy Systems," *J Polym Sci B Polym Phys*, vol. 33, pp. 43–54, 1995, doi: 10.1002/polb.1995.090330105.

[4] C. Bendjaouahdou and S. Bensaad, "Aging studies of a polypropylene and natural rubber blend," *International Journal of Industrial Chemistry*, vol. 9, no. 3, pp. 345–352, 2018, doi: 10.1007/s40090-018-0163-2.

[5] E. Manaila, M. D. Stelescu, and G. Craciun, "Degradation studies realized on natural rubber and plasticized potato starch based eco-composites obtained by peroxide cross-linking," *Int J Mol Sci*, vol. 19, no. 10, 2018, doi: 10.3390/ijms19102862.

[6] V. B. Gupta, L. T. Drzal, C. Y. C Lee, and M. J. Rich, "The temperature-dependence of some mechanical properties of a cured epoxy resin system," *Polym Eng Sci*, vol. 25, no. 13, pp. 812–823, 1985, doi: 10.1002/PEN.760251305.

[7] I. Miturska, A. Rudawska, M. Müller, and M. Hromasová, "The Influence of Mixing Methods of Epoxy Composition Ingredients on Selected Mechanical Properties of Modified Epoxy Construction Materials," 2021, doi: 10.3390/ma14020411.

[8] S. E. Hall *et al.*, "Mechanical Properties of High-Temperature Fiber-Reinforced Thermoset Composites with Plain Weave and Unidirectional Carbon Fiber Fillers," *Journal of Composites Science 2022, Vol. 6, Page 213*, vol. 6, no. 7, p. 213, Jul. 2022, doi: 10.3390/JCS6070213.

[9] M. S. Hassan *et al.*, "Selective Laser Sintering of High-Temperature Thermoset Polymer," *Journal of Composites Science*, vol. 6, no. 2, p. 41, Feb. 2022, doi: 10.3390/JCS6020041/S1.

[10] A. Marotta, N. Faggio, V. Ambrogi, P. Cerruti, G. Gentile, and A. Mija, "Curing Behavior and Properties of Sustainable Furan-Based Epoxy/Anhydride Resins," *Biomacromolecules*, vol. 20, no. 10, pp. 3831–3841, Oct. 2019, doi: 10.1021/acs.biomac.9b00919/asset/images/large/bm9b00919_0005.jpeg.

[11] A. Marotta, N. Faggio, and C. Brondi, “Curing Kinetics of Bioderived Furan-Based Epoxy Resins: Study on the Effect of the Epoxy Monomer/Hardener Ratio,” 2022, doi: 10.3390/polym14235322.

[12] S. Morsch, Z. Kefallinou, Y. Liu, S. B. Lyon, and S. R. Gibbon, “Controlling the nanostructure of epoxy resins: Reaction selectivity and stoichiometry,” *Polymer (Guildf)*, vol. 143, pp. 10–18, May 2018, doi: 10.1016/j.polymer.2018.03.065.

[13] N. Odagiri *et al.*, “Amine/epoxy stoichiometric ratio dependence of crosslinked structure and ductility in amine-cured epoxy thermosetting resins,” 2021, doi: 10.1002/app.50542.

[14] G. W. Go, D. B. Kim, W. G. Park, S. Y. Choi, and S. K. Oh, “Analysis of Expansion Characteristics According to Deterioration Conditions for Superabsorbent Polymer Content of a Polyurethane Waterproof Material with Water Expansion Properties,” *Applied Sciences 2022, Vol. 12, Page 2967*, vol. 12, no. 6, p. 2967, Mar. 2022, doi: 10.3390/APP12062967.

[15] M. Maghfouri *et al.*, “Drying shrinkage properties of expanded polystyrene (EPS) lightweight aggregate concrete: A review,” *Case Studies in Construction Materials*, vol. 16, p. e00919, Jun. 2022, doi: 10.1016/J.CSCM.2022.E00919.

[16] M. D. Hossain *et al.*, “Fire Behaviour of Insulation Panels Commonly Used in High-Rise Buildings,” *Fire 2022, Vol. 5, Page 81*, vol. 5, no. 3, p. 81, Jun. 2022, doi: 10.3390/FIRE5030081.

[17] I. Ekere *et al.*, “Bioconversion Process of Polyethylene from Waste Tetra Pak® Packaging to Polyhydroxyalkanoates,” *Polymers 2022, Vol. 14, Page 2840*, vol. 14, no. 14, p. 2840, Jul. 2022, doi: 10.3390/POLYM14142840.

[18] A. K. Chaudhary, · Shubham, P. Chitriv, K. Chaitanya, and · R P Vijayakumar, “Influence of ultraviolet and chemical treatment on the biodegradation of low-density polyethylene and high-density polyethylene by Cephalosporium strain,” *Environmental Monitoring and Assessment 2023 195:3*, vol. 195, no. 3, pp. 1–14, Feb. 2023, doi: 10.1007/S10661-023-10982-8.

[19] F. Bignotti, S. Pandini, F. Baldi, and R. de Santis, “Effect of the Resin/Hardener Ratio on Curing, Structure and Glass Transition Temperature of Nanofilled Epoxies”, doi: 10.1002/pc.21120.

[20] A. Wegmann, “Chemical resistance of waterborne epoxy/amine coatings,” *Prog Org Coat*, vol. 32, no. 1–4, pp. 231–239, Dec. 1997, doi: 10.1016/S0300-9440(97)00062-3.

[21] N. H. Othman, M. Mustapha, N. Sallih, A. Ahmad, F. Mustapha, and M. C. Ismail, “The Effect of Residual Solvent in Carbon−Based Filler Reinforced Polymer Coating on the Curing Properties, Mechanical and Corrosive Behaviour,” *Materials*, vol. 15, no. 10, May 2022, doi: 10.3390/ma15103445.

[22] M. J. Lodeiro and D. R. Mulligan, “Cure monitoring techniques for polymer composites, adhesives and coatings.”

[23] M. González González, J. C. Cabanelas, and J. Baselga, “Applications of FTIR on Epoxy Resins-Identification, Monitoring the Curing Process, Phase Separation and Water Uptake”, Accessed: Feb. 09, 2023. [Online]. Available: www.intechopen.com

[24] J. Cañavate, X. Colom, P. Pagès, and F. Carrasco, “Study of the curing process of an epoxy resin by ftir spectroscopy,” vol. 39, no. 5, pp. 937–943, Nov. 2007, doi: 10.1081/ppt-100101414.

[25] L. Wu and S. v Hoa, “Effects of Composition of Hardener on the Curing and Aging for an Epoxy Resin System”, doi: 10.1002/app.22493.

[26] F. Lionetto and A. Maffezzoli, “Monitoring the cure state of thermosetting resins by ultrasound,” *Materials*, vol. 6, no. 9, pp. 3783–3804, 2013, doi: 10.3390/ma6093783.

[27] M. J. Leeuwner, D. P. Wilkinson, and E. L. Gyenge, “Novel Graphene Foam Microporous Layers for PEM Fuel Cells: Interfacial Characteristics and Comparative Performance”, doi: 10.1002/fuce.201500031.

[28] V. T. Nguyen, A. S. Vaughan, P. L. Lewin, and A. Krivda, “The effect of resin stoichiometry and nanoparticle addition on epoxy/silica nanodielectrics; The effect of resin stoichiometry and nanoparticle addition on epoxy/silica nanodielectrics,” *IEEE Transactions on Dielectrics and Electrical Insulation*, vol. 22, no. 2, 2015, doi: 10.1109/tdei.2014.004785.

[29] S. L. Kim, J. Janiszewski, M. D. Skibo, J. A. Manson, and R. W. Hertzberg, “Effect of molecular weight distribution on fatigue crack propagation in poly(methyl methacrylate),” *Polym Eng Sci*, vol. 19, no. 2, pp. 145–150, 1979, doi: 10.1002/pen.760190218.

[30] E. v. Bystritskaya, T. v. Monakhova, and V. B. Ivanov, “TGA application for optimising the accelerated aging conditions and predictions of thermal aging of rubber,” *Polym Test*, vol. 32, no. 2, pp. 197–201, Apr. 2013, doi: 10.1016/j.polymertesting.2012.10.013.

[31] M. A. André S, J. Garmendia, A. Valea, A. Eceiza, and I. Mondragon, “Fracture Toughness of Epoxy Resins Modified with Polyethersulfone: Influence of Stoichiometry on the Morphology of the Mixtures,” *J Appl Polym Sci*, vol. 69, pp. 183–191, 1998, doi: 10.1002/(SICI)1097-4628(19980705)69:1<183::AID-APP21>3.0.CO;2.

[32] J. R. M. D’Almeida and S. N. Monteiro, “The influence of the amount of hardener on the tensile mechanical behavior of an epoxy system,” *Polym Adv Technol*, vol. 9, no. 3, pp. 216–221, 1998, doi: 10.1002/(sici)1099-1581(199803)9:3<216::aid-pat746>3.0.co;2-s.

[33] A. Shigang, H. Rujie, and P. Yongmao, “Effect of manufacturing defects on mechanical properties and failure features of 3D orthogonal woven C/C composites,” 2014, doi: 10.1016/j.compositesb.2014.11.003.

[34] S. Pitta, F. Roure, D. Crespo, and J. I. Rojas, “An experimental and numerical study of repairs on composite substrates with composite and aluminum doublers using riveted, bonded, and hybrid joints,” *Materials*, vol. 12, no. 18, 2019, doi: 10.3390/ma12182978.

[35] Harvey Tool - Carbide Composite Cutting End Mills - Compression Cutter. Available:http://www.harveytool.com/secure/Content/Images/CompressionCutter.jpg.

[36] S. Pitta, V. de la Mora Carles, F. Roure, D. Crespo, and J. I. Rojas, “On the static strength of aluminium and carbon fibre aircraft lap joint repairs,” *Compos Struct*, vol. 201, pp. 276–290, Oct. 2018, doi: 10.1016/j.compstruct.2018.06.002.

[37] M. Davis and J. Tomblin, "Best Practices in Adhesive-Bonded Structures and Repairs," U.S. Department of Transportation, Federal Aviation Administration, Washington, D.C., April 2007.

[38] F. Miami and K. Z. Yang, “MENs doped adhesive and influence on fracture toughness,” 2016.

[39] Ginger Gardiner (editor), High Performance Composites, "Certification of bonded composite primary structures," Composites World, North Carolina, 04 March 2014.

[40] M. Davis and J. Tomblin, "Best Practices in Adhesive-Bonded Structures and Repairs," U.S. Department of Transportation, Federal Aviation Administration, Washington, D.C., April 2007.

[41] L. J Hart-smith, G. Redmond, and M. J. Davis, “The Curse of Nylon Peel Ply,” SAMPE (Anaheim), 1996.

[42] D. Klapprott, H. Li, R. Wong, and G. Geisendorfer, “Key factors of the peel ply surface preparation process,” 2004.

[43] J. Scheirs, “High Performance Polymers for Diverse Applications,” *Modern Fluoropolymers* , Victoria, Australia: John Wiley & Sons Ltd, February 2000.

[44] P. Van Voast, P. Shelley, P. Blakley, A. Tracey, B. Flinn, G. Dillingham and B. Oakley, "Effect of Varying Levels of Peel Ply Contamination on Adhesion Threshold," in Society for the Advancement of Material Process and Engineering (SAMPE), Seattle, WA, 2010.

[45] C. Jeenjitkaew, Z. Luklinska, and F. Guild, “Morphology and surface chemistry of kissing bonds in adhesive joints produced by surface contamination,” *Int J Adhes Adhes*, vol. 30, no. 7, pp. 643–653, Oct. 2010, doi: 10.1016/J.IJADHADH.2010.06.005.

[46] J. Sun, H. Li, C. Wang, D. Yuan, L. P. Stubbs, and C. He, “The Effect of Residual Solvent N,N′-Dimethylformamide on the Curing Reaction and Mechanical Properties of Epoxy and Lignin Epoxy Composites,” *Macromol Chem Phys*, vol. 217, no. 9, pp. 1065–1073, May 2016, doi: 10.1002/MACP.201500453.

[47] A. H. Chowdhury, B. Jafarizadeh, N. Pala, and C. Wang, “Wearable Capacitive Pressure Sensor for Contact and Non-Contact Sensing and Pulse Waveform Monitoring,” *Molecules*, vol. 27, no. 20, p. 6872, Oct. 2022, doi: 10.3390/MOLECULES27206872/S1.

[48] J. Kostina *et al.*, “Influence of residual solvent on physical and chemical properties of amorphous glassy polymer films,” *Polym Int*, vol. 62, no. 11, pp. 1566–1574, Nov. 2013, doi: 10.1002/PI.4554.

[49] B. Aurela and T. Räisänen, “Residual solvent content in heatset offset print,” *Journal of High Resolution Chromatography*, vol. 16, no. 7, pp. 422–424, 1993, doi: 10.1002/JHRC.1240160708.

[50] G. Xue *et al.*, “Effect of Aromatic Solvents Residuals on Electron Mobility of Organic Single Crystals,” 2022, doi: 10.1002/aelm.202200158.

[51] J. N. Grima and C. Zerafa, “On the effect of solvent molecules on the structure and mechanical properties of organic polyphenylacetylene auxetic re-entrant network polymers,” *Phys Status Solidi B Basic Res*, vol. 250, no. 10, pp. 2030–2037, 2013, doi: 10.1002/pssb.201384245.

[52] G. Seisdedos *et al.*, “Assessment and Non-Destructive Evaluation of the Influence of Residual Solvent on a Two-Part Epoxy-Based Adhesive Using Ultrasonics,” *Applied Sciences 2023, Vol. 13, Page 3883*, vol. 13, no. 6, p. 3883, Mar. 2023, doi: 10.3390/APP13063883.

[53] J. Trinidad, L. Chen, A. Lian, and B. Zhao, “Solvent Presence and its Impact on the Lap-Shear Strength of SDS-Decorated Graphene Hybrid Electrically Conductive Adhesives Solvent Presence and its Impact on the Lap-Shear Strength of SDS-Decorated Graphene Hybrid Electrically Conductive Adhesives,” *Int J Adhes Adhes*, 2017, doi: 10.1016/j.ijadhadh.2017.06.012.

[54] K. Qiu, R. Tannenbaum, and K. I. Jacob, “Effect of processing techniques and residual solvent on the thermal/mechanical properties of epoxy-cellulose nanocrystal nanocomposites,” *Polym Eng Sci*, vol. 61, no. 4, pp. 1281–1294, Apr. 2021, doi: 10.1002/PEN.25685.

[55] K. Frank and J. Wiggins, “Effect of stoichiometry and cure prescription on fluid ingress in epoxy networks,” *J Appl Polym Sci*, vol. 130, no. 1, pp. 264–276, Oct. 2013, doi: 10.1002/APP.39140.

[56] B. Wan, M. F. Petrou, and K. A. Harries, “The Effect of the Presence of Water on the Durability of Bond between CFRP and Concrete”, doi: 10.1177/0731684406065140.

[57] K. Vine, P. Cawley, and A. J. Kinloch, “The Correlation of Non-Destructive Measurements and Toughness Changes in Adhesive Joints during Environmental Attack,” *J Adhes*, vol. 77, no. 2, pp. 125–161, 2001, doi: 10.1080/00218460108030735.

[58] M. R. Vanlandingham, R. F. Eduljee, and J. W. Gillespie, “Relationships between Stoichiometry, Microstructure, and Properties for Amine-Cured Epoxies,” 1999, doi: 10.1002/(SICI)1097-4628(19990131)71:5<699::AID-APP4>3.0.CO;2-D.

[59] G. R. Palmese and R. L. McCullough, “Effect of epoxy–amine stoichiometry on cured resin material properties,” *J Appl Polym Sci*, vol. 46, no. 10, pp. 1863–1873, 1992, doi: 10.1002/APP.1992.070461018.

[60] C. Grave, I. Mcewan, and R. A. Pethrick, “Influence of Stoichiometric Ratio on Water Absorption in Epoxy Resins”, doi: 10.1002/(SICI)1097-4628(19980919)69:12<2369::AID-APP8>3.0.CO;2-6.

[61] S. M. Seraji, H. Gan, N.-D. Le, J. Zhang, and R. J. Varley, “The effect of DOPO concentration and epoxy amine stoichiometry on the rheological, thermal, mechanical and fire-retardant properties of crosslinked networks,” 2022, doi: 10.1002/pi.6436.

[62] F. Meyer, G. Sanz, A. Eceiza, I. Mondragon, and J. Mijović, “The effect of stoichiometry and thermal history during cure on structure and properties of epoxy networks,” *Polymer (Guildf)*, vol. 36, no. 7, pp. 1407–1414, Mar. 1995, doi: 10.1016/0032-3861(95)95918-Q.

[63] F. N. Alhabill, R. Ayoob, T. Andritsch, and A. S. Vaughan, “Effect of resin/hardener stoichiometry on electrical behavior of epoxy networks,” *IEEE Transactions on Dielectrics and Electrical Insulation*, vol. 24, no. 6, pp. 3739–3749, Dec. 2017, doi: 10.1109/TDEI.2017.006828.

[64] L. Gao *et al.*, “Effects of the amine/epoxy stoichiometry on the curing behavior and glass transition temperature of MWCNTs-NH2/epoxy nanocomposites,” *Thermochim Acta*, vol. 639, pp. 98–107, Sep. 2016, doi: 10.1016/j.tca.2016.07.017.

[65] J. Szabelski, R. Karpí Nski, J. Jonak, and M. Frigione, “Adhesive Joint Degradation Due to Hardener-to-Epoxy Ratio Inaccuracy under Varying Curing and Thermal Operating Conditions,” 2022, doi: 10.3390/ma15217765.

[66] S. Pandini, F. Baldi, R. de Santis, and F. Bignotti, “Effect of the Resin/Hardener Ratio on Yield, Post-yield, and Fracture Behavior of Nanofilled Epoxies,” *POLYM. COMPOS*, vol. 32, pp. 1461–1472, 2011, doi: 10.1002/pc.21172.

[67] J. R. M. D’Almeida and S. N. Monteiro, “Analysis of the fracture surface morphology of an epoxy system as a function of the resin/hardener ratio,” *J Mater Sci Lett*, vol. 15, no. 11, pp. 955–958, Jun. 1996, doi: 10.1007/BF00241436/METRICS.

[68] H. Wang, S. Li, Y. Yuan, X. Liu, T. Sun, and Z. Wu, “Study of the epoxy/amine equivalent ratio on thermal properties, cryogenic mechanical properties, and liquid oxygen compatibility of the bisphenol A epoxy resin containing phosphorus,” *High Perform Polym*, vol. 32, no. 4, pp. 429–443, May 2020, doi: 10.1177/0954008319871340/FORMAT/EPUB.

[69] D. C. Washington, “The Airliner Cabin Environment and The Health of Passengers and Crew Committee on Air Quality in Passenger Cabins of Commercial Aircraft Board on Environmental Studies and Toxicology Division on Earth and Life Studies,” 2002, Accessed: Feb. 04, 2023. [Online]. Available: http://www.nap.edu/catalog/10238.html

[70] D. John, T. Paul, • Kazue Orikasa, • Cheng Zhang, B. Boesl, and A. Agarwal, “Engineered Aluminum Powder Microstructure and Mechanical Properties by Heat Treatment for Optimized Cold Spray Deposition of High-Strength Coatings”, doi: 10.1007/s11666-022-01455-4.

[71] J. Denny, A. N. Jinoop, C. P. Paul, R. Singh, and K. S. Bindra, “Fatigue crack propagation behaviour of inconel 718 structures built using directed energy deposition based laser additive manufacturing,” *Mater Lett*, vol. 276, Oct. 2020, doi: 10.1016/j.matlet.2020.128241.

[72] A. Kunneparambil Sukumaran, A. D. Thampi, E. Sneha, M. Arif, S. Rani, and A. P. J. Abdul, “Effect of bovine serum albumin on the lubricant properties of rice bran oil: a biomimetic approach”, doi: 10.1007/s12046-021-01717-xS.

[73] N. Bacca *et al.*, “Tribological and neutron radiation properties of boron nitride nanotubes reinforced titanium composites under lunar environment,” *J Mater Res*, vol. 37, 2022, doi: 10.1557/s43578-022-00708-w.

[74] P. Nautiyal *et al.*, “Interface Engineering and Direct Observation of Strengthening Behavior in Field-Sintered Boron Nitride Nanotube–Magnesium Alloy Composite,” *Adv Eng Mater*, vol. 22, no. 7, p. 2000170, Jul. 2020, doi: 10.1002/ADEM.202000170.

[75] L. Lou, T. Paul, B. A. Aguiar, T. Dolmetsch, C. Zhang, and A. Agarwal, “Direct Observation of Adhesion and Mechanical Behavior of a Single Poly(lactic-co-glycolic acid) (PLGA) Fiber Using an In Situ Technique for Tissue Engineering,” *Cite This: ACS Appl. Mater. Interfaces*, vol. 14, pp. 42876–42886, 2022, doi: 10.1021/acsami.2c09665.

[76] A. Nisar *et al.*, “Unveiling enhanced oxidation resistance and mechanical integrity of multicomponent ultra-high temperature carbides,” *Journal of the American Ceramic Society*, vol. 105, no. 4, pp. 2500–2516, Apr. 2022, doi: 10.1111/JACE.18281.

[77] A. Maffezzoli, E. Quarta, V. A. M. Luprano, G. Montagna, and L. Nicolais, “Cure Monitoring of Epoxy Matrices for Composites by Ultrasonic Wave Propagation,” *J Appl Polym Sci*, vol. 73, 1969.

[78] S. K. Dwivedi, M. Vishwakarma, and A. Soni, “Advances and Researches on Non Destructive Testing: A Review,” 2018. [Online]. Available: www.sciencedirect.comwww.materialstoday.com/proceedings

[79] S. Gholizadeh, “A review of non-destructive testing methods of composite materials,” *Procedia Structural Integrity*, vol. 1, pp. 50–57, 2016, doi: 10.1016/J.PROSTR.2016.02.008.

[80] M. Jolly *et al.*, “Review of Non-destructive Testing (NDT) Techniques and their Applicability to Thick Walled Composites,” *Procedia CIRP*, vol. 38, pp. 129–136, 2015, doi: 10.1016/J.PROCIR.2015.07.043.

[81] Dubon, J.; Seisdedos, G.; Ontiveros, M.; Boesl, B.; McDaniel, D. Bond Quality Evaluation Using Adhesive Doped with MagnetoElectric Nanoparticles. Am. Soc. Compos. 2021, https://doi.org/10.12783/asc36/35876.

[82] Seisdedos, G.; Hernandez, B.; Dubon, J.; Ontiveros, M.; Boesl, B.; McDaniel, D. Non-Destructive Evaluation of Mechanical Damage of Adhesives Using Magneto-Electric Nanoparticles. Am. Soc. Compos. 2021. https://doi.org/10.12783/asc36/35763.

[83] M. K. Lim and H. Cao, "Combining multiple NDT methods to improve testing effectiveness," *Constr Build Mater*, vol. 38, pp. 1310–1315, Jan. 2013, doi: 10.1016/j.conbuildmat.2011.01.011.

[84] R. P. Mahajan, K. K. Patankar, M. B. Kothale, S. C. Chaudhari, V. L. Mathe, and S. A. Patil, "Magnetoelectric effect in cobalt ferrite–bariumtitanate composites and their electrical properties," *PRAMANA – Journal of Physics*, 2002, vol. 58, pp. 1115–1124.

[85] Y. Zhang, C. Deng, J. Ma, Y. Lin, and C. W. Nan, "Enhancement in magnetoelectric response in Co Fe2 O4 -BaTi O3 heterostructure," *Appl Phys Lett*, vol. 92, no. 6, 2008, doi: 10.1063/1.2841048.

[86] V. Corral-Flores, D. Bueno-Baqués, and R. F. Ziolo, "Synthesis and characterization of novel CoFe2O4-BaTiO3 multiferroic core-shell-type nanostructures," *Acta Mater*, vol. 58, no. 3, pp. 764–769, Feb. 2010, doi: 10.1016/j.actamat.2009.09.054.

[87] M. Fiebig, "Revival of the magnetoelectric effect," *Journal of Physics D: Applied Physics*, vol. 38, no. 8. Apr. 21, 2005. doi: 10.1088/0022-3727/38/8/R01.

[88] R. A. Islam, V. Bedekar, N. Poudyal, J. P. Liu, and S. Priya, "Magnetoelectric properties of core-shell particulate nanocomposites," *J Appl Phys*, vol. 104, no. 10, 2008, doi: 10.1063/1.3013437.

[89] Q. A Pankhurst, J. Connolly, S. K Jones, and J. Dobson, "Applications of magnetic nanoparticlesin biomedicine," *Applied PhysicsI*, 2003 vol. 36, R167–R181, PII: S0022-3727(03)40035.

[90] M. Nair, R. Guduru, P. Liang, J. Hong, V. Sagar, and S. Khizroev, "Externally controlled on-demand release of anti-HIV drug using magneto-electric nanoparticles as carriers," *Nature Communications 2013 4:1*, vol. 4, no. 1, pp. 1–8, Apr. 2013, doi: 10.1038/ncomms2717.

[91] R. Guduru, P. Liang, C. Runowicz, M. Nair, V. Atluri, and S. Khizroev, "Magneto-electric Nanoparticles to Enable Field-controlled High-Specificity Drug Delivery to Eradicate Ovarian Cancer Cells," *Scientific Reports 2013 3:1*, vol. 3, no. 1, pp. 1–8, Oct. 2013, doi: 10.1038/srep02953.

[92] K. Yue, R. Guduru, J. Hong, P. Liang, M. Nair, and S. Khizroev, "Magneto-Electric Nano-Particles for Non-Invasive Brain Stimulation," *PLoS One*, vol. 7, no. 9, p. e44040, Sep. 2012, doi: 10.1371/JOURNAL.PONE.0044040.

[93] K. Petcharoen and A. Sirivat, “Magneto-electro-responsive material based on magnetite nanoparticles/polyurethane composites,” *Materials Science and Engineering: C*, vol. 61, pp. 312–323, Apr. 2016, doi: 10.1016/J.MSEC.2015.12.014.

[94] M. F. Uddin, H. Mahfuz, S. Zainuddin, and S. Jeelani, “Improving Ballistic Performance of Polyurethane Foam by Nanoparticle Reinforcement,” *J Nanotechnol*, vol. 2009, pp. 1–8, Jan. 2009, doi: 10.1155/2009/794740.

[95] P. Rosso, L. Ye, K. Friedrich, and S. Sprenger, “A toughened epoxy resin by silica nanoparticle reinforcement,” *J Appl Polym Sci*, vol. 100, no. 3, pp. 1849–1855, May 2006, doi: 10.1002/APP.22805.

[96] S. Y. Fu, X. Q. Feng, B. Lauke, and Y. W. Mai, “Effects of particle size, particle/matrix interface adhesion and particle loading on mechanical properties of particulate–polymer composites,” *Compos B Eng*, vol. 39, no. 6, pp. 933–961, Sep. 2008, doi: 10.1016/J.COMPOSITESB.2008.01.002.

[97] R. Wu, H. Zhang, R. Yang, W. Chen, and G. Chen, “Nondestructive Testing for Corrosion Evaluation of Metal under Coating,” 2021, doi: 10.1155/2021/6640406.

[98] Y. Liu, Q. Tian, and X. Guan, “Grain Size Estimation using phased array ultrasound attenuation,” *NDT and E International*, vol. 122, Sep. 2021, doi: 10.1016/j.ndteint.2021.102479.

[99] A. Gyekenyesi, “Techniques for monitoring damage in ceramic matrix composites,” *Review Article Journal of Intelligent Material Systems and Structures*, vol. 25, no. 13, pp. 1531–1540, 2014, doi: 10.1177/1045389X13510221.

[100] X. Wang, H. Xie, Y. Tong, B. Wang, and H. Hu, “Three-point bending properties of 3D_C/C_TiC_Cu composites based on acoustic emission technology,” *Mech Syst Signal Process*, vol. 184, Feb. 2023, doi: 10.1016/J.YMSSP.2022.109693.

[101] M. Matsukawa and I. Nagai, “Ultrasonic characterization of a polymerizing epoxy resin with imbalanced stoichiometry,” *Citation: The Journal of the Acoustical Society of America*, vol. 99, p. 2110, 1996, doi: 10.1121/1.415397.

[102] Last minute engineers. Available: https://lastminuteengineers.com/arduino-sr04-ultrasonic-sensor-tutorial/

[103] J. A. Reference: Slotwinski and G. v Blessing, “Ultrasonic Measurement of the Dynamic Elastic Moduli of Small Metal Samples,” 1999. [Online]. Available: www.astm.org

[104] C. Pantea, D. G. Rickel, and A. Migliori, “Digital ultrasonic pulse-echo overlap system and algorithm for unambiguous determination of pulse transit time,” *Rev. Sci. Instrum*, vol. 76, p. 114902, 2005, doi: 10.1063/1.2130715.

[105] K. Warnemuende, “Amplitude modulated acousto-ultrasonic non-destructive testing: damage evaluation in concrete,” Wayne State University, 2009.

[106] D. G. Aggelis and A. S. Paipetis, “Monitoring of resin curing and hardening by ultrasound,” *Constr Build Mater*, vol. 26, no. 1, pp. 755–760, Jan. 2012, doi: 10.1016/j.conbuildmat.2011.06.084.

[107] A. M. Visco, V. Brancato, and N. Campo, “Degradation effects in polyester and vinyl ester resins induced by accelerated aging in seawater”, doi: 10.1177/0021998311428533.

[108] Y. S. Rohana Yahya, A. R. Azura, and Z. Ahmad, “Effect of Curing Systems on Thermal Degradation Behaviour of Natural Rubber (SMR CV 60),” *Journal of Physical Science*, vol. 22, no. 2, pp. 1–14, 2011.

[109] G. v Salmoria, P. Klauss, A. T. N. Pires, J. Roeder, and V. Soldi, “Material Characterisation Investigations on cure kinetics and thermal degradation of stereolithography RenshapeÔ 5260 photosensitive resin”, doi: 10.1016/j.polymertesting.2008.05.008.

[110] W. K. Chin, H. Ja-Jen, and M. da Shau, “Curing behaviour and thermal properties of Epon 828 resin cured with diimide-diacid and phthalic anhydride,” *Polymer (Guildf)*, vol. 39, no. 20, pp. 4923–4928, Sep. 1998, doi: 10.1016/S0032-3861(97)10332-9.

[111] T. S. Wang and M. D. A. Shau, “Properties of epon 828 resin cured by cyclic phosphine oxide tetra acid,” *J Appl Polym Sci*, vol. 70, no. 10, pp. 1877–1885, 1998, doi: 10.1002/(SICI)1097-4628(19981205)70:10<1877::AID-APP2>3.0.CO;2-2.

[112] J. A. Gerber, W. L. Burmester, and D. J. Sellmyer, “Simple vibrating sample magnetometer,” *Review of Scientific Instruments*, vol. 53, no. 5, p. 691, Jun. 1998, doi: 10.1063/1.1137043.

[113] Dubon, J.; Seisdedos, G.; Watring, D.; Pajon, M.; Khizroev, S.; McDaniel, D.; Boesl, B. Multifunctional MEN-Doped Adhesives: Strengthening, Bond Quality Evaluation, and Variations in Magnetic Signal with Environ-mental Exposure. Appl. Sci. 2022, 12, 8238. https://doi.org/10.3390/ app12168238.

[114] Y. N. Joglekar and S. J. Wolf, “SPICE model of memristive device using Tukey window function,” *Circuits Syst. I, Reg. Papers*, vol. 9, no. 5, pp. 1–7, 2010, doi: 10.1109/TCT.

[115] C. Pantea *et al.*, "Digital ultrasonic pulse-echo overlap system and algorithm for unambiguous determination of pulse transit time," *Review of Scientific Instruments*, vol. 76, no. 11. pp. 1–9, 2005. doi: 10.1063/1.2130715.

[116] B. Stollenwerk, S. Stock, U. Siebert, K. W. Lauterbach, and R. Holle, "Uncertainty Assessment of Input Parameters for Economic Evaluation: Gauss's Error Propagation, an Alternative to Established Methods", doi: 10.1177/0272989X09347015.

[117] F. Lionetto and A. Maffezzoli, "Polymer Characterization by Ultrasonic Wave Propagation", doi: 10.1002/adv.20124.

[118] A. Bernath, L. Kärger, F. Henning, and A. Böker, "Accurate Cure Modeling for Isothermal Processing of Fast Curing Epoxy Resins", doi: 10.3390/polym8110390.

[119] W. W. Focke, I. van der Westhuizen, N. Musee, and M. T. Loots, "Kinetic interpretation of log-logistic dose-time response curves," *Scientific Reports 2017 7:1*, vol. 7, no. 1, pp. 1–11, May 2017, doi: 10.1038/s41598-017-02474-w.

[120] ASTM D638-03; Standard Test Method for Tensile Properties of Plastics. ASTM International: West Con-shohocken, PA, USA, 2012.

[121] V. Musaramthota, "Prediction of Fracture Toughness and Durability of Adhesively Bonded Composite Joints with Undesirable Bonding Conditions," Florida International University, 2015. doi: 10.25148/etd.FIDC000242.

[122] ASTM D5868-01, "Standard Method for Lap Shear Adhesion Fiber for FRP Bonding". ASTM International: West Conshohocken, PA, USA, 2014.

[123] "Standard Test Method for Determination of the Mode II Interlaminar Fracture Toughness of Unidirectional Fiber-Reinforced Polymer Matrix Composites 1", doi: 10.1520/D7905_D7905M-19E01.

[124] C. Soutis, "Carbon fiber reinforced plastics in aircraft construction," *Materials Science and Engineering: A*, vol. 412, no. 1–2, pp. 171–176, Dec. 2005, doi: 10.1016/J.MSEA.2005.08.064.

[125] Barbero, E.J. Introduction to composite materials design. 1 - 26 (CRC Press, 2011).

[126] Piehl, M.J., Bossi, R.H., Blohowiak, K.Y., Dilligan, M.A., & Grace, W.B. Efficient certification of bonded primary structures. SAMPE Technical Conference Proceedings. Society for the Advancement of Material and Process Engineering (2013).

[127] Dillard, D. Advances in Structural Adhesive Bonding. Woodhead Publishing. 286 – 287 (2016).

[128] Giurgiutiu, V., Zagrai, A., & Bao, J.J. Piezoelectric wafer embedded active sensors for aging aircraft structural health monitoring, Structural Health Monitoring 1, 41 – 61 (2002), DOI: 10.1177/147592170200100104.

[129] Aggelis, D.G., Barkoula, N.M., Matikas, T.E., & Paipetis, A.S. Acoustic structural health monitoring of composite materials: Damage identification and evaluation in cross ply laminates using acoustic emission and ultrasonics. Composites Science and Technology 72, 1127 – 1133 (2012), DOI:10.1016/j.compscitech.2011.10.011.

[130] Park, H.S., Lee, H.M., Adeli, H., and Lee, I. A new approach for health monitoring of structures: Terrestrial laser scanning. Computer-Aided Civil and Infrastructure Engineering 22, 19 – 30, (2006), DOI: 10.1111/j.1467-8667.2006.00466.x.

[131] Y. Tokura and S. Seki, "Multiferroics with Spiral Spin Orders," *Advanced Materials*, vol. 22, no. 14, pp. 1554–1565, Apr. 2010, doi: 10.1002/ADMA.200901961.

[132] T. M. El-Alaily, M. K. El-Nimr, S. A. Saafan, M. M. Kamel, T. M. Meaz, and S. T. Assar, "Construction and calibration of a low cost and fully automated vibrating sample magnetometer," *J Magn Magn Mater*, vol. 386, pp. 25–30, Jul. 2015, doi: 10.1016/J.JMMM.2015.03.051.

[133] P. Martins and S. Lanceros-Méndez, "Polymer-Based Magnetoelectric Materials," *Adv Funct Mater*, vol. 23, no. 27, pp. 3371–3385, Jul. 2013, doi: 10.1002/ADFM.201202780.

[134] W. Liu, A. E. Miroshnichenko, D. N. Neshev, and Y. S. Kivshar, "Broadband unidirectional scattering by magneto-electric core-shell nanoparticles," *ACS Nano*, vol. 6, no. 6, pp. 5489–5497, Jun. 2012, doi: 10.1021/nn301398a/asset/images/large/nn-2012-01398a_0005.jpeg.

[135] M. Nair, R. Guduru, P. Liang, J. Hong, V. Sagar, and S. Khizroev, "Externally controlled on-demand release of anti-HIV drug using magneto-electric nanoparticles as carriers," *Nature Communications 2013 4:1*, vol. 4, no. 1, pp. 1–8, Apr. 2013, doi: 10.1038/ncomms2717.

[136] R. Guduru, P. Liang, C. Runowicz, M. Nair, V. Atluri, and S. Khizroev, "Magneto-electric Nanoparticles to Enable Field-controlled High-Specificity Drug Delivery to Eradicate Ovarian Cancer Cells," *Scientific Reports 2013 3:1*, vol. 3, no. 1, pp. 1–8, Oct. 2013, doi: 10.1038/srep02953.

[137] Graham, C.D. High-sensitivity magnetization measurements. Journal of Materials Science & Technology 2 (2000).

[138] B. Wetzel, P. Rosso, F. Haupert, and K. Friedrich, "Epoxy nanocomposites - fracture and toughening mechanisms," *Eng Fract Mech*, vol. 73, no. 16, pp. 2375–2398, Nov. 2006, doi: 10.1016/J.ENGFRACMECH.2006.05.018.

[139] T. H. Hsieh, A. J. Kinloch, K. Masania, A. C. Taylor, and S. Sprenger, “The mechanisms and mechanics of the toughening of epoxy polymers modified with silica nanoparticles”.

[140] K. C. Jajam and H. v Tippur, “Quasi-static and dynamic fracture behavior of particulate polymer composites: A study of nano- vs. micro-size filler and loading-rate effects,” 2012, doi: 10.1016/j.compositesb.2012.01.042.

[141] B. B. Johnsen, A. J. Kinloch, R. D. Mohammed, A. C. Taylor, and S. Sprenger, “Toughening mechanisms of nanoparticle-modified epoxy polymers,” *Polymer (Guildf)*, vol. 48, no. 2, pp. 530–541, Jan. 2007, doi: 10.1016/J.POLYMER.2006.11.038.

[142] H. Zheng *et al.*, “Multiferroic BaTiO3-CoFe2O4 Nanostructures,” *Science (1979)*, vol. 303, no. 5658, pp. 661–663, Jan. 2004, doi: 10.1126/science.1094207/suppl_file/zhengh.som.pdf.

[143] P. Nautiyal, B. Boesl, A. Agarwal. “In-Situ Mechanics of Materials,” Springer International Publishing, (2020), DOI: 10.1007/978-3-030-43320-8

[144] O. A. Ahmad, A. M. al Kassasbeh, and M. A. al Rawashdeh, “Fabrication of Polymer Concrete of Light Weight and High Performance,” *International Journal of GEOMATE*, vol. 20, no. 77, pp. 116–122, Jan. 2020, doi: 10.21660/2020.77.44329.

[145] G. Cheng, M. Sahli, J.-C. Gelin, and T. Barriere, “Process parameter effects on dimensional accuracy of a hot embossing process for polymer-based micro-fluidic device manufacturing”, doi: 10.1007/s00170-014-6135-6.

[146] C. J. Culbreath, B. Gaerke, M. S. Taylor, S. D. McCullen, and O. T. Mefford, “Effect of infill on resulting mechanical properties of additive manufactured bioresorbable polymers for medical devices,” *Materialia (Oxf)*, vol. 12, Aug. 2020, doi: 10.1016/J.MTLA.2020.100732.

[147] A. Smirnov and A. Genis, “Effect of process parameters on the structure and physicomechanical properties of nonwoven materials manufactured by aerodynamic spinning from polymer solution,” *Fibre Chemistry*, vol. 34, no. 6, pp. 24–29, 2002.

[148] D. John, T. Paul, S. M. A. K. Mohammed, G. Seisdedos, B. Boesl, and A. Agarwal, “Profilometry-Based Indentation Plastometry for Evaluating Bulk Tensile Properties of Aluminum-Silicon Carbide Composites,” *Adv Eng Mater*, p. 2201890, Mar. 2023, doi: 10.1002/ADEM.202201890.

[149] N. Caluk and A. Azizinamini, “Introduction to the concept of modular blocks for lunar infrastructure,” *Acta Astronaut*, Mar. 2023, doi: 10.1016/j.actaastro.2023.03.004.

[150] N. A. Jayasree, A. G. Airale, A. Ferraris, A. Messana, L. Sisca, and M. Carello, "Process analysis for structural optimisation of thermoplastic composite component using the building block approach," *Compos B Eng*, vol. 126, pp. 119–132, Oct. 2017, doi: 10.1016/J.COMPOSITESB.2017.06.007.

[151] Office of Aviation Research Washington. Effects of Surface Preparation on the Long-Term Durability of Adhe-sively Bonded Composite Joints. 2004, DOT/FAA/AR-03/53.

[152] E. Moutsompegka, K. Tserpes, M. Noeske, M. Schlag, and K. Brune, "Experimental Investigation of the Effect of Pre-Bond Contamination with Fingerprints and Ageing on the Fracture Toughness of Composite Bonded Joints," *Applied Composite Materials*, pp. 1001–1019, 2019, doi: 10.1007/s10443-019-09763-9.

[153] V. M. Drakonakis, J. C. Seferis, and C. C. Doumanidis, "Curing pressure influence of out-of-autoclave processing on structural composites for commercial aviation," *Advances in Materials Science and Engineering*, vol. 2013, 2013, doi: 10.1155/2013/356824.

[154] Musaramthota, V.; Pribanic, T.; Mcdaniel, D.; Zhou, X. Effect of surface contamination on composite bond in-tegrity and durability. Joint Advanced Materials and Structures, Baltimore, MD, USA, 2012.

[155] Hernandez, B.; Gutierrez-Duran, G.; Dubon, J.; Pajon, M.; Rojas-Sanchez, J. F.; Boesl, B.; Mcdaniel, D. Effect of surface contamination with mitigation methods on adhesive composite bond integrity and durability. Proceed-ings of the SAMPE, Charlotte, NC, USA, 2019.

[156] Gupta, S; Thorat, G; Murthy, Z. V. P. Mixed Matrix PVA-GO-TiO 2 Membranes for the Dehydration of Isopro-pyl Alcohol by Pervaporation. Macromolecular Research 2020, vol. 28, n. 6, pp. 587-595, doi: 10.1007/s13233-020-8070-8.

[157] Y.-Y. Lua, X. Cao, B. R. Rohrs, and D. Scott Aldrich, "Surface Characterizations of Spin-Coated Films of Ethylcellulose and Hydroxypropyl Methylcellulose Blends," 2007, doi: 10.1021/la0629680.

[158] Moiz, S. A.; Khan, I. A.; Younis, W. A.; Masud, M. I.; Ismail, Y.; Khawaja, Y. M. Solvent induced charge transport mechanism for conducting polymer at higher temperature. Mater. Res. Express 2020, doi: 10.1088/2053-1591/abb497.

[159] J. T. Kwon, B. S. Moon, J. K. Shin, S. H. Lee, S. H. Lee, and Y. S. Lee, "A new polyfluorene containing repeated ethylenoxy units linked to glycerol as side chains: Synthesis and application as an electron injection material in the fabrication of polymer light-emitting diodes," *Synth Met*, vol. 162, no. 23, pp. 2163–2170, Dec. 2012, doi: 10.1016/J.SYNTHMET.2012.09.010.

[160] ASTM D5868−01 “Standard Method for Lap Shear Adhesion Fiber for FRP Bonding”. ASTM International: West Conshohocken, PA, USA, 2014.

[161] R. Li and / Pccp, “PCCP Physical Chemistry Chemical Physics,” 2018, doi: 10.1039/c7cp07829c.

[162] M. R. Loos, L. A. F. Coelho, S. H. Pezzin, and S. C. Amico, “The effect of acetone addition on the properties of epoxy,” *Polimeros*, vol. 18, no. 1, pp. 76–80, 2008, doi: 10.1590/S0104-14282008000100015.

[163] C. Yi, P. Rostron, N. Vahdati, E. Gunister, and A. Alfantazi, “Curing kinetics and mechanical properties of epoxy based coatings: The influence of added solvent,” *Prog Org Coat*, vol. 124, pp. 165–174, Nov. 2018, doi: 10.1016/J.PORGCOAT.2018.08.009.

[164] Dubon, J.; Seisdedos, G.; Watring, D.; Pajon, M.; Khizroev, S.; McDaniel, D.; Boesl, B. Multifunctional MEN-Doped Adhesives: Strengthening, Bond Quality Evaluation, and Variations in Magnetic Signal with Environ-mental Exposure. Appl. Sci. 2022, 12, 8238. https://doi.org/10.3390/ app12168238.

[165] W. K. Chin, H. Ja-Jen, and M. da Shau, “Curing behaviour and thermal properties of Epon 828 resin cured with diimide-diacid and phthalic anhydride,” *Polymer (Guildf)*, vol. 39, no. 20, pp. 4923–4928, Sep. 1998, doi: 10.1016/S0032-3861(97)10332-9.

[166] N. O. Garifullin, B. A. Komarov, A. T. Kapasharov, and G. v Malkov, “Dependence of the Physical-Mechanical Properties of Cured Epoxy-Amine Resin on the Ratio of its Components,” 2019, doi: 10.4028/www.scientific.net/KEM.816.146.

[167] S. Pandini, F. Bignotti, F. Baldi, L. Sartore, G. Consolati, and G. Panzarasa, “Thermomechanical and Large Deformation Behaviors of Antiplasticized Epoxy Resins: Effect of Material Formulation and Network Architecture”, doi: 10.1002/pen.24555.

[168] P. Skourlis and R. 1 Mccullouch, “An Experimental Investigation of the Effect of Prepolymer Molecular Weight and Stoichiometry on Thermal and Tensile Properties of Epoxy Resins”, doi: 10.1002/(SICI)1097-4628(19961017)62:3<481::AID-APP6>3.0.CO;2-M.

[169] R. Hardis, J. L. P. Jessop, F. E. Peters, and M. R. Kessler, “Cure kinetics characterization and monitoring of an epoxy resin using DSC, Raman spectroscopy, and DEA,” *Compos Part A Appl Sci Manuf*, vol. 49, pp. 100–108, 2013, doi: 10.1016/j.compositesa.2013.01.021.

[170] C. Pantea *et al.*, “Kinetics of SiC formation during high P-T reaction between diamond and silicon,” 2005, doi: 10.1016/j.diamond.2005.04.013.

[171] M. A. García del Cid, M. G. Prolongo, C. Salom, C. Arribas, M. Sánchez-Cabezudo, and R. M. Masegosa, “The effect of stoichiometry on curing and properties of epoxy-clay nanocomposites,” *J Therm Anal Calorim*, vol. 108, no. 2, pp. 741–749, May 2012, doi: 10.1007/S10973-012-2215-8.

VITA

GONZALO SEISDEDOS RODRIGUEZ

Born, Barcelona, Spain

2019	B.S., Mechanical Engineering Florida International University Miami, Florida
Fall 2019 – Fall 2021	PhD Student in Materials Science and Engineering Florida International University Miami, Florida
Summer 2021	Intern at Los Alamos National Laboratory Los Alamos, New Mexico
Fall 2021	M.S., Materials Science and Engineering Florida International University Miami, Florida
Spring 2021 - Present	FIU NSF PREM IMPAQT Fellow Florida International University Miami, Florida
Spring 2021 - Present	PhD Candidate in Materials Science and Engineering Florida International University Miami, Florida

PUBLICATIONS AND PRESENTATIONS

Seisdedos, G.; Viamontes, E.; Salazar, E.; Ontiveros, M.; Pantea, C.; Davis, E.S.; Rockward, T.; McDaniel, D.; Boesl, B. Assessment and Non-Destructive Evaluation of the Influence of Residual Solvent on a Two-Part Epoxy-Based Adhesive Using Ultrasonics. Appl. Sci. 2023, 13, 3883. https://doi.org/10.3390/app13063883

J. Dubon, G. Seisdedos, M. Ontiveros, B. Boesl, D. McDaniel. Bond Quality Evaluation Using Adhesive Doped with Magneto-Electric Nanoparticles. *American Society for Composites* (2021). DOI: 10.12783/asc36/35876.

John, D.; Paul, T.; Sukumaran, A. K.; Seisdedos, G.; Boesl, B.; Agarwal, A. Profilometry‐Based Indentation Plastometry for Evaluating Bulk Tensile Properties of Aluminum‐Silicon Carbide Composites. Adv Eng Mater 2023, p. 2201890, 2023, doi: 10.1002/ADEM.202201890.

G. Seisdedos, B. Hernandez, J. Dubon, M. Ontiveros, B. Boesl, D. McDaniel. Non-Destructive Evaluation of Mechanical Damage of Adhesives Using Magneto-Electric Nanoparticles. *American Society for Composites* (2021). DOI: 10.12783/asc36/35763.

Dubon, J.; Seisdedos, G.; Watring, D.; Pajon, M.; Khizroev, S.; McDaniel, D.; Boesl, B. Multifunctional MEN-Doped Adhesives: Strengthening, Bond Quality Evaluation, and Variations in Magnetic Signal with Environmental Exposure. *Appl. Sci.* 2022, 12, 8238. https://doi.org/10.3390/ app12168238.

Presentation: J. Dubon, G. Seisdedos, M. Ontiveros, B. Boesl, D. McDaniel. Bond Quality Evaluation Using Adhesive Doped with Magneto-Electric Nanoparticles. *American Society for Composites* (2021)

Presentation: G. Seisdedos, B. Hernandez, J. Dubon, M. Ontiveros, B. Boesl, D. McDaniel. Non-Destructive Evaluation of Mechanical Damage of Adhesives Using Magneto-Electric Nanoparticles. *American Society for Composites* (2021). DOI: 10.12783/asc36/35763.